Université Lille I - Sciences et Technologies

Laboratoire de Mécanique de Lille (UMR CNRS 8107)
Ecole Doctorale SPI Lille Nord-de-France

Année 2013 - N° d'ordre : 41100

THESE

Pour obtenir le grade de

Docteur de l'Université Lille I - Sciences et Technologies

Discipline : Génie Civil

Présentée par

Zaobao LIU

Evaluation et amélioration des modèles numériques pour l'analyse de la stabilité des pentes

Soutenue publiquement le 22 Avril 2013 devant le jury composé de

M. D. HOXHA, Professeur, Université d'Orléans	**Rapporteur**
M. Q.U. JIANG, Professeur, Université de Wuhan	**Rapporteur**
M. H.B. BIAN, Maître de conférences, Université Metz,	**Membre**
M. F. PELLET, Professeur, INSA Lyon	**Membre**
M. T. VERDEL, Professeur, Ecole des Mines de Nancy	**Membre**
M. J.F. SHAO, Professeur, Université Lille I	**Directeur de thèse**

Remerciements

Any attempt to enumerate the people and opportunities with which my life has been richly blessed would be like trying to count the stars in the heavens. Yet among these stand four individuals whose profound impact deserves special acknowledgements and to whom I would like to dedicate this thesis.

To my mentor, Prof. Jianfu Shao, who, welcomed me in his lab, gave me the opportunity to develop this experience abroad and challenged me every day to make me a better researcher. According to my research experiences, he suggested and guided the work and offered his continuing advice and encouragement throughout the course of this thesis. His patient, thought-provoking guidance and instruction have guided this dissertation to a successful completion. The time and care he put into his work set an example I hope to follow in my future job.

To my co-tutor supervisor, Prof. Weiya Xu, who accepted me as a freshman in his reputed group and trained me a lot in the scientific field. He offered me the opportunity to study abroad and kept guiding me throughout the course of this thesis. His advice, unsurpassed knowledge and the internationalized outlook had profoundly broadened my insight and strengthened the quality of the work. Also, I appreciate him very much since he had helped me a lot to cope with life during my period being a graduate student and PhD student.

To my mother, Fubao Guo, who provided an example of hard work and pride in a well done job, and inspired me a lot in love of science and engineering. The time he spent, the opportunities he provided, the instruction and encouragement he gave continue to bless my life.

Most importantly, to my wonderful wife, Dan Xue. You have supported me in the darkest times and believed in me even when I did not believe in myself. Your tireless effort enabled me to take every time to complete this work. You not only supported my decision but also made the past five years some of the best of my life. I’ve always loved your joyful spirit and this spirit provided the boost that made even the longest hours enjoyable. This would not have been possible if not for you. No words can express how grateful I am for your love and support and how very much I love and appreciate you.

The four individuals to whom this thesis is dedicated each provided a special contribution to this thesis. Many other individuals and organizations also have contributed to and supported the research presented herein and I would like to gratefully acknowledge their contributions.

I would like to thank Prof. PELLET from the Départment de génie civil of INSA Lyon; Prof. HOXHA from Polytech-Orléans; Prof. JIANG from Wuhan University; MCF. Dr. BIAN from Université Paul Verlaine Metz and Prof. VERDEL from Ecole des mines de Nancy for serving on my

dissertation committee and for providing valuable guidance and suggestions. Special thanks are due to Prof. HOXHA for the careful review and many suggestions that he provided in the original manuscript and to Prof. PELLET for his thorough review and many suggestions.

I would like to express my sincere gratitude to the Chinese Scholarship Council for providing financial support for my research and living expenses abroad. I also would like to thank the Jiangsu Higher–education Innovation Project grant NO.2009B_158Z for supporting me in my early research. Also, I appreciate the staffs in Jinping Projects of Chendu Hydroelectric Design Institute and Ertan Hydropower Development Company, Ltd. for providing me the related data in this work. Especially, I am very grateful to Mr.Zhong Zhou and Dr. Shaohui Duan for their support and help for me during my four stays in the field of Jingping 1 Hydropower Station.

I would like to thank Dr.Yun Jia, Dr.Yuanyuan Zheng, Dr.Shouyi Xie and Dr.Hanbin Bian for providing me the sincere help and specific instruction in daily life in Lille. This had made life easier for me and as a result I could concentrate on my thesis work. I really appreciate the joy of discussion in the group seminary upheld by Prof. Nicolas Burlion and Prof. Schozilas. Their humor and insightful comments at each seminar made the research enjoyable and wonderful. I also would like to thank Dr.Yun Huang, Dr.Tao Zeng, Dr.Yue Liang, Dr.Caifeng Jin, Dr.He Yang, Dr. Wei Chen, Dr.Emma Lanoye, Dr. Dawei Hu Dr. Wanqin Shen and Dr.Thomas for their daily help and instruction in preparing this dissertation.

I am particularly grateful for the support and encouragement of the wonderful group of peers at the Laboratory of Mechanics of Lille. Not only has it been a pleasure to work and study with you, but your suggestions, comments, and criticisms along the way have been most helpful. In particular, Lifeng Zheng, Yu Zhang, Mingyao Li, Qier Wu, Amid, Chi Yao, Taogen Liu and Lin Li have all provided assistance and encouragement that made this thesis easier and more enjoyable.

I would like to offer special thanks to Marie-Christine Nodot, whose constant behind-the-scenes efforts make the Laboratory of Mechanics of Lille a much brighter place to work. Their efforts with everything from administrative details to arranging office works created an atmosphere that makes the laboratory a joy palce to work at. I also would like to express my appreciation to Mr. Olivier Colot, Mme.Tram Nguyen and Mme.Fabienne Leclercq of the Ecole Doctoral Lille, who constantly ensured that all the administrative requirements of the Department and Graduate College were met and did this with a manner that made visits to address these requirements enjoyable rather than a burden.

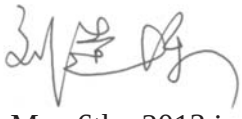

May 6th , 2013 in Lille

Evaluation et amélioration des modèles numériques pour l'analyse de la stabilité des pentes

Résumé

La rupture des pentes et l'éclatement des roches, qui représentent deux types de risques naturels fréquents dans le monde, peuvent engendrer des conséquences économiques importantes et des pertes en vie humaine. Malgré que les phénomènes soient étudiés depuis de longues années, il reste encore des questions ouvertes et sans réponse et il est donc encore nécessaire poursuivre les recherches sur cette thématique. Le présent travail de thèse est consacré la modélisation numérique de la stabilité des grandes pentes et de l'éclatement des massifs rocheux en utilisant des méthodes basées sur l'intelligence artificielle en proposant des modifications et des améliorations de telles méthodes.

En se basant sur des observations de déplacements de terrain, le glissement de terrain, qui est phénomène commun de la rupture de pentes, est étudié par le processus de Gauss afin de prédire son apparition temporelle. Ensuite, la question d'évaluation de la stabilité des pentes est abordée en utilisant la stratégie de machine à vecteurs de pertinence (RVM) avec des hyper-paramètres adaptatifs. Une approche itérative est proposée afin de déterminer les valeurs optimales des hyper-paramètres. Afin d'améliorer la prédiction, l'évaluation complète de la stabilité des pentes est réalisée en proposant un modèle basé sur la théorie de flou (CM) associé à un processus analytique d'hiérarchisation pondérée (WAHP). Ce modèle est utilisé à l'évaluation de la stabilité de la pente de rive gauche de la centrale hydroélectrique de Jinping 1, dans la région Sud-Ouest de Chine. Enfin, dans la dernière partie, la problématique de l'éclatement des massifs rocheux est abordée en utilisant des modèles basés sur la théorie du flou, en se basant sur une synthèse de 164 cas réels. Des comparaisons entre les résultats numériques et des données de terrain sont présentées pour de différents cas étudiés dans cette thèse.

Mots clés : risque naturel, glissement de roches--prévision, pentes (mécanique des sols), pente et versants rocheux--stabilité, éclatement de roche, modélisation numérique intelligente, processus Gaussiens, machine à vecteurs de pertinence, machine à vecteurs de support, théorie du flou

Evaluation and improvement of some numerical models for the analysis of slope stability and rock burst

Abstract

Slope failures and rock burst, which are two typical types of geological hazards, create tremendous economic damages and cause massive losses to the health of domestic humans or animals every year throughout the world. The severe situation implies that they are still in need to be further studied despite the fact that they have been discussed for a long time. The present work is devoted to presenting the analysis of slope failures and rock burst using some computational intelligent models with modifications and improvements.

Then landslide, a common type of slope failure, is analyzed for time occurrence prediction using the Gaussian Process by means of field-observed displacement series. After that, the problem of slope stability evaluation is discussed using the strategy of relevance vector machine (RVM) with adaptive hyper-parameter. An iteration approach is presented to find optimal hyper-parameter values in this chapter. Afterwards, the comprehensive evaluation of slope stability is carried out with the cloud model (CM) and weighted analytical hierarchy process (WAHP) closely related to the left abutment slope of Jinping 1 Hydropower Station, southwest of China. Finally, prediction of rock burst classification is engaged using the cloud models synthesized with the attribution weights on the basis of 164 rock burst cases. In each modeling of the associated problems, comparisons are given on the performance of each strategy as well as some evaluations.

Keywords: geotechnical hazard; applied soft computing; landslide; slope stability; rock burst ; computational intelligent model; Gaussian process; relevance vector machine; support vector machine; cloud model

General Introduction

Geological hazards, like the slope failures and rock burst, would result in severe outcomes during the construction of infrastructures and hydroelectric projects. The analysis of the two types of hazards involves many variable factors for the reason that they are created by different mechanisms. For example, slope failures are probably related to the strength of the geo-materials (soils or rocks) and the geometry of the slopes; rock burst is mainly induced due to overstress of the ground in hard rocks. The present work is closely related to the analysis of slope stability and rock burst using computational intelligent models. It focuses on the improvements of intelligent models for application in the analysis of slope stability and rock burst classification as well as evaluations of the performances of these models.

Early research on slope failures can be found in research publications such as (Tayer 1937; Saito 1965; Janbu 1973; Chen and Snitbhan 1975; Fukuzono 1985). These publications represent the initial start on this topic. After that, various kinds of work contribute to this issue for applying new methods for slope stability analysis. The limit equilibrium analysis is the widely used and the most acceptable kind of method which in fact encounters difficulties in solving for the factor of safety. Then the numerical methods like the finite element method (FEM), discrete element method (DEM) are studied and utilized to model slope failure problems. Recently, the intelligent computational methods, for instance the artificial neural network (ANN) and support vector machines (SVM), are addressed in the analysis of slope failures. As for research on rock burst classification, it starts with the work on the prediction criteria (Neyman et al. 1972; Turchaninov et al. 1972; Russenes 1974; Hoek and Brown 1980). Based on these works, the predictive methods or models are extensively discussed for rock burst classification as presented in Chapter 4.

In this work, the analyses on slope stability and rock burst classification are implemented using different computational intelligence methods. Some improvements are proposed for each method in order to utilize them properly as well as obtain valuable modeling results. The content of the thesis is organized into 6 chapters as shown below.

In Chapter 1, landslide, a typical slope failure type, is studied by means of field observed displacement for time prediction with the method of Gaussian Process (GP). The observed landslide displacement is a typical time series data which represents the overall feature of landslides. Drifting away the complicated inducing factors, landslide displacement is the comprehensive external outcome of its underlying dynamic evolutionary process for the potential landslides. The displacement is used as one of the principal means to indicate the status of slopes. Study of landslide displacement had been recognized as an effective way to know the landslide event for a long time. Firstly the noisy predictive

problem is introduced from the view of nonlinear mapping with observed data of slope displacement. Secondly the Gaussian Process is demonstrated as a regression method for modeling the displacement series of slopes. The typical features of Gaussian process, like the covariance functions, modeling training and the loss functions, are also introduced for better understanding. Thirdly, the discussed method is implemented to analyze the observed one of the displacement series in Wolong Temple New Landslide. The dynamic cross validation method is applied to improve the predictive performance of the strategy. Comparisons of the predicted results of the previous work, different covariance functions and other techniques (RBF neural network, support vector machine) are discussed in order to deliver a comprehensive evaluation of the Gaussian process. The results turn out that the composition of different covariance function does not necessarily give improvement in predictive performances for a specified modeling problem. And covariance functions should be accorded with the characteristic of the modeling object so as to give satisfactory predictive results. Also, the proposed strategy performs better than the RBF neural network and the support vector vachine in the trend prediction of the displacement series, though it cannot give superior point predictions in some cases. Finally, a criterion for landslide is given that it would be a signal for forecasting of landslide occurrence if the intersection angle arrives at 45º at the turnings on the predicted curve when modeling the observed displacement of the creep-typed slope.

In Chapter 2, the state of art model--relevant vector machine (RVM) is improved with optimal hyper-parameter value and thus the adaptive RVM (ARVM) is presented for slope stability evaluation. The RVMs, as well as the kernel functions, is introduced briefly in the Bayesian framework for the prediction of slope stability. An iteration approach is presented in the study for searching the optimal hyper-parameter values of the kernels. The effect of hyper-parameter values on the performance of RVMs is investigated as well as that of the kernel type and the size of samples for modeling. Also, comparisons are illustrated on the performances of the ARVM and other approaches like the artificial neural network (ANN) and the support vector machines(SVM) for slope stability analysis. The results turn out that the hyper-parameter values have certain effects on the performance of RVMs, and the kernel type and the size of samples for modeling may result in different optimal hyper-parameter values. The comparative results prove that the ARVM is feasible and effective as a potential tool for analysis of slope stability analysis.

As for Chapter 3, it focuses on the comprehensive stability evaluation of complicated high slopes. This chapter aims to introduce the cloud models to evaluate the stability of complicated rock slopes with the help of the weighted analytical hierarchy process. The work is closely related to the left abutment slope of Jinping 1 Hydropower Station, southwest of China. A brief introduction is given firstly on both conventional and unconventional methods for slope stability evaluation problems as

well as the cloud models. Secondly, the characterization of the discussed slope and the evaluation systems are discussed concerning to the problems on site characterization, potential slope failure, slope reinforcement and treatment, categories of evaluating factors, classification of the factors and empirical rock slope stability classification. The factors adopted for evaluating slope stability are obtained according to slope conditions and with reference to the previous rock mass rating systems. The classifications of these factors are obtained from China slope design standard and the previous work related to this slope. Afterwards, the method of cloud model is introduced with special regard to slope stability problems. The cloud generators are presented to generate the cloud model outputs as well as the cloud transformation process which is also essential for the performance of the models. Meanwhile, the weighted AHP is presented for comprehensive evaluation of slope stability with the outputs of cloud models. Finally, basing on the data collected, the implementation of the presented approach is executed to evaluate the stability of the left abutment slope of Jinping 1 Hydropower Station southwest of China. The results turn out that the stability status of the slope at that time is lying between the stability level II (stable) and I (very stable), prone to level II. Also, the result is validated by other techniques carried out in another point of view by former researchers.

In Chapter 4, prediction of rock burst classification is discussed with the cloud models synthesized by attribution weights which are noted as the weighted cloud model (WCM). Rock burst is one of the frequent failures during the opening of underground tunnels. This chapter focuses on the prediction of rock burst classification with case instances using the cloud models and considering the attribution weight. Firstly cloud models are introduced briefly related to the rock burst classification problem. Then the attribution weight method is presented to quantify the relative contribution of each rock burst indicator for classification. The approach is implemented to predict the classification of rock burst intensity for the 164 rock burst instances collected. The clustering figures are generated by cloud models for each rock burst class. The computed weight values of the indicators give out that the stress ratio $Ts = \sigma_\theta/\sigma_c$ is the most vulnerable parameter and that the elastic strain energy storage index W_{et} and the brittleness factor $B = \sigma_c/\sigma_t$ takes the second and third place, respectively, for contributing to the rock burst classification. Besides, different models with varying indicators are also investigated to find out the effect of the indicators. The result shows that the indicator $Ts = \sigma_\theta/\sigma_c$ is the most sensitive in generating predictive results. The obtained results are accorded with that of attribution weight values. Finally, the predictive performance of the strategy introduced in this work is compared with that of the neural network (including general regression neural network and probability neural network) and support vector machines. The results turn out that the SVM and the cloud models with attribution weight can perform better than the neural networks and simple cloud models in the generalization of the test data samples, while the neural networks have significantly better

performance in training the data samples. Thus it can be concluded that cloud models are feasible and applicable for prediction of rock burst classification considering the attribution weights and can be recognized as a potential method for classification prediction of rock bursts.

Finally the summary and recommendations are given in Chapter 5 as well as some limitations of the study in the thesis.

The overview of the content of this thesis is shown below in Figure 0-1.

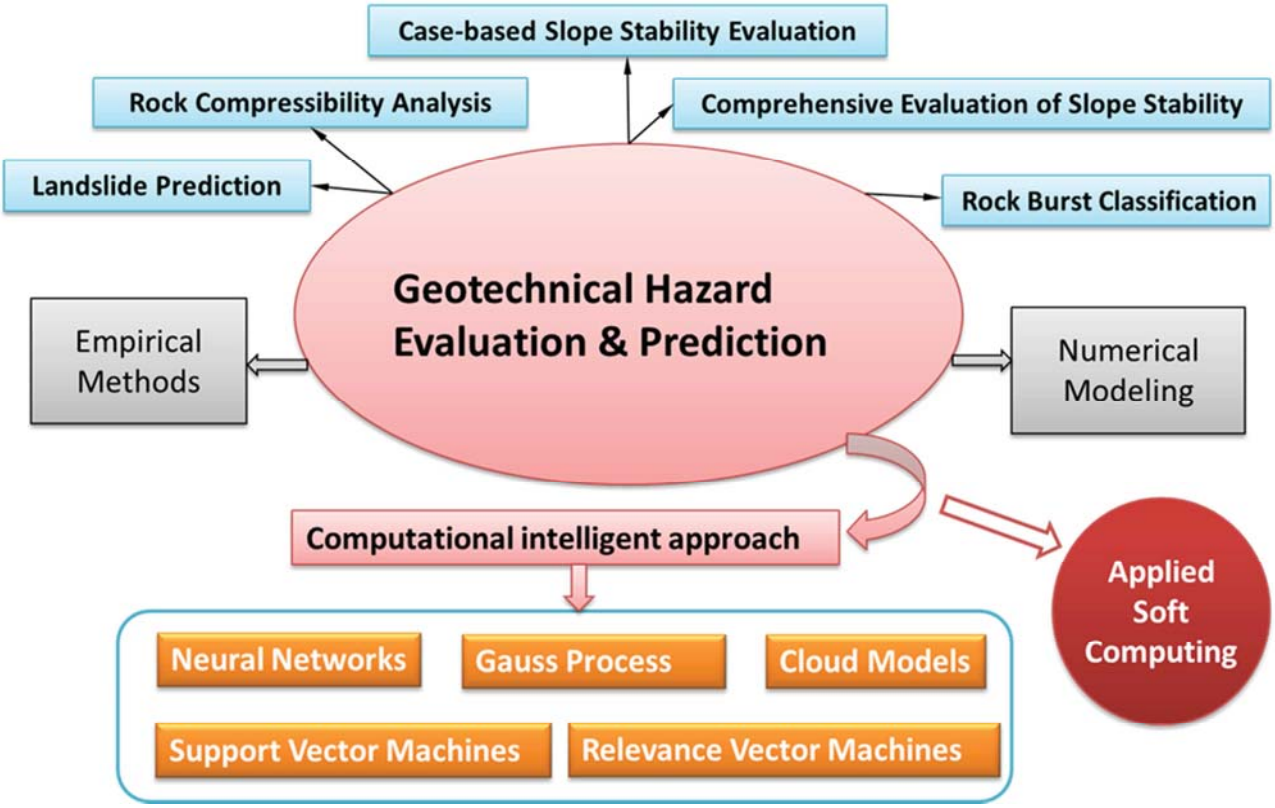

Figure 0-1 Overview of the content of the thesis

Table of Contents

List of Tables

List of Figures

List of Symbols

F	Factor of safety
γ	Bulk density
c	Cohesion
φ	Internal friction angle
β	Inclination
H	Slope height
r_u	Pore water pressure
σ_c	Uniaxial compressive strength
f_i	Slope fault number
K_v	Integrality index
V_{pm}	Velocity of elastic P-wave in the rock mass
V_{pt}	Velocity of elastic P-wave in rock sampling
S_k	Number of ungrouped joints per cubic meter
J_v	Number of joint per cubic meter
σ_θ	Shear strength
σ_t	Tensile strength
$Ts = \sigma_\theta/\sigma_c$	Tangential stress
W_{et}	Elastic strain energy storage index
$B = \sigma_c/\sigma_t$	Brittle index of rock
x_i	Dependent variable
y_i	Independent variable
X	Vector or matrix of the dependent variable
Y	Vector or matrix of the independent variable
T_i	The i^{th} principle component of independent variable
U_i	The i^{th} principle component of dependent variable
e_1	Eigen value
v_1	Unit Eigen vector
θ_1^2	Maximum Eigen value
$E_1;\ F_1$	Residual error matrix
l	Number of principal component
$\phi(x)$	Mapping function

$w=[w_0\ , w_1\ ,...,\ w_N]^t$	Weight vector
$K(x_i,x_j)=\phi(x_i)\phi(x_j)$	Kernel function
$C>0$	Penalty factor of SVM
P_{best}	Particle best solution
G_{best}	Global best solution of particle
L_{best}	Best location of particles
$g_j(\boldsymbol{x})$	Gaussian basis function
$m(x)$	Mean function
$k(x,x')$	Covariance function
σ_f^2	Signal variance
E_x	Expectation
E_n	Entropy
H_e	Hyper entropy

Chapter 1 Landslide displacement analysis and prediction using Gaussian process

1.1 Introduction

Numerous slopes are triggered to come up with landslides, collapses, crumbles and other kinds of disasters, which causes huge biotic and economic loss worldwide each year. The severe situation has motivated the assessment and prediction of slope instability together with the mitigation efforts in engineering construction for disaster prevention and control. Slope instability could be triggered by various inducing factors such as rainfall, earthquake, excavating activity and so on. In practice, most large-scale slope projects and critical landslides are decorated with a complete safety monitoring system to feedback and control the slope deformation and its stability status. The safety monitoring system expresses the slope stability status by real-time monitoring the observed outcome information, like displacement and stress, during its potential dynamic and complicated evolution. Drifting away the complicated inducing factors, slope deformation is the comprehensive external outcome of its underlying dynamic evolutionary process for potential landslides, and it has been used as the main measure means for indicating the status of slope stability.

Even though landslide analysis via its deformation analysis has been recognized for a long time, researchers have been keeping study on proper prediction or forecasting models for slope instability. Many have ever succeeded in forecasting landslide event, enabling mitigation measures in advance to cut down the potential loss. From the 1990s, according to the records of the Ministry of Land and Resources of China, landslides were forecasted successfully in Yuntai Mountain between Zhenjiang and Jiangsu province on the 9th Jul. 1991, Huangci Village of Yongjing city in Gansu province on the 31th Jan.1995, and Jiaojia Carbonization Plant of Yongjing in Gansu province on the 6th Feb.1996(MRLChina 2010). And the large-scale mountain landslide took place in Litai Village Naxi District Luzhou City Sichuan on June 20th 2002; over 600 casualties were avoided from suffering thanks to continuous monitoring and timely disaster precautions(Zhou and Yao 2009).

Time series are commonly used in many fields to reveal the characteristics of complicated systems. The observed landslide displacement is a typical time series data which represent the overall features of landslides. Drifting away the complicated inducing factors, landslide displacement is the comprehensive external outcome of its underlying dynamic evolutionary process for potential landslides. The displacement has been used as one of the main means to indicate the status of slopes. Study of landslide displacement has been recognized as an effective way to know the landslide event

for a long time. Researchers have been keeping study on proper prediction models for monitoring displacement series of landslide. Landslide displacement prediction is the fundamental work for prevention of landslide disasters despite that it is far away from being completely forecasted. Study on landslide displacements is an effective tool for better understanding of landslide movements. Models or methods have been proposed with proper criteria for the issue of modeling specific landslide displacement series, mainly including the grey forecasting model, the neural network and the support vector machine etc.

In the view of treating landslide as a grey system, (Liu et al. 2009) conducted a study on the landslide displacement prediction with modified GM(1.1) model for unequal interval observation series. While the predictive accuracy of GM model would depend largely on the number of samples for modeling and the exact sample size was difficult to identify reasonable.

Many former researchers have reported the outperformance of different ANNs for study of slope displacement and movement. (Feng et al. 1996) stated a real-time prediction model for roof pressure in coal mines using a multilayer feed-forward neural network and achieved contented accuracy. (Sakellariou and Ferentinou 2005) promoted the study on estimation of slope stability using neural networks based on collective data set of historical slopes worldwide and they also studied the relative importance of the parameters affecting slope stability. (Wang et al. 2005) presented the Back Propagation Neural Networks (BPNN) with five input nodes, two hidden layers, and two output nodes to evaluation slope instability by using a training data set of landslide samples throughout the regional observations. (Ferentinou and Sakellariou 2007) presented a study on prediction of slope performance obtained by using the back-propagation algorithm, the theory of Bayesian neural networks and the Kohonen self-organizing maps. The reasonable results indicated that the method conducted by them was promising and should be further exploited.

In the application of support vector machines, many works investigated the support vector machines for modeling displacement and movement of slopes to give satisfactory predictive results. (Feng et al. 2004) presented the support vector machine (SVM) to obtain a global optimization model for evaluation of the non-linear displacement behavior of geo-materials in conditions of large project dimensions, small sample sizes and nonlinearity. They found that SVM can appropriately describe the evolutionary law of deformation of geo-materials at depth and provide predictions for the future 6-10 time steps with acceptable accuracy and confidence. (Matías et al. 2010) proposed a partially linear SVM(PLSVM) method with the kernel composed of a linear kernel and a nonlinear kernel. They found that the PL-SVM improved on the results of other autoregressive approaches for predicting monthly movement in a mine slope with an impact on the safety of the mining operation. (Xu and Xu 2010a) conducted the prediction of slope displacement series using a hybridization of SVMs and Markov

chains and found that the integrated model promoted contently the accuracy of predictive results. P. (Samui and Kotharib 2011) examined the capability of a least square support vector machine (LSSVM) model for slope stability analysis and they carried out a comparative study between the LSSVM and an artificial neural network (ANN). Their study concluded that the developed LSSVM is a robust model for slope stability analysis. Various models were presented by former researchers for time series prediction.

Some models mentioned above gave an estimation of slope stability according collection of historical data on slope cases, while precise data acquisition is quite a difficult task for some parameters of slopes, especially some descriptive data. Thus some others promoted models for prediction of landslide displacement based on observations, which is another way for analysis of slopes and can be called the phenomenal way. However, these methods are not sufficient enough to prevent searching new methods for the study of landslide displacement for that they all have some restrictions. For example, the performance of grey model is closely related to the number of data that is modeled. And no coincide has been made on the best quantity of data for modeling. ANNs are thought to be powerful for the ability to deal with nonlinear problems while the parameters and results of ANNs are sometimes difficult to be physically explained. The SVM is proposed for machine learning on the principle of minimizing the empirical risk. Its performance is greatly affected by the types of kernel function and other parameters. (Mehdi and Mehdi 2011) reviewed broadly the literatures on time series prediction when they proposed a hybridization of neural networks and ARIMA models for time series forecasting. They concluded that improving forecasting especially time series forecasting accuracy was an important yet often difficult task facing decision makers in many areas. The research for improving the effectiveness of forecasting models would never stop despite the numerous time series models available. This work is still in need to present prediction method which can take into account of the previous knowledge of the landslide system.

A new regression method was inspired since 1996 by Neal's work (Neal 1996) on Bayesian learning for neural network analysis. Gaussian process has been proved to be an attractive method for modeling noisy data based on priors over functions. Problems with noisy free and stationary series ((Williams and Rasmussen 1996; Belhouari and Vesin 2001; Belhouari and Bermak 2004) have been studied using Gaussian Process; in this chapter it discussed modeling on the noisy and non-stationary landslide displacement series.

Gaussian process is based on Bayesian leaning. The advantages lie that it utilizes not only the model information and data message, but also makes the best of prior knowledge about the studied object. What's more, the prior knowledge can be free of special restrictions but indispensable. The prior distribution need not be objective while it can partially or completely depend on the subjectivities.

Thus it gains superiority in discussing strong empirical systems like the landslide. And this has bloomed its development and applications in many fields (Li and Sun 2009; Elguebaly and Bouguila 2011).

It can be concluded from the literatures that a predictive model may be able to generate satisfactory results for one set of training samples, while it might not be able to outperform for another input data with different behaviors. The clue may lie that some are linear models, while some others are nonlinear. Linear models could perform well for linear systems; nonlinear ones can generate pretty good results for nonlinear systems. But linear models could not contently account for nonlinear systems and vice-versa. Landslide displacement is complicated with typical nonlinear features.

Despite of the above achievements, landslide displacement modeling is still in need to be further studied since it deals with the natural data, which concerns with not only calculations and numerical analysis, but also concepts, perception, judgment and employment of experience that cannot be strictly represented numerically. The following section introduces the Gaussian process for landslide displacement analysis and prediction(Liu et al. 2012).

1.2 Prediction problems of slope displacement

Slope is a nonlinear open system coupling affected by the geo-environment of the rock mass, hydrological condition, underground water, rainfall, manual activities, even the seismic and the like. It is severely difficult to uncover the complicated evolutionary process for slopes in complex conditions. The displacement behavior of slopes is aggravated by its material structures, reinforcements, excavation blasting, human activities, tectonic activities, seismic forces, high stresses, high water pressure, temperature gradient, strong geo-chemical reaction and their coupled effects (Feng et al. 2004). The measured displacement series is noisy, non-stationary and variable over time. Modeling the measured displacement is important and feasible for analysis and prediction of slope stability status. The prediction of slope displacement is aimed at estimating and predicting its future displacement in magnitude and tendency based on the historical displacement time series.

Once a certain model is proved to be suitable for prediction of landslide displacement, then forecasting of landslide occurrence could be considered with proper thresholds and criteria for potential slope instability. The predictive model is processed as the main issue for the prediction problem of slope displacement. Regard a set of nodes $d$such that the observed target is denoted as $X = \left\{ x_{k-d+1}, x_{k-(d-1)+1}, \cdots, x_k \right\}$ and the next x_{k+1} is the prediction target or the modeling output. Since the measurement conditions are usually influenced complicatedly by multitudinous factors, let ε, y^i, $f(x,\theta)$ be the overall effects of noise corrupting the data, the observation and the predictive distribution

of slope displacement, respectively, then the aim of prediction is to obtain the mapping of observations using observed input data $\boldsymbol{x} = [x_{k-d+1}, x_{k-(d-1)+1}, \cdots, x_k]$. Thus the prediction problem for slope displacement can be denoted as

$$y^i = f(x^i, \theta) + \varepsilon^i \qquad i = 1, \cdots, n \quad \text{.....(1.1)}$$

The goal of prediction is to obtain the non-linear mapping $f(\boldsymbol{x}, \theta)$, where θ denote the unknown parameters to be determined by training with the input data using proper techniques. In fact, as an important application field of neural networks, the mapping $f(\boldsymbol{x}, \theta)$ can be given by a specified network. The outcome of the RBF network is computed as a linear superposition (Bishop, C.M., 1995) as

$$f(\boldsymbol{x}, \theta) = \sum_{j=1}^{M} w_j g_j(\boldsymbol{x}) \quad \text{.....(1.2)}$$

Where w_j and $g_j(\boldsymbol{x})$ are the weights of the output layer and the Gaussian basis functions, respectively. And $g_j(\boldsymbol{x})$ are defined as

$$g_j(\boldsymbol{x}) = \exp\left\{ -\frac{\left\| \boldsymbol{x} - \boldsymbol{\mu}_j \right\|^2}{2\sigma_j^2} \right\} \quad \text{.....} \quad (1.3)$$

Where $\boldsymbol{\mu}_j$ and σ_j denote means and variances respectively. Thus the parameters θ can be defined as $\theta = \left[w_j, \mu_j, \sigma_j^2 \right]$ $(j = 1, \cdots, M)$, which would be estimated by a special training algorithm like Back Propagation Algorithm.

Unlike the method of neural network, predictions by non-parametric methods, for example the support vector machine (Xu and Xu 2010a) is gained without representing the unknown slope system as an explicit parameterized mapping. A new method for regression was inspired on Bayesian learning and an attractive method for modeling non-stationary noise landslide displacement data are proposed hereafter based on priors over function. And Gaussian Process is applied with proper prior covariance and dynamic crossing validation method.

1.3 Gaussian process based approach

The Gaussian process represents the posterior distribution over functions based on training data

and prior distribution. The graphical model of Gaussian process is shown in Fig. 1.1 to give a visualized view, where the squares denote the known variables and circles the unknown ones.

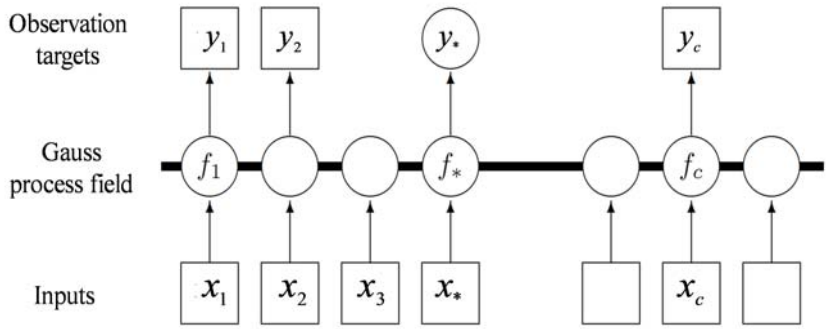

Fig. 1.1 Graphical description of Gaussian Process

1.3.1 Basic equations

A Gaussian process $f(x)$ is a collection of random variables, any finite set of which have a joint Gaussian distribution (Rasmussen and Williams 2006). Its statistical characteristics are completely specified by its mean function $m(x)$ and covariance function $k(x,x')$, i.e.

$$\begin{aligned} f(x) &\sim GP(m(x), k(x,x')) \\ m(x) &= \mathrm{E}[f(x)] \\ k(x,x') &= \mathrm{E}[(f(x)-m(x))-(f(x')-m(x'))] \end{aligned} \quad \text{.....(1.4)}$$

Given the observations $D=\left\{\boldsymbol{x}^{(i)}, y^{(i)} \mid i=1,2,\cdots,n\right\}$ and the predictive input x_* (also named test input), the goal of Gaussian process modeling is to obtain the output y_* for the distribution $P(y_* \mid D, x_*)$. Suppose the prior distribution of observation target y satisfies $y \sim N(0, k(x,x'))$ and the independent noise ε obeys $\varepsilon \sim N(0, \sigma_n^2)$, thus the covariance of noisy observations is obtained

$$\begin{aligned} &\mathrm{cov}(y_p, y_q) = k(x_p, x_q) + \sigma_n^2 \delta_{pq} \quad \text{or} \\ &\mathrm{cov}(y) = K(X,X) + \sigma_n^2 I \end{aligned} \quad \text{.....(1.5)}$$

Where $K(X,X)$ is a positive definite covariance matrix with size $n \times n$ and its elements denote the correlations of different observation samples. Consequently the joint distribution of the observed targets and the predictions can be signified as

$$\begin{bmatrix} y \\ f_* \end{bmatrix} \sim N\left(0, \begin{bmatrix} K(X,X)+\sigma_n^2 & K(X,X_*) \\ K(X_*,X) & K(X_*,X_*) \end{bmatrix}\right) \quad \text{.....(1.6)}$$

For notation simplicity, if $K=K(X,X), K_*=K(X,X_*)$, the regression equation of Gaussian process for noisy observed target is obtained

$$f_* \mid X, y, X_* \sim N(\bar{f}_*, \mathrm{cov}(f_*)) \quad \text{.....(1.7)}$$

$$\bar{f}_* = \mathrm{E}[f_* \mid X, y, X_*] = K_*^{\mathrm{T}}[K+\sigma_n^2 I]^{-1} y \quad \text{.....(1.8)}$$

$$\mathrm{cov}(f_*) = K(X_*,X_*) - K_*^{\mathrm{T}}[K+\sigma_n^2 I]^{-1} K_* \quad \text{.....(1.9)}$$

The regression output of Eq.(1.7) is not a single value but a probability distribution of predictions. This advantage can be used to obtain the prediction intervals that describe a degree of confidence of the predictions.

1.3.2 Covariance functions

Covariance functions specify the relationships between the input data and output elements. Note that although Eq.(1.7) gives the predictive distribution of the observed target, the lateral prior function $K(X,X)$ need to be specified in advance. Although there are many possible choices of prior covariance functions, an arbitrary function of input pairs (X, X_*) will not, in general, be a valid covariance function. The covariance function is the crucial element for Gaussian process regression, as it encodes pre-assumptions about the lateral function which we wish to learn and it defines the similarity between the inputs and test point with the predictive output. But from the modeling point of view, the goal is to specify prior covariance functions that contain our prior beliefs on the structure of the lateral function we are modeling. Formally, it aims to specify a function which will generate a positive definite covariance matrix for any set of input data and represent the relationships between input data and output predictions.

One covariance function used universally has the square exponential term

$$K_{\mathrm{se}}(\boldsymbol{x_p}, \boldsymbol{x_q}) = \sigma_f^2 \exp\left(-\frac{1}{2}(\boldsymbol{x_p}-\boldsymbol{x_q})^T M(\boldsymbol{x_p}-\boldsymbol{x_q})\right) + \sigma_n^2 \delta_{pq} q \quad \text{.....(1.10)}$$

Where σ_f^2, σ_n^2 and M denote the observed target variable, the noise variance and the length

scale, respectively. And $\theta=(\sigma_f^2,\sigma_n^2,\{M\})^T$ are the hyper-parameters to be adjusted by model training. The properties of the covariance function depend on the values of hyper-parameters. This covariance function expresses the idea that nearby inputs will have highly correlated outputs. One extreme case is $\boldsymbol{x_p}-\boldsymbol{x_q}=0$. The simplest non-stationary covariance function is the one corresponding to a linear trend so that $K\left(\boldsymbol{x_p},\boldsymbol{x_q}\right)\neq K\left(|\boldsymbol{x}_p-\boldsymbol{x}_q|\right)$, which is

$$K_{\mathrm{ns}}\left(\boldsymbol{x}_p,\boldsymbol{x}_q\right)=v_0+v_1\sum_{l=1}^{d}x_l^p x_l^q \quad \text{.....(1.11)}$$

It has been proved that the addition and multiplication of simple covariance functions are powerful in constructing various covariance functions (Belhouari and Bermak 2004). There are a variety of other covariance functions such as the Matérn class, the polynomial, the rational quadratic and the like (Rasmussen and Williams 2006).

For landslide observation modeling on non-stationary displacement series, the hyper-parameters of prior functions are denoted as $\theta=(\sigma_f^2,\sigma_n^2,\{M\},v_1,v_2,\cdots)^T$, which will be specified by model training.

1.3.3 Model training

Model training is aimed to obtain the values of hyper-parameters in Eq.(1.7), actually in the prior distributions, based on the observed data of landslide displacement series. Noting the predictive distribution of Gaussian process regression, the value of hyper-parameters can be achieved in a maximum likelihood framework by adjusting the hyper-parameters so as to maximize the log likelihood of hyper-parameters.

Starting with Bayesian theory, the marginal likelihood $p(y\mid X)$ is the integral of the likelihood times the prior distribution, referring to the marginalization over the lateral function f

$$p(y|X)=\int p(y|f,X)\,p(f\mid X)\,df \quad \text{.....} \qquad (1.12)$$

The prior of Gaussian process is Gaussian, $f\,|X\sim N(0,K)$

$$\log p(f|X)=-\frac{1}{2}f^T K^{-1}f-\frac{1}{2}\log|K|-\frac{n}{2}\log 2\pi \quad \text{.....} \qquad (1.13)$$

The likelihood is a factorized Gaussian, $y|f \sim N(f, \sigma_n^2 I)$. Let $K_y = K + \sigma_n^2 I$, the log marginal likelihood is obtained as follows since the factorization of Gaussians is also of Gaussian.

$$\log p(y|X) = -\frac{1}{2} y^T (K_y)^{-1} y - \frac{1}{2} \log |K_y| - \frac{n}{2} \log 2\pi \quad \text{.....(1.14)}$$

The hyper-parameters θ are implied potentially in the log marginal likelihood Eq.(1.14). Since

$$\frac{\partial}{\partial \theta} K_y^{-1} = -K_y^{-1} \frac{\partial K_y}{\partial \theta} K_y^{-1} \quad \text{and} \quad \frac{\partial}{\partial \theta} \log |K_y| = tr\left(K_y^{-1} \frac{\partial K_y}{\partial \theta} \right) \quad \text{.....(1.15)}$$

Then the partial derivatives of the log marginal likelihood with respect to each hyper parameter can be obtained

$$\begin{aligned} \frac{\partial}{\partial \theta_j} \log p(y|X) &= \frac{1}{2} y^T K_y^{-1} \frac{\partial K_y}{\partial \theta_j} K_y^{-1} y - \frac{1}{2} tr\left(K_y^{-1} \frac{\partial K_y}{\partial \theta_j} \right) \\ &= \frac{1}{2} tr\left(\left(K_y^{-1} y (K_y^{-1} y)^T - K_y^{-1} \right) \frac{\partial K}{\partial \theta_j} \right) \end{aligned} \quad \text{.....} \quad (1.16)$$

To adjust the values of hyper-parameters, the initial values are first given randomly in a regular scope within the hyper-parameters space, and then training is proceeded on the input data with an iteration method, such as the conjugate gradient (Steihaug 1983) or particle swarm optimization algorithm (Chau 2006), to search for the optimal values hyper-parameters.

1.3.4 Loss function

It can be perceived from the previous section that, given the observed data set and test point, Gaussian process regression implements model training and search the optimal hyper-parameters in the theoretical frame of maximum marginalization using the prior distributions, and then it computes the predictive distribution of the observed target with the optimized hyper-parameters by Eq.(1.7). However in practical application decisions must be made about how to act, say a point-like prediction which is optimal in some sense. To this end, a loss function $L(y_{true}, y_{guess})$ is in need to specify the loss incurred by guessing the true value y_{true} with y_{guess}. For instance, the loss function could be an absolute deviation or a relative deviation between the guess value and true value.

The predictive goal is to obtain the point prediction value y_{guess}. It is incapable to estimate directly

what the state with minimum decision loss is on condition that the true value y_{true} is previous unknown. Loosely speaking, the loss function can be defined by the expected loss and optimized by minimization of expected loss function (Rasmussen and Williams 2006), i.e.

$$\tilde{R}(y_{guess} \mid X_*) = \int L(y_*, y_{guess})\, p(y_* \mid X_*, D) dy_*$$
$$y_{optimal} \mid X_* = \arg\min \tilde{R}(y_{guess} \mid X_*) \quad \text{.....} \quad (1.17)$$

Those decision loss functions commonly used are absolute error loss function ($AEL = \mid y_{guess} - y_* \mid$) and square error loss function ($SEL = (y_{guess} - y_*)^2$), also with their variant versions. It has been proved in statistics that the estimation obtained by minimizing absolute loss AEL is the median of probability $p(y_* \mid X_*, D)$ and that obtained by minimizing the square error loss is the mean value of $p(y_* \mid X_*, D)$. And in this chapter, the variant versions of loss functions were also used for point predictions.

Attention should be paid that Gaussian process regression derives the predictive distribution without any reference to the loss function. It just depends on the prior and the marginalization over the functions with data input of observation target. It is the fundamental difference between the Bayesian based methods and non-Bayesian paradigms. In non-Bayesian methods, model training are typically implemented by minimizing the empirical loss, for example, the support vector machine. In contrast, there is a clear separation in Bayesian method between the loss function and likelihood. The likelihood function expresses the how the noisy measurements are assumed to deviate from the underlying noise free function. On the contrary, the loss function captures the consequences of making a specific choice of guessing value, given an actual true state. The likelihood and loss function need not have anything in common (Barber and Saad 1996).

1.4 Using Gaussian process to model landslide displacement series

Discussion on the analysis and prediction of the New Landslide of Wolong Temple were presented in this section to illustrate the attractiveness of Gaussian process in modeling non-stationary displacement series of landslides. Some extra data managing skills was also proved to be effective in promoting of predictive accuracy and tendency.

1.4.1 Observations of Wolong Temple landslide

The New Landslide in Wolong Temple occurred in a loess tableland. Tear cracks were noticed since the beginning of 1971 and it was monitored since the 11th March by pile driving into the earth.

The landslide occurred in the early morning on May 5th with severe destruction of sliding movement. The dataset listed in Table 1.1 is the observed displacements of the cracks labeled No.5, which has been recognized as the key monitoring point to indicate the stability status of the slope. As it can be drawn from the column of Dis. in Table 1.1, the displacements of the landslide developed slowly initially but increased dramatically by the end of the observed displacement series. The characteristics of the displacement series were studied by different methods in previous works. (Yuan et al. 2005) presented the Negative Selection Algorithm for identifying the mutation point of the displacement curve and found that the jump spot occurred at the 49th point of the displacement series. (Dong et al. 2007) presented a model using the Tokens theory for predicting the landslide displacement based on support vector machines (SVM) and they concluded that the RBF kernel function had the priority in promoting of generalization accuracy combined with SVM. Now our purpose is to model the observations using the Gaussian process and the dynamic cross validation technique to give predictive performance on predictions (generations).

Table 1.1 Observed displacements of the crack labeled No.5

Day/d	Disp./mm	Day/d	Disp./mm	Day/d	Disp./mm	Day/d	Disp./mm
15	1.0	28	8.2	41	12.0	54	23.0
16	1.5	29	8.4	42	13.0	55	24.0
17	1.7	30	8.7	43	13.4	56	25.2
18	2.5	31	9.0	44	14.0	57	26.0
19	3.2	32	9.2	45	15.0	58	27.0
20	4.0	33	9.4	46	16.1	59	28.2
21	4.4	34	10.0	47	16.4	60	30.0
22	5.1	35	10.1	48	17.2	61	31.0
23	5.9	36	10.3	49	17.6	62	32.0
24	6.3	37	10.4	50	18.2	63	33.0
25	7.0	38	10.5	51	19.0	64	42.0
26	7.3	39	10.8	52	19.2	65	47.0
27	7.8	40	11.1	53	20.0	66	61.0

1.4.2 Dynamic crossing validation

The dynamic crossing validation was implemented to promote the predictive performance of Gaussian process regression. The observed displacement series were divided into two independent data sets: the training set and the test set. The predictive performance was checked to represent the

generalization error for the derived regression model. The procedure of cross validation was implemented as follows:

(a) Supposing the observed data set be $S=(s_1,s_2,\cdots s_n)$, divide S into a series of subsets $S_{iTr}=(s_i,s_{i+1},\cdots s_{i+d})$, $i=1,2,\cdots,(n-d)$, with the same size d; then $(n-d)$ subsets would be generated;

(b) Let m be the size of test sets, thus the test sets could be denoted as $S_{iTe}=s_{i+d+1},s_{i+d+2},\cdots s_{i+d+m}$;

(c) Generate models on the dataset S using Gaussian process regression method and implement training process with training set to adjust and optimize the hyper-parameters; and then with the test input output the results of the test sets $S^{p}_{iTe}=s^{p}_{i+d+1},s^{p}_{i+d+2},\cdots,s^{p}_{i+d+m}$;

(d) Repeat the step (a) ~(c) for $(n-d)$ rounds, then the predictive output for the test sets would be $S_{predict}=(s^{p}_{d+1},s^{p}_{d+2}\cdots,s^{p}_{n})$.

Loosely the parameter d can be recognized as the length of training set, and m that of the test set. Generally speaking, for the effectiveness of the regression model, the value of d would be no less than 12 so as to keep the generated model eligible for catching patterns underlying the observed datasets. Meanwhile, m should not be too large for reduction of the generalization error.

1.4.3 Modeling preparations

Generally, two problems should be settled before the Gaussian process can give predictions: the prior covariance function and the corresponding hyper-parameters. The prior covariance can be specified manually based on empirical experiences or expert judgments which provide structural information of covariance functions. And the numerical values of hyper-parameters make the characteristics of the covariance differ broadly and will be optimized by model training with proper techniques.

Here another prior covariance function was also chosen: the Matérn class functions with isotropic distance measure, i.e.

$$K_{\mathrm{Mc}}(\boldsymbol{x_p},\boldsymbol{x_q})=\sigma_f^2 f(\sqrt{d}*r)*\exp(-\sqrt{d}*r) \quad \text{.....(1.18)}$$

Where $f(t)=1+t$, $r=\sqrt{(x^p-x^q)^T*P^{-1}(x^p-x^q)}$, P is l times the unit matrix and σ_f^2 is the signal variance, The corresponding hyper-parameters are l and σ_f^2 with initial value $l=1/4,\sigma_f^2=1$. The training and test process were implemented using the displacement series in Table 1 with

$d = 15, m = 1$.

In order to test the performance of modeling on the non-stationary displacement series using Gaussian process regression, dynamic crossing validation was applied to strengthen the ability of the model to give more precise predictions. Hyper-parameters are adjusted by the strategy of model training techniques introduced in the former section. The conjugate gradient method is applied for iteration computing and optimizing the values of hyper-parameters. To avoid local minimum during the training process, we would randomly initialize several selective values within the space of hyper-parameters during the implementation procedures. If the values of hyper-parameters are specified, we can obtain the predictions of test input by substituting values of hyper-parameters in Gaussian process regression Eq. (1.7).

The data for modeling often have a large size in length in practical application for analysis and prediction of long-term monitoring displacement series of landslides, which causes approximation problems for these large datasets in data processing. There are several choices of the approximation methods, for example, namely as the subset of regressors, the Nyström method, the subset of data points, the projected process approximation, the Bayesian committee machine and the iterative solution of linear systems (Rasmussen and Williams 2006). In this chapter we perform short-term point predictions and take the method of a Subset of Data Points which is indicated in the process of dynamic crossing validation.

1.5 Results and analysis

In this section, comparison and discussion are organized into three stages. The former is a comparison of Gaussian process introduced in this chapter with previous work; the second is result comparison of different covariance functions using Gaussian process; the third part is result discussion on different methods applied for predictive results based on the observation of the landslide.

1.5.1 Comparison with a previous work

The relative error loss (*REL*) is defined to evaluate the performances of different covariance functions $REL = \left| \frac{y_i - y_i^*}{y_i} \right| \times 100\%, (i = 1, 2, \ldots, n)$, y_i, y_i^* is the i^{th} observation and prediction.

Predictive results and the corresponding *RELs* are comparatively shown in Table 1.2 for the strategy of the present work in this chapter and the previous work in the literature (K.Liu et al. 2009). The distributive characteristics of the predictive *REL* are both shown in Fig.1.2 for the present and previous works. It can be seen that the previous method is moderate since the height of error histogram of the previous work are much larger than that of the present strategy using GPR with dynamic

crossing validation techniques for most predictive points, which was especially highlighted at the turning point of the observed curve of displacement. Also, it can be seen that the error histograms jumps swiftly at the turning point of the observed data curve for both methods which implies that it is detective for predictions on catastrophe points using continuous methods. Whereas the predictive errors present in Fig.1.2 shows that the prediction strategy proposed in this research can grasp and track the displacement fluctuations and turnings in a very short time.

Besides the relative error loss for each point prediction, two other overall loss functions are also promoted to evaluate quantitatively the overall performance of the regression strategy present above. The average relative error loss (AREL) and the average square error loss (ASEL) are defined as $AREL = \frac{1}{n}\sum_{i=1}^{n}\left|\frac{y_i^* - y_i}{y_i}\right| \times 100\%$, $ASEL = \frac{1}{n}\sum_{i=1}^{n}(y_i^* - y_i)^2$ to give comparisons with previous work.

Table 1.2 Comparisons of predictions and the errors of the present and previous work

Time /d	a /mm	predictions/mm		relative error loss%		Time /d	a /mm	predictions/mm		average error loss %	
		b	c	b	c			b	c	previous	present
30	8.7	8.65	8.69	0.57	0.17	49	17.6	17.72	18.02	0.68	2.40
31	9.0	8.78	8.93	2.44	0.78	50	18.2	17.89	17.73	1.70	2.58
32	9.2	8.85	9.24	3.80	0.48	51	19.0	18.31	18.64	3.63	1.90
33	9.4	9.26	9.43	1.49	0.29	52	19.2	18.33	19.50	4.53	1.58
34	10.0	9.31	9.59	6.90	4.07	53	20.0	18.13	19.72	9.35	1.38
35	10.1	9.32	10.27	7.72	1.70	54	23.0	20.26	20.43	11.91	11.15
36	10.3	10.22	10.40	0.78	0.97	55	24.0	20.62	24.09	14.08	0.38
37	10.4	10.51	10.52	1.06	1.17	56	25.2	20.93	25.46	16.94	1.04
38	10.5	10.77	10.55	2.57	0.49	57	26.0	28.92	26.42	11.23	1.63
39	10.8	10.66	10.59	1.30	1.94	58	27.0	29.65	26.84	9.81	0.59
40	11.1	10.73	10.90	3.33	1.79	59	28.2	28.92	27.68	2.55	1.84
41	12.0	10.78	11.25	10.17	6.23	60	30.0	29.82	28.94	0.60	3.54
42	13.0	12.76	12.55	1.85	3.49	61	31.0	31.28	30.99	0.90	0.02
43	13.4	13.61	13.90	1.57	3.77	62	32.0	32.80	32.11	2.50	0.35
44	14.0	14.27	13.88	1.93	0.88	63	33.0	33.80	32.94	2.42	0.17
45	15.0	15.57	14.44	3.80	3.71	64	42.0	35.26	33.82	16.05	19.48
46	16.1	16.74	15.67	3.98	2.70	65	47.0	36.76	41.70	21.79	11.28
47	16.4	17.95	17.07	9.45	4.07	66	61.0	61.15	51.85	0.25	15.00
48	17.2	17.28	16.40	0.47	4.66						

Hint: the column *a* represents the original observing data; column *b* represents previous results; column *c* represents the present results of this chapter.

The *AREL* and *ASEL* of the previous and present strategies are shown in Table 1.3. As it can be drawn from Table 1.3, the *AREL* of the present strategy is 3.23%, about 60.9% of that of previous work; the *ASEL* of the present strategy is 4.68, about 80.1% of that of previous method. Thus the

performance of predictions using the present method in this chapter has been greatly promoted in contrast to that of previous work.

The reason for moderate performance of the previous work in the literature lies that Gaussian process is a member of Bayesian learning methods but it is confused in the literature. In Bayesian theory, model learning is implemented to compute and adjust the hyper-parameters in the frame of marginalization over the likelihood function. It is different in nature with those learning methods in the frame of minimizing empirical loss. The former is implemented with probabilistic characteristics. And prior knowledge about the studied system is embedded with a certain form, for example the covariance functions. These are the key points of Gaussian process. As for the literature (K.Liu et al. 2009), it described that Genetic Algorithm was used to optimize the hyper-parameters. But prudential readers would notice that it applied Genetic Algorithm to adjust the hyper-parameters using a fitness function (essentially a loss function) after the training and prediction for each processing step and carry out computations using a iteration method till the termination conditions, for instance 100 processing steps, were satisfied. It did not implement model learning process in the frame of marginal likelihood but in the form of loss function. Thus it could not generate the satisfactory results as the strategy introduced in this research. Actually, those biological algorithms could be applied to optimize the hyper-parameters instead of the usually used conjugate gradient method for iteration computations but they cannot be mixed with loss functions.

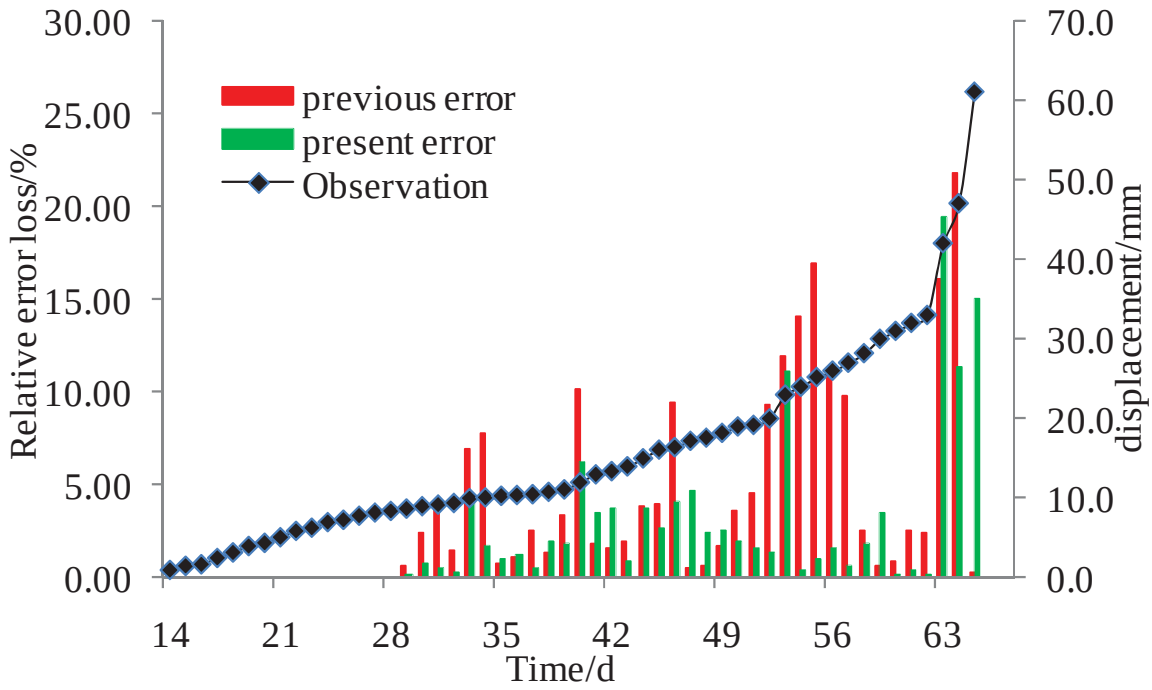

Fig.1.2 Comparisons of relative error loss for each prediction

Table 1.3 Comparisons of predictive loss functions

Method	AREL/%	ASEL
Previous	5.30	5.84
Present	3.23	4.68

1.5.2 Comparisons of different covariance functions

Several terms of covariance functions introduced above, K_{se}, K_{Mc}, K_{ns} and the composites, are adopted in this chapter in order to investigate the influences of different prior covariance functions to the strategy of Gaussian process. The corresponding predictive results are listed in Table 1.4. The *RELs* for each point prediction is also shown in Table 1.4.

Table 1.4 Predictive performances of Gaussian process with different covariance functions

Day/d	Observation	predictions of different covariance functions /mm					relative error loss of different covariance functions /%				
		K_{se}	K_{Mc}	$K_{se}+K_{ns}$	$K_{ns}+K_{Mc}$	$K_{se}+K_{Mc}$	K_{se}	K_{Mc}	$K_{se}+K_{ns}$	$K_{ns}+K_{Mc}$	$K_{se}+K_{Mc}$
30	8.70	8.56	8.65	9.50	8.73	8.68	0.14	0.05	0.80	0.03	0.02
31	9.00	8.80	8.88	9.85	8.95	8.89	0.20	0.12	0.85	0.05	0.11
32	9.20	9.11	9.17	9.15	9.20	9.17	0.09	0.03	0.05	0.00	0.03
33	9.40	9.28	9.36	9.36	9.41	9.36	0.12	0.04	0.04	0.01	0.04
34	10.00	9.44	9.55	9.61	9.60	9.55	0.56	0.45	0.39	0.40	0.45
35	10.10	10.29	10.21	10.32	10.28	10.21	0.19	0.11	0.22	0.18	0.11
36	10.30	10.47	10.42	10.54	10.48	10.42	0.17	0.12	0.24	0.18	0.12
37	10.40	10.62	10.56	10.68	10.61	10.56	0.22	0.16	0.28	0.21	0.16
38	10.50	10.56	10.58	10.58	10.61	10.58	0.06	0.08	0.08	0.11	0.08
39	10.80	10.66	10.54	10.66	10.67	10.54	0.14	0.26	0.14	0.13	0.26
40	11.10	10.89	10.89	11.12	11.12	10.94	0.21	0.21	0.02	0.02	0.16
41	12.00	11.14	11.16	11.46	11.44	11.22	0.86	0.84	0.54	0.56	0.78
42	13.00	11.77	11.79	12.29	12.26	12.52	1.23	1.21	0.71	0.74	0.48
43	13.40	12.59	14.10	13.93	13.81	14.03	0.81	0.70	0.53	0.41	0.63
44	14.00	13.57	13.98	13.47	13.54	13.80	0.43	0.02	0.53	0.46	0.20
45	15.00	13.99	14.33	14.22	14.30	14.25	1.01	0.67	0.78	0.70	0.75
46	16.10	15.69	15.56	15.31	15.49	15.83	0.41	0.54	0.79	0.61	0.27
47	16.40	16.84	16.88	16.68	16.92	17.02	0.44	0.48	0.28	0.52	0.62
48	17.20	16.95	17.11	17.00	16.21	16.52	0.25	0.09	0.20	0.99	0.68
49	17.60	17.78	17.79	17.72	17.76	18.04	0.18	0.19	0.12	0.16	0.44
50	18.20	17.99	18.07	18.05	18.08	18.00	0.21	0.13	0.15	0.12	0.20
51	19.00	18.39	18.55	18.52	18.60	18.64	0.61	0.45	0.48	0.40	0.36
52	19.20	19.17	19.35	19.27	19.41	19.49	0.03	0.15	0.07	0.21	0.29
53	20.00	19.57	19.66	19.61	19.72	19.56	0.43	0.34	0.39	0.28	0.44
54	23.00	20.41	20.37	20.34	20.41	20.40	2.59	2.63	2.66	2.59	2.60
55	24.00	22.12	22.20	22.21	22.19	24.33	1.88	1.80	1.79	1.81	0.33

56	25.20	23.84	25.76	23.90	25.65	23.83	1.36	0.56	1.30	0.45	1.37
57	26.00	25.81	26.76	25.86	26.35	26.55	0.19	0.76	0.14	0.35	0.55
58	27.00	27.25	26.87	27.28	26.58	26.91	0.25	0.13	0.28	0.42	0.09
59	28.20	28.51	27.48	28.50	27.48	28.21	0.31	0.72	0.30	0.72	0.01
60	30.00	29.61	28.73	28.41	28.74	29.30	0.39	1.27	1.59	1.26	0.70
61	31.00	30.94	30.75	30.74	30.71	31.21	0.06	0.25	0.26	0.29	0.21
62	32.00	32.07	31.99	31.91	31.98	31.97	0.07	0.01	0.09	0.02	0.03
63	33.00	32.95	32.98	32.85	33.00	33.09	0.05	0.02	0.15	0.00	0.09
64	42.00	34.13	34.02	33.91	34.00	34.06	7.87	7.98	8.09	8.00	7.94
65	47.00	38.87	39.28	39.03	39.26	42.51	8.13	7.72	7.97	7.74	4.49
66	61.00	53.60	53.07	52.89	51.78	48.22	7.40	7.93	8.11	9.22	12.78

Several conclusions can be obtained from the predictive performances shown in Table 1.4. Predicted results of Gaussian process with different covariance functions all have good accuracy, with *RELs* than 3%, for point predictions at the non-fluctuation positions on the displacement curve. But predictive performances at the fluctuation positions are moderate, mostly less than 10%, though not very good. Results do not differ very much from each other obtained by single covariance (K_{se} or K_{mc}) and the composite covariance functions. Also, K_{se} and K_{mc} perform similarly in the modeling prediction problem of Wolong Temple landslide displacement. And the compositions of K_{se} or K_{mc} with K_{ns} do not give good promotion of *RELs* in our predictive modeling problem, while the composition of K_{se} and K_{mc} has slightly promoted the overall predictive performances. The reason may lie that K_{ns} is not suitable for accounting the characteristics of the displacement series of Wolong Temple and the existence of K_{ns} descends the predictive performance. Thus it can be summarized here that compositions of different covariance function do not necessarily give promotions in predictive performances for a specified modeling problem. And covariance functions should be accorded with the characteristics of the modeling system so as to give satisfactory predictive results.

1.5.3 Comparison with other methods

It was discussed the comparative results of different Gaussian process strategies in the previous section. Compassions with other methods such as the support vector machine (SVM) and the artificial neural networks (ANNs) will be discussed hereby. It first introduces the variant terms of covariance functions in the kernel form to show the consistency of Gaussian process with other learning methods. Then it compares the predictive results obtained by different predictive strategies for the last seven point predictions of the landslide displacement series.

It can be noticed that the coefficient $K_*^{\mathrm{T}}[K+\sigma_n^2 I]^{-1}$ in the mean Eq.(1.8) does not depend on the observed target y, but only on the input X , hence predictive mean $\overline{f}_*$ is linear combination of observed target y; this is the property of Gaussian process. The variance in Eq.(1.9) is the difference between $K(X_*, X_*)$, simply the prior covariance, and a positive term representing the information the observations give us about the function. From another point of view, the mean $\overline{f}_*$ in Eq.(1.8) is the linear combination of n kernel functions each of which is centered on a training point i.e. $\overline{f}(\mathrm{x}_*)=\sum_{i=1}^{n}\alpha_i k(x_i, x_*)$ where $\alpha=(K+\sigma_n^2 I)^{-1}y$.

Therefore it can be concluded that Gaussian process is consistent with other kernel learning methods. In fact it has been proved that most kernel learning methods could be accorded with Gaussian process with specific restrictions (Rasmussen and Williams 2006). Thus, comparisons of Gaussian process with ANNs and SVM are to be discussed hereafter on the predictive performance for modeling the landslide displacement. Only the last seven point predictions are discussed for comparison since it has been shown that Gaussian process could obtain quite satisfactory results of the other predictions as given in Table 1.2 and Table 1.4.

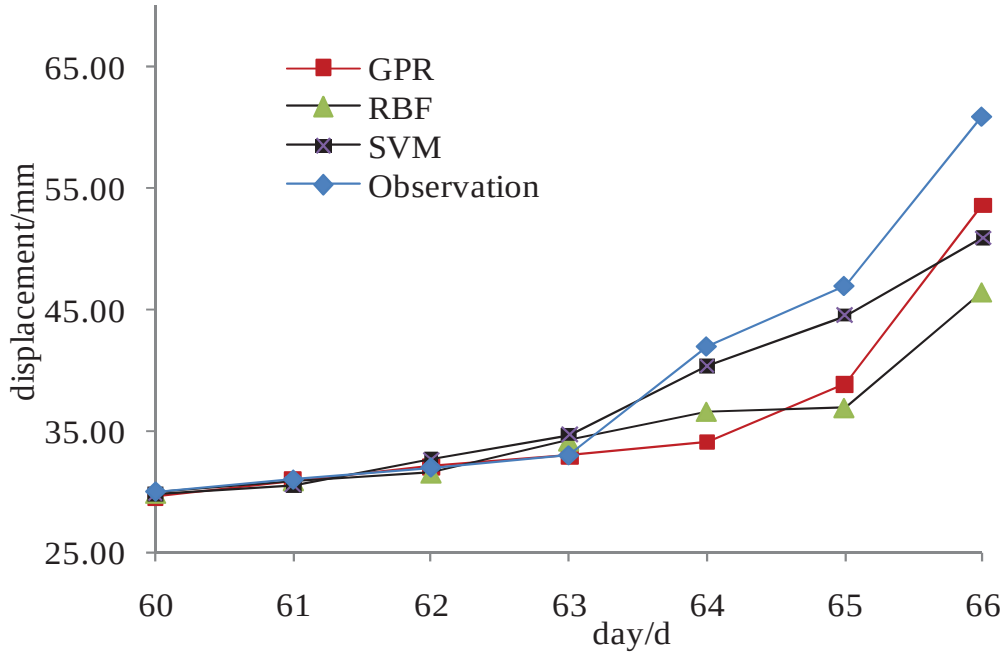

Fig. 1.3 Predictive performances of different strategies

The predicted results obtained by RBF network and SVM (Dong et al. 2007) are comparatively

given in Fig. 1.3 with that of Gaussian process. It can be seen that the three strategies (GPR, RBF network and SVM) all give very good point predictions for days from 60 to 62 but divergent results for days from 63 to 66 till the landslide occurrence. The observations start jumping for the day 63, which leads to moderate performances for all the three strategies. Fortunately, the results of Gaussian process regression show that the predictive results it generates have the same trends with that of the observation even though it cannot perform very well for point values, while the results given by RBF and SVM are inferior for trend keeping though they give better point predictions for some days. The ultimate goal of modeling slope displacements is for forecasting of landslide occurrence. And the trend prediction is an essential element for both long-term and short-term forecasting of landslides, as well as imminent warning. It can be concluded in this end that GPR performs better than RBF and SVM on the predictive modeling of the landslide displacement.

1.6 Further discussion

Predictive modeling on landslide displacement is an effective phenomenal way of revealing future features of landslides. It can provide reference for landslide occurrences in advance with proper warning criteria. It has been shown above that the performance of the a present in this research in contrast to the previous works, and now concentration could be made on the lateral information the GPR predictions expressed for warning criteria of landslides. It shows the observed displacement process and the corresponding predictions by GPR of the landslide in Fig. 1.4. As it can be drawn from Fig. 1.4, the displacement of this landslide had stepped over four stages, divided by three apparent inflections, before the sliding movement occurred. The linear trends of the displacement curve at each inflection point are drawn with continuous solid lines and the boundary lines of each stage are marked with dash lines for understanding better the involution stages. It must be recognized that the linear trend at each inflection point is derived approximately from a line that can pass through as many data points as possible. Also, one can find that the intersection angle at each inflection point is different from each other and enlarged as the landslide displacement develops with time. The values of the intersection angles were no less than 10°, and the intersection angle at the last inflection (labeled as 3) is more than 45°, after which the landslide occurred. Thus, this characteristic can be considered as a criterion for forecasting of such kind of landslide.

There are mainly two important indexes to evaluate a model's ability on landslide time forecasting from the observed displacement series: the trends of underlying displacement and the retardation time of forecasting, given the threshold value for landslide occurrence. Drawing back to the attractive performance of the GPR strategies, it can be noted that the prediction strategy of the paper could adapt well with the displacement curves even at the inflection points. Fatherly, the trends close to sliding

time were nearly the same with that of the observation since the trend line for both the observation and GPR curves are somewhat parallel to each other. On the other hand, once the observed displacement jumped to a new range, the GPR model can adapt it swiftly in the next prediction. To this point, if the intersection angle of the predicted curve is to $45°$, it would be a signal for forecasting of landslide occurrence when modeling the observed displacement series. Thus it can be regarded as a threshold value of criterion for the landslide forecasting. Whereas one could also recognize that despite of its attractive ability on tendency tracking, the displacement predictions of GPR with dynamic crossing validation is somewhat hysteretic to the observations at sudden turnings of the curves. Also, the landslide forecasting criterion here will be responsible only for slopes with typical creep-typed displacement curves like Wolong Temple New Landslide.

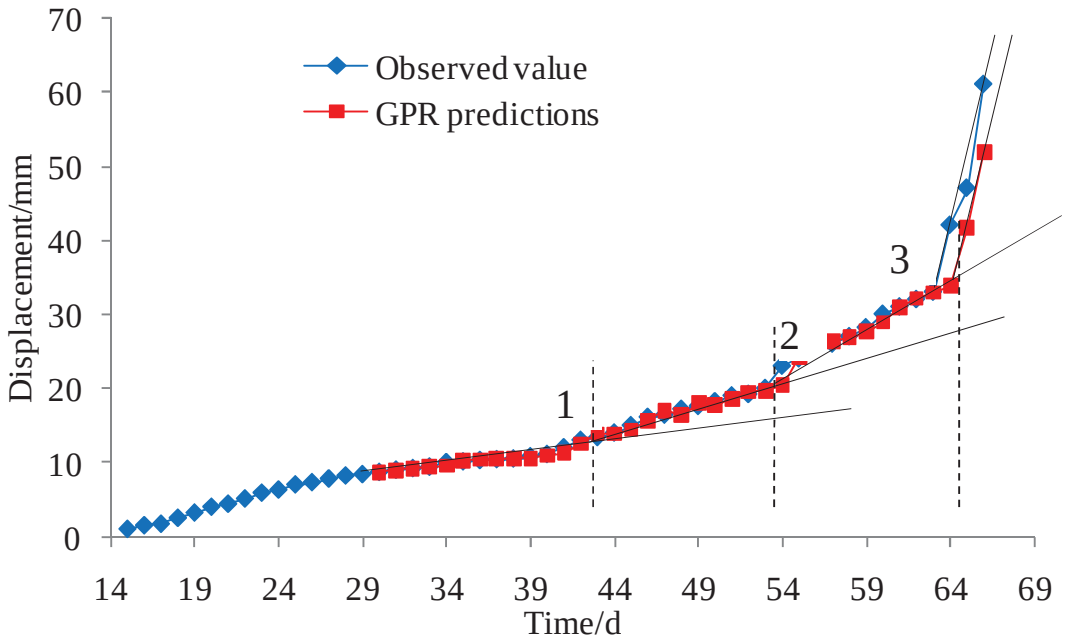

Fig. 1.4 Actual displacements and the GPR predictions

Actually, some criteria have been proposed for landslides forecasting, but the corresponding threshold values for each criterion are difficult to identify. A portion of the criteria is the displacement rate, the rainfall thresholds, the safety factors and the like. With the increasing sophistication of the site-investigation of slopes, the criteria with good reliability, feasibility and efficacy will utilize intensively the information from monitoring systems. The landslide discussed in this article is the creep-typed slope and the displacement curve changes slowly. Also, there exist landslides with stepped or shock-type displacement curves. The stepped displacement curves often exist in slopes formed by deposits. And the threshold values for forecasting criterion are to be discussed fatherly. As it should to be, using a reliable and precise prediction model for slope displacement prediction like Gaussian

process in this research, landslide forecasting can be implemented loosely with proper threshold values of displacement criterion.

1.7 Conclusions

The Gaussian process utilizes the monitored data for model training. It can cover expert prior knowledge in the priority functions, which has progressed its application in the fields that empirical experience is important. Its hyper-parameters are optimized by model training to minimize the likelihood but empirical risk functions. These are why it can outperform than other techniques only dealing with data series. Based on the results of this chapter, conclusions can be drawn as follows:

(1) Gaussian process is a good technique for modeling of landslide displacement series. It has the superior ability of point predictions for landslide displacement modeling with proper prior covariance functions. Also, it can provide satisfactory results for tendency tracking of the displacement series. Thus it can be regarded as a good strategy for tendency predictions of phenomenal data of complex systems.

(2) The covariance functions and the relevant hyper-parameters are the main causes for moderate or good performances of the Gaussian process strategy with dynamic crossing validation in this chapter. Model training of Gaussian process is executed by means of minimizing the likelihood of hyper-parameters. The predictive *AREL* and *ASEL* of the strategy in this chapter is about 60.9% and 80.1% of that in previous work. Thus training target function cannot be confused with loss functions. Also, comparison works show that the strategy introduced in this chapter is superior to the RBF network and the SVM since only it can track well the tendency of the displacement curve of Wolong Temple Slide event at the sudden inflection. And this ability is very important for a model to predict landslide occurrence.

(3) It would be a signal for forecasting of landslide occurrence if the intersection angle is to $45°$ at the turnings on the predicted curve when modeling the observed displacement of the creep-typed slope. The landslide is a complex system involving many disciplines. Displacement modeling is a phenomenal analytical method for landslide study; further studies need be continued on landslide predictions by the composition of displacement study and evolutionary mechanism analysis.

Nevertheless, the criterion proposed in this study should be fatherly validated by more landslide cases for its generalization ability. Meanwhile, studies should be also carried out on the topic of warning criteria for slopes of different kinds of displacement characteristics like the mutant type and stepped type.

Chapter 2 Case-based slope stability evaluation with adaptive relevant vector machines

2.1 Introduction

A slope can be recognized as a special structural body composed of geo-materials. Its stability is a big challenge to the safety of the ground as well as people associated with its affecting region. The study of slope stability has contributed a lot to describe the stability of slopes. In conventional methods, the safety factor (F_s) is widely used to describe the stability condition of slopes. If $F_s > 1$, a slope is thought stable; if $F_s < 1$, a slope is thought unstable; if $F_s = 1$, a slop is thought in its critical status of stability. In this context, many methods have been developed to calculate the value of F_s including the analytical method, the numerical method. This rule is valid for most slope cases. However, in some cases the above rule does not work correctly for the calculated F_s value since that all the methods used to calculate F_s have some assumptions which may not be the actual situation. And the F_s value calculated by different methods would be probably varying for the same slope. In this way, a slope with calculated $F_s > 1$ may be unstable in practice. In fact, many slope cases have been reported to be unstable with $F_s > 1$ (Sah et al. 1994; Sakellariou and Ferentinou 2005; Wang et al. 2005). Therefore, determination of slope stability concerning F_s value is not valid in some cases. Consequently, some other methods are in need to be developed to approach this problem.

Fortunately, besides the above methods, other newly developed methods have been being studied to give out the stability of slopes from another point of view. The purpose of these methods is directly to predict the stability status of a slope but by judgment of the F_s value. These methods have been developed based on widely collected slope case data with various parameters related to slope stability. Some unknown potential modes are thought lying in the case data for the slopes of different stability status. Generally, the stable slopes have their unknown modes of slope parameter values which are thought to be different from that of the failed slopes. In this way, the stability of slopes can be identified by means of distinguishing the different modes. In many cases, the purpose of study on slopes is to judge whether a slope is stable according to the parameter values but to find out the lying unknown modes which may be too difficult to be described explicitly. Many inference methods and artificial intelligence techniques can learn the modes from the collected slope cases and then can generate predictions if new group of parameter values are given. In the past decade, some techniques have been applied to undertake this problem.

These methods are related to the grey inference, the fuzzy inference, neural network, and the support vector machines (SVM). A tool based on ANN and grey system was developed for analyzing and predicting future ground movement based on geotechnical properties and historical behavior of the collected data (Lu and Rosenbaum 2003). They concluded that the combination of ANN and grey Systems methods offers potential to improve prediction of the likely state of stability for a slope. The intelligent forecast procedure was presented for slope stability with evolutionary artificial neural network (Li and Liu 2004). It demonstrated that the forecast of slope stability using artificial neural network was feasible and a well-trained artificial neural network revealed an extremely fast convergence, a better generalization and a high degree of accuracy in the intelligent forecast for the slope stability. The authors delivered their work on slope stability evaluation using back propagation neural networks (Wang et al. 2005). In their study, a slope case in hydra-electric stations was studied with the proposed method based on the collected data. A study on slope stability prediction was introduced using neural networks (Sakellariou and Ferentinou 2005). They applied the network with back-propagation learning algorithm to estimate the factor of safety (Fs) as a function approximation problem, and the stability status as a function approximation problem or a classification problem. They concluded that their results were superior to those obtained by means of standard analytical methods. The prediction and estimation of slope stability was illustrated according to the status of stability and failure mechanism for dry and wet slopes by using the back-propagation algorithm, the theory of Bayesian neural networks and the Kohonen self-organizing maps (Ferentinou and Sakellariou 2007). They also estimated the slope stability controlling variables by combining computational intelligence tools with generic interaction matrix theory. An ANN system consisting of multilayer perceptron networks was developed to predict slope stability in a specified location, based on the available site investigation data from Noabad in Mazandaran of Iran (Choobbasti et al. 2009). Some other applications of the neural networks have been also presented for slope stability analysis (Kaunda et al. 2010; Das et al. 2011). The above methods used the ANN as the modeling tool to approach the evaluation of slope stability.

On the application of the SVM method in slope stability analysis, a study was presented in (Yao et al. 2008) on landslide susceptibility mapping using the technique of SVM for a case of natural slope in Hong Kong, China. The results gave out that two-class SVM possessed better prediction efficiency than logistic regression and one-class SVM. A study was conducted on the support vector machine based reliability analysis method for slope reliability analysis (Zhao 2008). It showed that the proposed approach was applicable to slope reliability analysis which involved implicit performance functions. A study was delivered on slope stability analysis with the support vector machine approach (Samui 2008). In this study, the SVM predicted the factor of safety as a regression

problem and the stability status as a classification problem. The results showed that the SVM model gave better results than that of the previously published ANN model for the prediction of safety factor and SVM gave an accuracy of 85.71% in the case of stability status. A least square support vector machine (LSSVM) was utilized for slope stability analysis (Samui and Kotharib 2011). The study showed that the developed LSSVM was a robust model for slope stability analysis. These studies approached the problem of slope stability with the SVM based techniques.

Recently, on the application of fuzzy theory in slope stability analysis, the fuzzy slope mass rating (FSMR) system was applied for assessment of rock slope stability based on the rock mass rating system (Daftaribeshelia et al. 2011). Their results showed that the method was capable of giving out sensible results. A stability assessment model was executed for epimetamorphic rock slopes using the adaptive neuro-fuzzy inference system based on the collected case data (Chen et al. 2011). The results proved that the model they proposed was applicable for slope stability assessment. The evolutionary risk preference inference model was proposed using fuzzy support vector machine for road slope collapse prediction (Chenga et al. 2012). Their results showed that the decision maker risk preference ratio was significantly lower than the error tolerance of ±10%. A comparative study was delivered on the predictive ability of the decision tree, support vector machine and adaptive neuron-fuzzy models in landslide susceptibility mapping (Pradhan 2012). Their results showed that adaptive neuron-fuzzy models had better prediction capability among all models in the specific problem. A research was presented on the prediction of slope stability using fuzzy logic, adaptive neuro fuzzy inference system (ANFIS), and statistical method, multiple linear regression (MLR) (Mohamed et al. 2012). Their result showed that ANFIS could predict the safety factors with high accuracy compare with MLR. Also, many applications of the soft computing techniques have been presented for approaching the problems in earth science and geotechnical engineering (Ahangar-Asr et al. 2010; Liu et al. 2012; Mohamadnejad et al. 2012; Li et al. 2013; Liu et al. 2013).

Despite of those achievements, the above methods still have certain limitations. The accuracy of the grey inference method depends intensively on the number of data samples and it is difficult to find out the optimized sample number. It is very difficult sometimes to define the structures as well as the interpretations of the neural networks. And often the neural networks are easy to suffer from the local minimum problems. As for the SVMs, they make unnecessarily liberal use of basis functions since the number of support vectors required typically grow linearly with the size of training set. It is difficult to estimate the penalty parameter and the kernel of SVMs must satisfy the Mercer's condition. And the results of SVMs are not probabilistic (Tipping 2001). Therefore, some reasonable methods are still in need to be developed for slope stability analysis.

The present work is devoted to slope stability analysis and prediction by utilization of relevant

vector machine (RVM) (Tipping 2001). The RVM is proposed by Tipping on Bayesian framework using kernel methods (Tipping 2000). The RVM typically utilizes dramatically fewer kernel functions than an equivalent SVM while it is capable of generalizing comparable performance (Tipping 2004). This study aims to demonstrate the following points: (1) to exploit the ability of the RVM models for evaluation of slope stability based on case data; (2) to discover the effect of the width parameter, the kernel type and the sample size on the predictive accuracy and build the adaptive relevant vector machine (ARVM) approach; (3) to give a comparative study on the predictive performance of ARVM and other methods on slope stability evaluation.

2.2 Slope stability evaluation mechanism

There are many types of slope failure such as the circular slip failure(SCF), the wedge slip failure(WSF) and the toppling failure etc. Different slope failure type is controlled by different associated factors. In this chapter, only the common CSF is discussed. The sketch of CSF is shown in Fig. 2.1. The stability of the type of CSF can be written as $F = f(\gamma, c, \varphi, \beta, H, R_u)$, where γ, c, φ is the bulk density, the cohesion, the internal friction angle of the slope material, respectively; β, H is the inclination and slope height, respectively; R_u is the pore pressure coefficient which is defined as the ratio of the pore-water pressure to the overburden pressure, i.e. $R_u = \frac{u_w}{\sum \gamma_i h_i}$.

It should be noted that our target is to model directly the stability status of slope regardless of the factor of safety since the latter functions not very well in some cases mentioned previously due to the variability of computing method and assumptions. Based on the formulated parameters in F, Some slope cases of CSF have been collected (Sakellariou and Ferentinou 2005; Wang et al. 2005; Chen et al. 2011). These cases are given in Table 1.2. In the column “stability” of Table 1, “0” labels the Failed slope; “1” labels the Stable slope.

The slope stability condition with respect to each parameter value in the circular slip mechanism is shown in Table 2.2. It is apparent as shown in Fig. 2.2 that none of the parameter can distinguish the stability of the slope cases. The ARVM is applied to learn the disciplines lying among those data and give evaluations on the slope stability. Consequently, all the parameters are considered in the ARVM approach to learn the disciplines lying in the data and give predictions on slope stability. The program of this method is developed in Matlab2012a. It should be noted that the output of Eq.(2.8) is an estimate of slope stability in the form of conditional probability. The output comprises two probabilistic values corresponding to the two kinds of slope status (Stable or Failed). A probabilistic output is thought to be true if the element labeling “Stable” is bigger than 0.50 for the true “Stable” slope or if the element labeling “Failed” is bigger than 0.50 for the true “Failed” slope in the program.

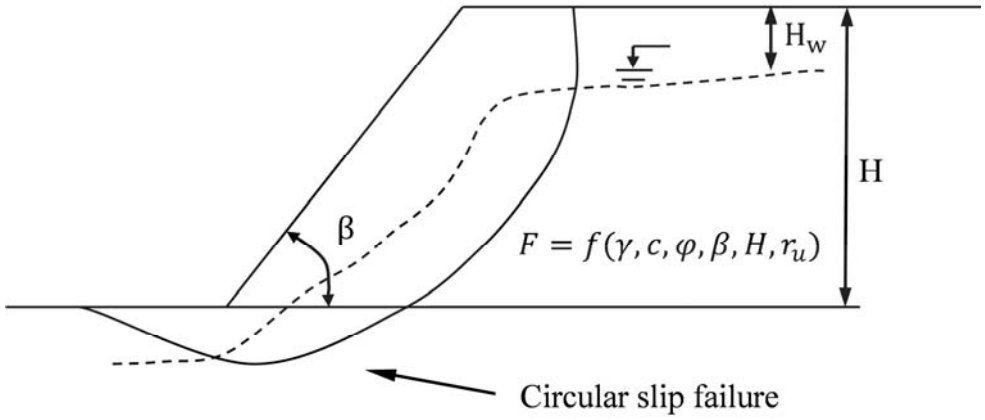

Fig. 2.1 The sketch of circular slip failure of a slope

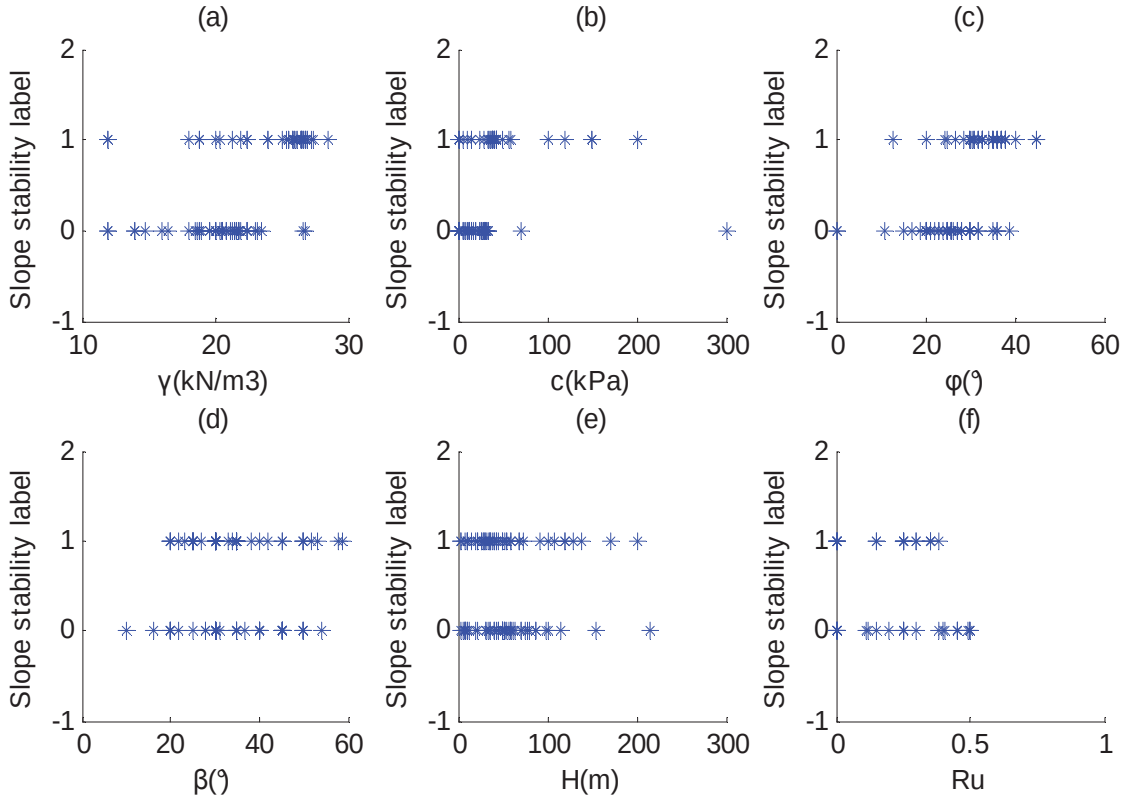

Fig. 2.2 Slope stability label with respect to each parameter value

Table 2.1 Slope cases of circular slip failure

Case No.	γ (kN/m3)	c(kPa)	φ	β	H(m)	Ru	Stability	Moisture	Location
1	18.68	26.34	15	35	8.23	0	0	Dry	Congress street, open cut slope, Chicago, USA
2	16.5	11.49	0	30	3.66	0	0	Dry	Bright ling sea slide UK
3	18.84	14.36	25	20	30.5	0	1	Dry	Unknown
4	18.84	57.46	20	20	30.5	0	1	Dry	Unknown
5	28.44	29.42	35	35	100	0	1	Dry	Case 1: open pit iron ore mine, India
6	28.44	39.23	38	35	100	0	1	Dry	Case 2: open pit iron ore mine, India
7	20.6	16.28	26.5	30	40	0	0	Dry	Open pit chromite mine, Orissa, India

Case No.	γ (kN/m3)	c(kPa)	φ	β	H(m)	Ru	Stability	Moisture	Location
8	14.8	0	17	20	50	0	0	Dry	Sarukuygi landslide,Japan
9	14	11.97	26	30	88	0	0	Dry	Case 1:open pit iron ore mine,Goa,India
10	25	120	45	53	120	0	1	Dry	Mercoirol open pit coal mine, France
11	26	150.05	45	50	200	0	1	Dry	Marquesade open pit iron ore mine, Spain
12	18.5	25	0	30	6	0	0	Dry	Unknown
13	18.5	12	0	30	6	0	0	Dry	Unknown
14	22.4	10	35	30	10	0	1	Dry	Case 1: Highvale coal mine, Alberta, Canada
15	21.4	10	30.34	30	20	0	1	Dry	Case 2: Highvale coal mine, Alberta, Canada
16	22	20	36	45	50	0	0	Dry	Case 1: open pit coal mine, Newcastle,coalfield, Australia
17	22	0	36	45	50	0	0	Dry	Case 2: open pit coal mine, Newcastle,coalfield, Australia
18	12	0	30	35	4	0	1	Dry	Unknown
19	12	0	30	45	8	0	0	Dry	Unknown
20	12	0	30	35	4	0	1	Dry	Unknown
21	12	0	30	45	8	0	0	Dry	Unknown
22	23.47	0	32	37	214	0	0	Dry	Pima open pit mine, Arizona, USA
23	16	70	20	40	115	0	0	Dry	Case 1: Wyoming, USA
24	20.41	24.9	13	22	10.67	0.35	1	Wet	Seven Sisters Landslide, UK
25	19.63	11.97	20	22	12.19	0.405	0	Wet	Case 1: The Northolt slide, UK
26	21.82	8.62	32	28	12.8	0.49	0	Wet	Selset Landslide, Yorkshire, UK
27	20.41	33.52	11	16	45.72	0.2	0	Wet	Saskatchewan dam, Canada
28	18.84	15.32	30	25	10.67	0.38	1	Wet	Case 2: The Northolt slide, UK
29	18.84	0	20	20	7.62	0.45	0	Wet	Sudbury slide, UK
30	21.43	0	20	20	61	0.5	0	Wet	Folkstone Warren slide, Kent, UK
31	19.06	11.71	28	35	21	0.11	0	Wet	River bank side, Alberta, Canada
32	18.84	14.36	25	20	30.5	0.45	0	Wet	Unknown
33	21.51	6.94	30	31	76.81	0.38	0	Wet	Unknown
34	14	11.97	26	30	88	0.45	0	Wet	Case 2: open pit iron ore mine, Goa, India
35	18	24	30.15	45	20	0.12	0	Wet	Athens slope, Greece
36	23	0	20	20	100	0.3	0	Wet	Open pit coal mine Allori coal?eld, Italy
37	22.4	100	45	45	15	0.25	1	Wet	Case 1: open pit coal mine, Alberta, Canada
38	22.4	10	35	45	10	0.4	0	Wet	Case 2: open pit coal mine, Alberta, Canada
39	20	20	36	45	50	0.25	0	Wet	Case 3: open pit coal mine, Newcastle coalfield, Australia
40	20	20	36	45	50	0.5	0	Wet	Case 4: open pit coal mine, Newcastle coalfield, Australia
41	20	0	36	45	50	0.25	0	Wet	Case 5: open pit coal mine, Newcastle coalfield, Australia
42	20	0	36	45	50	0.5	0	Wet	Case 6: open pit coal mine, Newcastle coalfield, Australia
43	22	0	40	33	8	0.35	1	Wet	Case 1: Harbour slope, Newcastle, Australia
44	24	0	40	33	8	0.3	1	Wet	Case 2: Harbour slope, Newcastle, Australia
45	20	0	24.5	20	8	0.35	1	Wet	Case 3: Harbour slope, Newcastle, Australia
46	18	5	30	20	8	0.3	1	Wet	Case 4: Harbour slope, Newcastle, Australia
47	26.49	150	33	45	73	0.15	1		Slope in Hydraulic power station China
48	26.7	150	33	50	130	0.25	1		Slope in Qing River power station China
49	26.89	150	33	52	120	0.25	1		Slope in Qing River basin power station China
50	26.57	300	38.7	45.3	80	0.15	0		Slope in Qing River basin power station China
51	26.78	300	38.7	54	155	0.25	0		Slope in Qing River basin power station China
52	26.81	200	35	58	138	0.25	1		Slope in Qing River basin power station China
53	26.43	50	26.6	40	92.2	0.15	1		Slope in Qing River basin power station China
54	26.7	50	26.6	50	170	0.25	1		Slope in Qing River basin power station China
55	26.8	60	28.8	59	108	0.25	1		Slope in Qing River basin power station China
56	20	8	20	10	10		0		Slope in Tailie elementary school
57	27.3	37.3	31	30	30		1		Slope on the right of Circle E of Tailie Overpass

Case No.	γ (kN/m3)	c(kPa)	φ	β	H(m)	Ru	Stability	Moisture	Location
58	20.6	26.31	22	25	35		0		Landslide on the left of K71+625～K71+700
59	21.6	6.5	19	40	50		0		Slope of Pingxite Bridge
60	22.4	28.9	24	28	35		0		Slope on the right of K76+085～K76+200
61	23.2	31.2	23	30	33		0		Slope on the left of K77+920～K78+100
62	26.8	37.5	32	30	26		1		Slope on the left of K79+165～K79+300
63	27.4	38.1	31	25	42		1		Slope on the right of K79+920～K80+035
64	21.8	32.7	27	50	50		0		Landslide on the right of ZAK0+315～ZAK0+407
65	21.8	27.6	25	35	60		0		Slope on the left of K83+260～K83+360
66	26.5	35.4	32	30	21		1		Slope on the right of K88+300～K88+420
67	26.5	36.1	31	35	39		1		Slope on the right of K88+700～K88+876
68	27	35.8	32	30	69		1		Slope on the right of K89+730～K89+841
69	27	38.4	33	25	22		1		Slope on the right of K90+225～K90+345
70	21.4	28.8	20	50	52		0		Slope on the left of K98+520～K98+710
71	26	42.4	37	38	55		1		Slope on the left of K99+120～K99+260
72	26	39.4	36	25	30		1		Slope on the left of K100+280～K100+410
73	25.6	38.8	36	25	26		1		Slope on the left of K100+615～K100+915
74	20	30.3	25	45	53		0		Landslide on the left of K103+330～K103+450
75	25.8	34.7	33	30	50		1		Slope on the left of K104+610～K104+805
76	21.8	28.8	26	35	99		0		Landslide on the left of K104+892～K105+052
77	21.8	31.2	25	30	60		0		Landslide on the left of K105+260～K105+330
78	24	41.5	36	30	51		1		Slope on the left of K106+268～K106+577
79	24	40.8	35	35	50		1		Slope on the left of K106+992～K107+085
80	20.6	27.8	27	35	70		0		Landslide on the left of K107+856～K107+968
81	20.6	32.4	26	35	55		0		Landslide on the left of K108+960～K109+010
82	25.8	38.2	33	27	40		1		Slope on the left of K109+841～K109+900
83	25.8	39.4	33	25	45		1		Slope on the left of K110+200～K110+274
84	21.1	33.5	28	40	31		0		Landslide on the left of K110+421～K110+500
85	21.1	34.2	26	30	75		0		Landslide on the left of K110+980～K110+240
86	26.6	42.4	37	25	52		1		Slope on the right of K112+720～K112+815
87	26.6	44.1	38	35	42		1		Slope on the left of K113+500～K113+580
88	26.6	40.7	35	35	60		1		Slope on the left of K114+060～K114+167
89	25.8	41.2	35	30	40		1		Slope on the left of K114+224～K114+258
90	25.8	43.3	37	30	33		1		Slope on the left of K117+200～K117+412
91	21.7	32	27	45	60		0		Front slope of tunnel in SongjieyaK122+310
92	20.6	28.5	27	40	65		0		Landslide on the right of K122+350～K122+455
93	21.5	29.8	26	40	70		0		Landslide on the left of K127+440～K127+590
94	26.5	42.9	38	34	36		1		Slope on the left of K127+761～K127+882
95	20.8	15.6	20	30	45		0		Landslide on the left of K137+650～K137+730
96	20.8	14.8	21	30	40		0		Landslide on the left of K138+624～K138+797
97	19.6	29.6	23	40	58		0		Landslide on the right of K75+760～K76+000
98	25.4	33	33	20	35		1		Slope on the right of ZBK0+000～ZBK0+185
99	22.4	29.3	26	50	50		0		Landslide on the left of K84+602～K85+185
100	26.2	41.5	36	35	30		1		Slope on the right of K91+614～K91+660
101	26.2	42.3	36	23	36		1		Slope on the right of K91+720～K91+771
102	25.6	39.8	36	30	32		1		Slope on the left of K100+950～K101+300
103	25.6	36.8	34	35	60		1		Slope on the left of K102+691～K102+880
104	26.2	42.8	37	30	37		1		Slope on the right of K118+360～K118+549

Case No.	γ (kN/m3)	c(kPa)	φ	β	H(m)	Ru	Stability	Moisture	Location
105	26.2	43.8	38	35	68		1		Slope on the right of K119+823～K119+951
106	20.6	32.4	26	30	42		0		Landslide on the right of K124+340～K124+562
107	26.5	41.8	36	42	54		1		Slope on the right of K131+280～K131+380
108	20.8	15.4	21	30	53		0		Landslide on the left of K138+840～K138+930

2.3 Adaptive relevance vector machine for classification

Generalized linear models perform a nonlinear projection of the input space into a transformed space by means of a set of nonlinear basis function which is named as a kernel function in machine learning. In supervised learning, a training data set is used to train a model to obtain some parameters. This data set comprises a set of *N* input vectors $\{\mathbf{x}_n\}_{n=1}^N$ and the corresponding target value $\{t_n\}_{n=1}^N$. This target t_n could be a sample from a set of class label values for the classification problem. The aim of training is to learn a mapping $f(x)$ from the training set $\{x_n, t_n\}_{n=1}^N$ in order to predict the target t_* for the new input x_*. A commonly used form of the function $f(x)$ can be noted as

$$y = f(\mathbf{x};\mathbf{w}) = \sum_{i=1}^{M} w_i \phi_i(x) + w_0 = w^t \phi(x) \quad \text{..... (2.1)}$$

In the above equation, $w = [w_1, w_2, ..., w_M]^t$ is the weight parameter which is to be adjusted with the training dataset; $\phi(x) = [\phi_1(x), \phi_2(x), ..., \phi_M(x)]^t$ is the basis function which is fixed and user-defined but of any form. The training objective is to estimate the parameters *w* given a set of training data $\{x_n, t_n\}_{n=1}^N$ and fixed functions $\varphi_i(x)$.

2.3.1 Relevant vector machine

Here the RVM is briefly introduced by using a Bayesian framework for classification. "Relevance vector machine" (RVM) is a Bayesian framework for learning in general models. RVM actually relies on a particular form of Eq.(3.1), similar to that used for "support vector machine" (SVM)(Vapnik 1998; Schölkopf et al. 1999; Herbrich 2002)

$$f(x\ ;\ w) = \sum_{i=1}^{N} w_i K(x,\ x_i) + w_0 = w^t \varphi(x) \quad \text{.....(2.2)}$$

with $\varphi(x) = [1,\ K(x,\ x_1),\ K(x,\ x_2),\ ....,\ K(x,\ x_n)]^t$ and $w = [w_0\ , w_1\ ,...,\ w_N\ ]^t$. Note that the

constant term w_0 is introduced in the vector of unknown parameters w. The kernel function $K(x, x_i)$ so defines on basis function per "data point" x in the training set. RVM regression employs model (2.2) with an additive noise term to link the vector input x_n and scalar target variable t_n

$$t_n = f(x_x; w) + \in_n \quad \text{.....(2.3)}$$

where $\in_n$ is a zero-mean white noise process with variance σ^2, i.e., $p(\in_n | \sigma^2) = N(\in_n | 0, \sigma^2)$,. Considering noise precision β instead of its variance σ^2, i.e., posing $\beta = \sigma^2$, and assuming the independence of the samples t_n the likelihood of the complete training data set is

$$p(t \mid X, w, \beta) = (2\pi\beta^{-1})^{-N/2} \exp\left(-\frac{1}{2}\beta \left\| t - \Phi w \right\|^2 \right) \quad \text{.....(2.4)}$$

where $t = [t_1, ..., t_N]^t$, $X = [X_n]_{n=1}^N$ and $\Phi = [\varphi(x_1), \varphi(x_2), ..., \varphi(x_n)]^t$ is a $N \times (N+1)$ design matrix. With more parameters $(N+1)$ than training data samples (N), direct maximum-likelihood estimation of w would lead to over-fitting. In the RVM Bayesian framework, zero-mean Gaussian shrinkage priors are imposed on every w_i and, assuming the independence of the parameters, we have

$$p(w_i | \alpha_i) = \mathrm{N}(w_i | 0, \alpha_i^{-1}) \Rightarrow p(w|\alpha) = \prod_{i=0}^{N} N(w_i | 0, \alpha_i^{-1}) \quad \text{.....(2.5)}$$

with $\alpha = [\alpha_0, \alpha_1, ..., \alpha_N]^t$, a $N+1$ vector of hyper-parameters representing the precision on the parameters. Finally uniform hyper-priors are assumed for all the precision hyper-parameters, α and β. An interesting property of these hyper-priors is that when the evidence of the model is maximized with respect to the hyper-parameters the corresponding parameters to be zero. This is a type of "automatic relevance determination"(MacKay 1994) leading to a sparse set of parameters w. Using Bayes rule and the properties of Gaussian functions, the posterior distribution of the weight can also be described by a Gaussian:

$$p(w|X, t, \alpha, \beta) = N(W | m, \Sigma) \quad \text{.....(2.6)}$$

where the mean m and covariance xxx are given by

$$m = \beta \Sigma \Phi^t t$$
$$\Sigma = (A + \beta \Phi^t \Phi)^{-1} \quad \text{.....(2.7)}$$

with $A = diag(\alpha_0, ..., \alpha_N)$ a diagonal matrix of precisions.

In practice, the values of α and β are estimated by maximizing the marginal likelihood $p(t|X, \alpha, \beta)$, i.e., using a type-II maximum-likelihood method (Berger 1985). Only the most probable values are thus calculated, an approximation to estimating and using their full distribution. With this simplification, the marginal likelihood can be obtained by integrating out the weight parameters

$$p(t|X, \alpha, \beta) = \int p(t|X, w, \beta) p(w|\alpha) dw = N(t|0, \beta^{-1} I + \Phi A^{-1} \Phi^t) \quad \text{.....(2.8)}$$

Values of α and β that maximizes (the log of) (Eq.2.8) can then be obtained iteratively, using the following update rules

$$\alpha_i^{new} = \frac{1 - \alpha_i \Sigma_{ii}}{m_i^2}$$
$$(\beta^{new})^{-1} = \frac{\|t - \Phi m\|^2}{N - \sum_{i-1}^{N} (1 - \alpha_i \Sigma_{ii})} \quad \text{.....(2.9)}$$

where m_i is the i^{th} element of the estimated posterior weight w and Σ_{ii} the i^{th} diagonal element of the posterior covariance matrix Σ from Eq.(2.7).

Once the iterative procedure has converged to the "most probable: values α_{MP} and β_{MP}, the distribution of target value t_* for a new data point x_* is also Gaussian and estimated through

$$p(t_*|X, t, \alpha_{MP}, \beta_{MP}) = \int p(t_*|X, w, \beta_{MP}) p(w|X, t, \alpha_{MP}, \beta_{MP}) dw$$
$$= N(t_*|m^t \varphi(x_*), \sigma_*^2) \quad \text{.....(2.10)}$$

with the variance estimated as

$$\sigma_*^2 = \beta_{MP}^{-1} + \varphi(x_*)^t \Sigma \varphi(x_*) \quad \text{.....(2.11)}$$

where Σ is given by Eq.(2.7) with α and β set at their optimal value.

In our problem of slope stability, our target is to predict whether a slope is stable or not, thus it is a binary two-class problem with target variable $t_n \in \{0, 1\}$. Thus the problem is to predict the posterior probability belonging to either of the two classes, given the input x_n. Therefore Eq.(2.1) is generalized by applying a logistic sigmoid function $\sigma(a) = \frac{1}{1+\exp(-a)}$, such that

$$f(x; w) = \sigma(w^T \phi(x)) = \frac{1}{1+\exp(-w^T \phi(x))} \quad \text{.....(2.12)}$$

Adopting the Bernoulli distribution, the likelihood of the training data set is defined as

$$p(t \mid X, w) = \prod_{n=1}^{N} \sigma(w^T \phi(x_n))^{t_n} (1-\sigma(w^T \phi(x_n))^{1-t_n} \quad \text{.....(2.13)}$$

Using the Laplace approximation with a fixed value of α, the posterior distribution over w can be obtained by maximizing (Psorakis et al. 2010):

$$\begin{aligned} \log p(w \mid X, t, \alpha) &= \log(p(t \mid X, w)\, p(w \mid \alpha)) - \log p(t \mid X, \alpha) \\ &= \sum_{n=1}^{N} (t_n \log f(x_n; w) + (1-t_n) \log(1- f(x_n; w))) - \frac{1}{2} w^t A w + const \end{aligned} \quad (2.14)$$

The mean and variance obtained by the Laplace approximation for w are

$$\begin{aligned} w_{MP} &= \Sigma_{MP} \Phi^t B t \\ \Sigma_{MP} &= (\Phi^t B \Phi + A)^{-1} \end{aligned} \quad \text{.....(2.15)}$$

Where B is a $N \times N$ diagonal matrix with $b_{nn} = f(x_n; w)(1- f(x_n; w))$. Using this Laplace approximation, the log marginal likelihood is expressed as

$$\begin{aligned} \log p(t \mid X, \alpha) &= \log \int p(t \mid X, w) p(w \mid \alpha) dw \\ &= \log p(t \mid X, w_{\mathrm{MP}})\, p(w_{\mathrm{MP}} \mid \alpha) (2\pi)^{1/2} \left|\Sigma_{MP}\right|^{1/2} \end{aligned} \quad \text{.....(2.16)}$$

The values of α by maximizing Eq.(2.16) then can be obtained iteratively using the following update rule

$$\alpha_i^{new} = \frac{1-\alpha_i \Sigma_{ii}}{m_i^2} \quad \text{.....(2.17)}$$

Where m_i is the i^{th} element of the estimated posterior weight w; Σ_{ii} is the i^{th} diagonal element of the posterior covariance matrix Σ in Eq.(2.15).

Once the iterative procedure converges to the most optimal value α_{MP}, the target value t_* for a new data input x_* is estimated by

$$p(t_*|X, t, \alpha_{MP}) = \int p(t_*|X, w)p(w|X, t, \alpha_{MP})dw \quad \text{.....(2.18)}$$

2.3.2 Kernel function

There are many kernel functions that could be used in Eq.(2.1)(Tipping 2000; Clark and Everson 2012). In this chapter, three kernel functions, i.e. the Gaussian kernel, the Laplace kernel and the Cauchy kernel, are investigated to find out the effect of the so-called width or length-scale hyper-parameter. The Gaussian kernel function is

$$\emptyset(X_m, X_n) = \exp(-\frac{\|X_m - X_n\|^2}{r^2}) \quad \text{.....(2.19)}$$

The Laplace kernel function is

$$\emptyset(X_m, X_n) = \exp(-\sqrt{\frac{\|X_m - X_n\|^2}{r^2}}) \quad \text{.....(2.20)}$$

The Cauchy kernel function is

$$\emptyset(X_m, X_n) = \frac{1}{1+\frac{\|X_m - X_n\|^2}{r^2}} \quad \text{.....(2.21)}$$

Each kernel has a hyper-parameter r^2 which should be specified before model training. In the following section, the hyper-parameter $r^2$of each kernel function is adapted to discover its effect on the model performance.

2.3.3 Adapting the kernel parameter

Unlike the optimizing of the weight w, the hyper-parameter r^2 is user-defined before model training. The objective function is defined as the following equation(Dixon 2009) in order to evaluate the predictive performance:

$$\text{Predictive Accuracy(PA)} = \frac{(\text{TPR+TNR})}{\text{TPR+FPR+TNR+FNR}} \times 100\% \quad \text{.....(2.22)}$$

where, TPR is True positive rate, percentage of stable slope correctly detected; TNR is True negative rate, the percentage of failed slope correctly detected; FPR is False positive rate, percentage of stable slope wrongly classified as failed slope; FNR is False negative rate, the percentage of failed wrongly classified as stable slope.

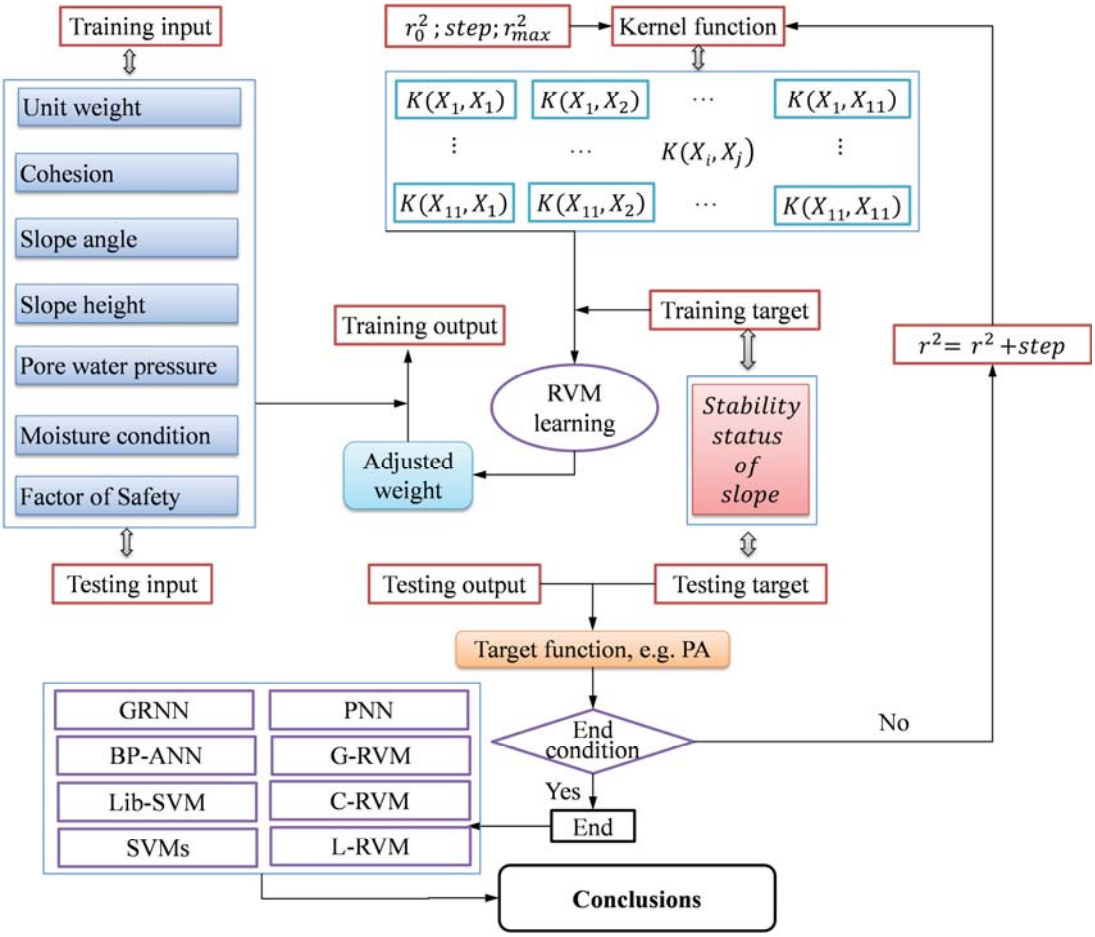

Fig. 2.3 Implementation of adaptive RVM for slope stability analysis

The adapting of the kernel parameter processes in the following steps:

(a) Initializing the hyper-parameter r^2 in a proper range and specifying the initial r_0^2 and an appropriate step value for iteration;

(b) Specifying one of the kernel functions;

(c) Training the RVM model with the dataset by Eq.(2.16) to obtain an optimal value α_{MP} and by Eq.(2.14) for the weight w;

(d) Computing the posterior distribution output $\mathrm{P}(t|X,w)$ in Eq.(2.13);

(e) Calculating the PA value in Eq.(2.12);

(f) Updating hyper-parameter $r_{k+1}^2 = r_k^2 + step$, looping into (b) till $r^2 = \max(r^2)$;

(g) Finding out the maximum PA value for each kernel function and the corresponding r^2 as the optimal hyper-parameter.

With the above steps, the predictive outputs of different kernels are obtained and the optimal r^2 value of each kernel is also figured out.

The implementation of the approach is given in Fig. 2.3.

2.4 Results and discussion

The effect of hyper-parameter is exploited in this chapter as well as the kernel type and sample size. The effects of different kernels are firstly investigated. Then the effect of the hyper-parameter in the kernel function is investigated with the strategy described in Section 2.3. Meanwhile, Model 1~4 is defined in order to show the effect of sample size to the predictive performance of ARVM. The former 46 cases are modeled in Model 1. The frontal 55 cases are modeled in Model 2. All the cases are modeled in Model 3 and the last 53 cases are modeled in the Model 4 to show the effect of data quality on consistency. Each model is executed with different kernels and variant hyper-parameter values.

At last, this strategy of ARVM is applied to evaluate the stability of slopes in the same dataset as the other approached like ANNs and SVMs in order to illustrate comparatively its performance. The comparison is given on the view of obtaining good PA value and less number of relevant vectors.

2.4.1 Kernel effect and parameter effect

The predictive performances of the Model 1, Model 2, Model 3 and Model 4 are given in Fig. 2.4-(a), (b), (c), (d), respectively, for all the three kernels introduced with respect to the width hyper-parameter values. The overall performance of the models is given in Table 2.2.

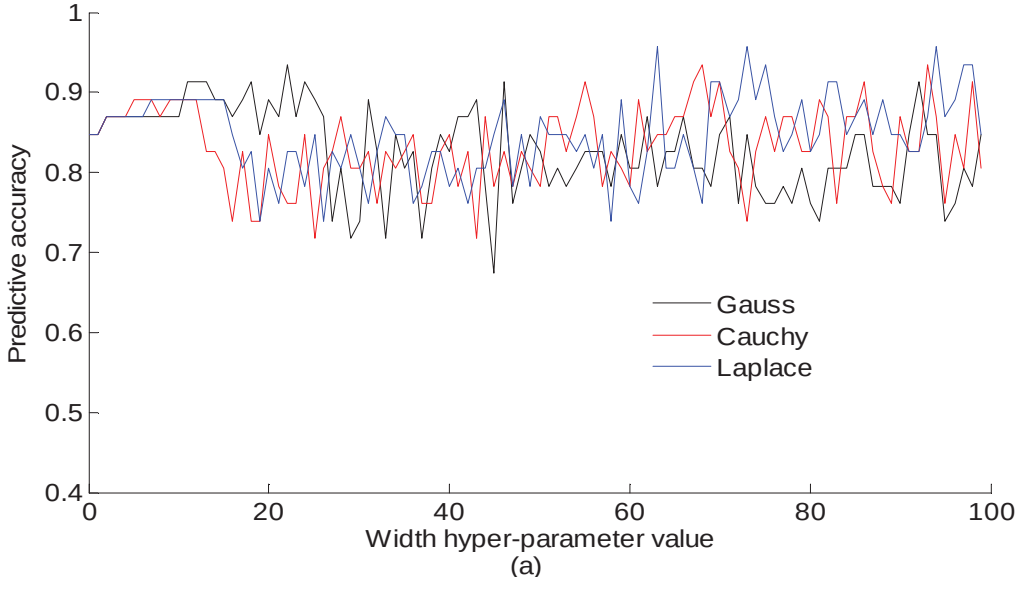

(a)

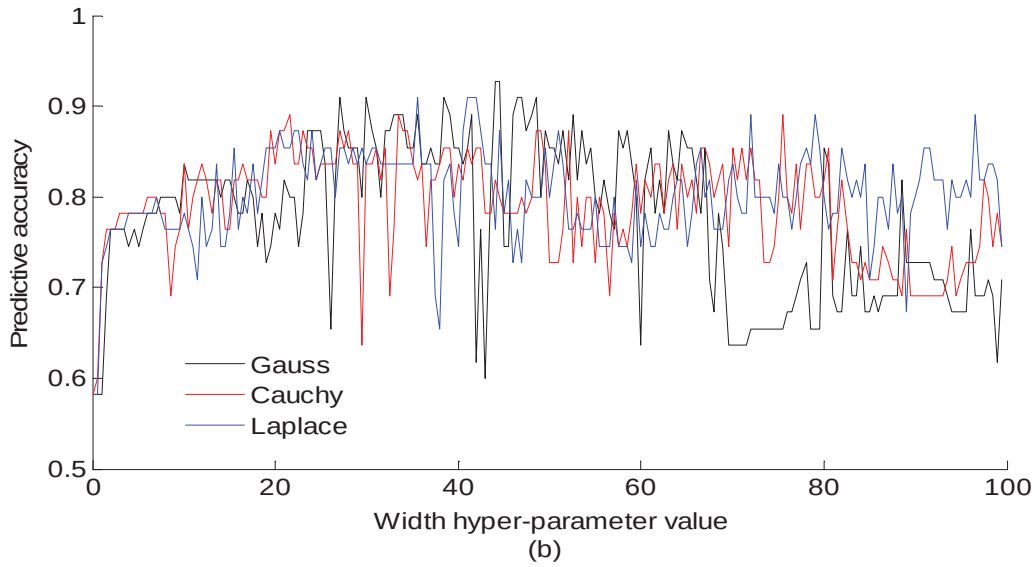

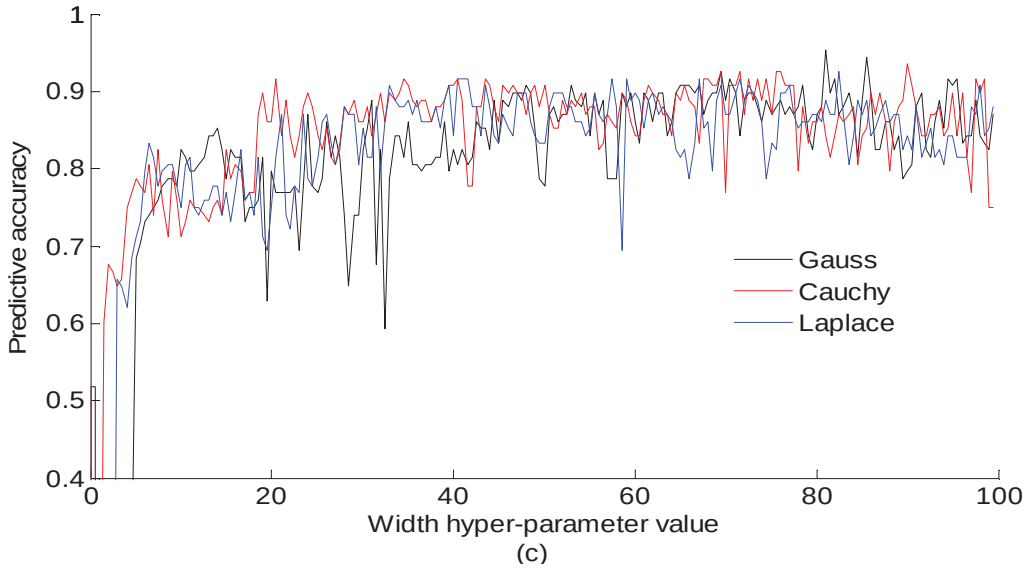

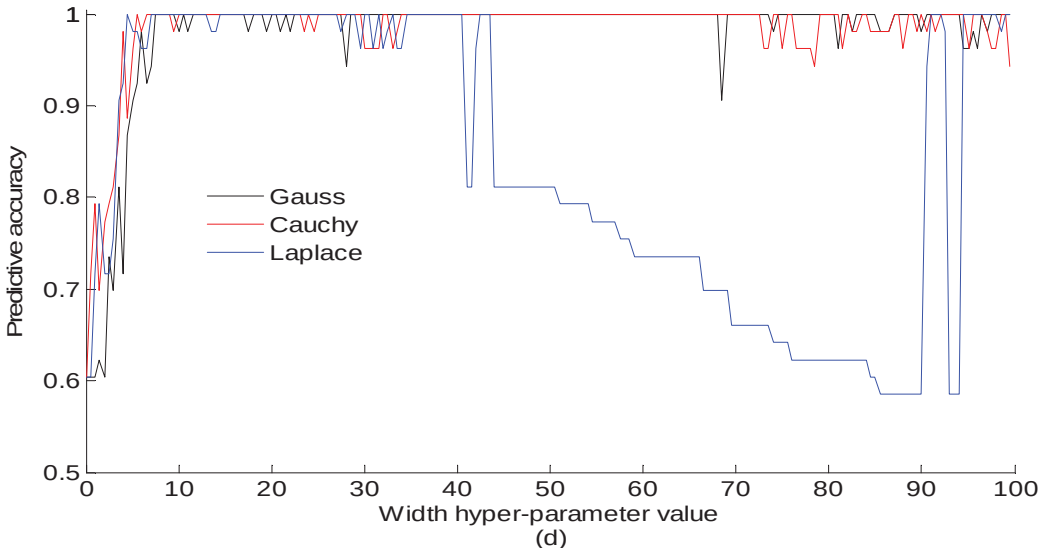

Fig. 2.4 Effects of kernel type and value of width hyper-parameter on predictive accuracy

It can be drawn from Model 1 in Fig. 2.4-(a) that the predictive accuracy varies intensively as the value of width hyper-parameter changes for each kernel type. It is shown in Fig. 2.4-(a) that the PA value ranges from 0.68 to 0.95 for the Gaussian kernel function. It leaps dramatically as the width value changed slightly. There are many width values such that the PA reached 0.95 which is the best model performance. The relationship between PA and the width value is rough-and-tumble judging from Fig. 2.4-(a), which implies that the effect of width value to predictive performance cannot be easily figured out as a common function. Thus pilot calculation is proposed as a compromise to look for the optimal width value for the purpose of obtaining the best PA. It should be confessed that the pilot calculation was time-consuming.

The rambling feature of PA value with respect to width value for Cauchy kernel and Laplace kernel are mainly similar to that of Gaussian kernel in Fig. 2.4-(a). All the three kernels can generate satisfactory results. It can be noted that an optimal width value of Gaussian kernel does not mean that it was an optimal value for the Cauchy kernel or Laplace kernel. That's to say each kernel performs best with different optimal width values. The width parameter of Gaussian kernel can generate good PA value at a relatively small value (near to 20), compares with that of Cauchy kernel (near to 70) and Laplace kernel (near to 60). It implies that Gaussian kernel could perform best with a relative small width value than Cauchy kernel and Laplace kernel. The Gaussian kernel thus can converge faster than the other two when carrying out the pilot calculation for optimal width value. To this point, Gaussian kernel performs a bit better than the Cauchy kernel and Laplace kernel.

As for Model 2 in Fig. 2.4-(b), the rambling feature of PA value with respect to width value is mainly the same as that in Model 1. Again, each of the three kernels can generate best PA value with several width values, which implies that these kernels are also suitable with proper width values for the modeling of 55 cases. Like that in Model 1, the Gaussian kernel converges much faster than the Cauchy kernel and the Laplace kernel to a get a best PA value in Model 2. The PA values of Gaussian kernel show a much more rambling than that of Laplace kernel and Cauchy kernel. Thus this time the hyper-parameter values result in variant predictive performances for the three kernels but the kernel type makes no apparent influence on predictive performance.

The rambling feature of PA value with respect to width value is still the same for Model 3 shown in Fig. 2.4-(c) as that in Model 1 and Model 2 for each kernel function. Thus different width hyper-parameter values can generate variant predictive performance. The maximum PA values that the three kernels can generate are smaller than the corresponding values in Model 1 and Model 2. The Cauchy kernel can get the result of PA=0.96 and the Gaussian kernel can get the result of PA=0.95; the Laplace kernel can get the result of PA=0.94. All these PA values are relatively satisfactory. The Cauchy kernel works slightly better than the other two kernels.

The rambling feature of PA value with respect to width value is more intensive for Model 4 in Fig. 2.4-(d), especially that of Gaussian kernel. Again, many width values can generate the corresponding best PA value for each kernel. The predictive performance is mainly similar to each other for the three kernels. The features of the predictive performance curves are generally different from that in Model 1 and Model 2.

Based on the above analysis, comments can be achieved that the predictive performance is not steady with respect to the width hyper-parameter value of each kernel, i.e. the width hyper-parameter has apparent effect on the predictive performance of RVMs. All the three kernel functions can perform well in the above Model 1~Model 3. Comparing the results of Model 1~Model 4, conclusion can be made that the kernel type has no evident effect on the predictive performance given an optimal width hyper-parameter value, based on the fact that none of the three kernels can always perform better than the others in every model.

2.4.2 Sample size effect

The divergent performance of different Model shown in Table 2.2 implies that the sample size might have effect on the predictive performance. In fact, this effect can be caused probably by the quality of the dataset on consistency of different models. It can be seen easily that the rambling predictive performance curve of Model 4 is quite different from that of Model 1 and Model 2, which implies that the potential disciplines in these dataset might be a bit different. Model 1 and Model 2 have good consistency of data quality. The predictive performance of Model 3 can be recognized as a compromise of Model 2 and Model 4. The compromising process is undertaken automated by ARVMs during model training. The different samples make the optimal width hyper-parameter value of each model different but the predictive performance is mainly the same with the corresponding optimal parameter value. Therefore in all, the quality of data samples on consistency is important for the performance of ARVMs and it makes the optimal hyper-parameter values different.

Table 2.2 Predictive performance of different sample size

Model	Model 1			Model 2			Model 3			Model 4		
	GK	CK	LK	GK	CK	LK	GK	CK	LK	GK	CK	LK
An optimal width value	99	115	115	44	121.5	35.5	142.51	120.01	166.01	12.5	10.5	9.5
NO. of support vectors	10	11	9	9	10	8	9	9	10	6	7	7
Predictive accuracy	0.96	0.96	0.98	0.93	0.93	0.91	0.96	0.96	0.94	1.00	1.00	1.00

Notes: GK-the Gaussian kernel; CK-Cauchy kernel; LK-Laplace kernel.

2.4.3 Comparison of different techniques

Besides, the approach discussed in this paper is comparatively studied with other techniques.

Comparisons of the predictive performances of different approaches like the GRNN and PNN (Specht 1990, 1991) are given in Table 2.3. The results of BP-ANN are reported with 46 cases using the function approximation technique (Sakellariou and Ferentinou 2005); the results of RBF-SVM, P-SVM and S-SVM are reported with 46 slope cases comprised 32 training samples and 14 test samples (Samui 2008). The G-RVM, C-RVM and L-RVM apply the Gaussian kernel, the Cauchy kernel and Laplace kernel, respectively. The comparisons are thus demonstrated with the same data set, i.e.32 training samples and 14 test samples. The results are comparatively shown in Fig. 2.5.

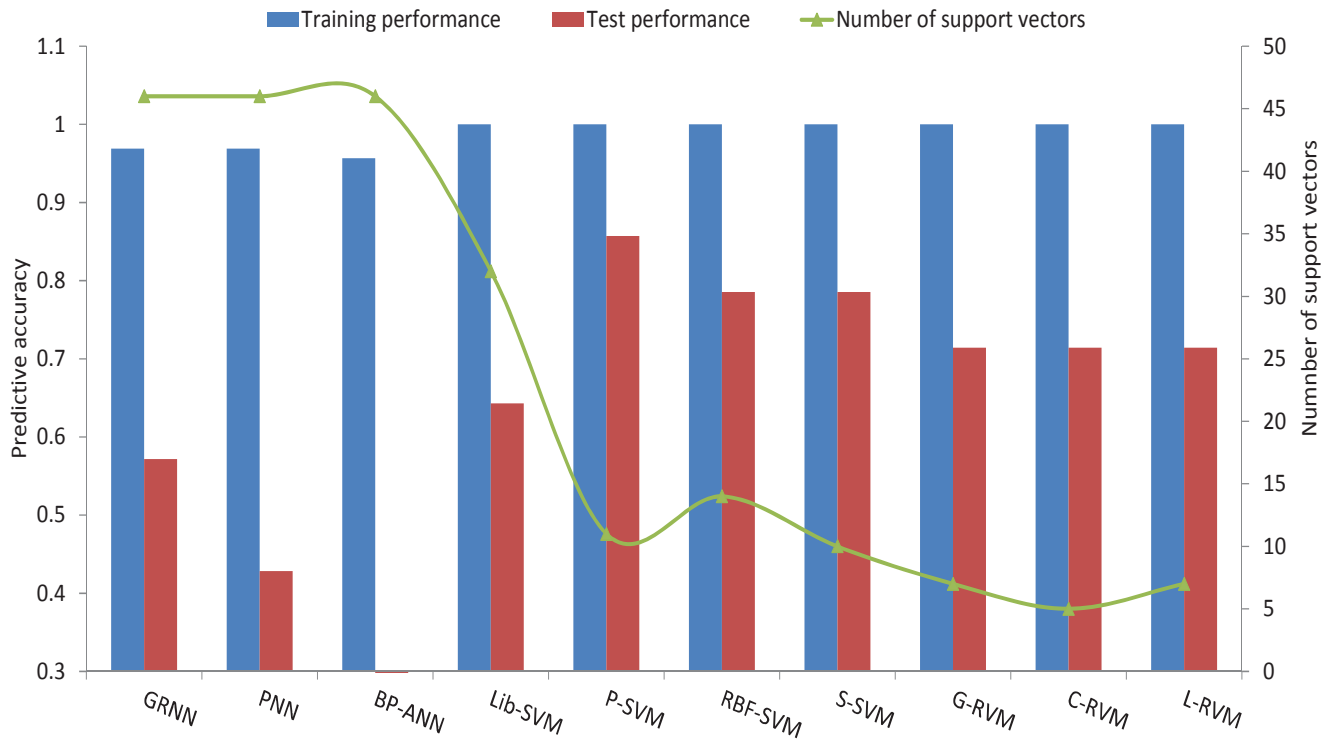

Notes: GRNN: general regression neural network; PNN: probabilistic neural network; BP-ANN: back propagation neural network; P-SVM, RBF-SVM and S-SVM denote the support vector machine with polynomial kernel, radial basis function and spline kernel, respectively; G-RVM, C-RVM and L-RVM denote the relevance vetor machine with Gaussian kernel, Cauchy kernel and Laplace kernel , respectively.

Fig. 2.5 Predictive performance of different approaches

As given in Table 2.3, all the approaches can perform well to obtain good PA values for the training samples but perform not very well for testing samples. The Neural Networks use all the samples for model training and then give model output. The SVM and RVM train with the samples and then give the model output depending on the support vectors (a sample was treated as a vector). It is known to all that the less the number of support vectors the less calculation the corresponding approach will take for the same problem. The testing performance of GRNN and PNN is poor as given in Table 2.3. The LIBSVM approach(Chang and Lin 2011) which is a widely used SVM classifier, generates results with 100% accuracy for training and 64.29% accuracy for testing. The

P-SVM, RBF-SVM, S-SVM approach gives 100% accuracy for training and 85.71%, 78.57%, 78.57% accuracy for testing, respectively. The G-RVM, C-RVM, L-RVM performs excellent in training and gives the accuracy value of 71.43%, i.e. 10 of the 14 samples are correctly predicted which is not a bad performance.

The numbers of support vectors for the RVMs are about a half of that for the corresponding SVMs. Thus the RVMs can perform much faster than other approaches if a new unknown test sample is given for a trained network. In fact, the three RVMs can obtain the same performance in Table 2.3 with many other width hyper-parameter values despite that only one value is given. The hyper-parameter value is not as important as that in SVMs for generating good results. Therefore in stability prediction of the slope cases, the RVMs perform as well as the SVMs in training and better than the LibSVM in testing, while not so well as P-SVM, RBF-SVM, S-SVM in testing. However, the number of support vectors of the RVMs is only half of that of the SVMs. To this point, the RVMs are advantageous to the SVMs.

Table 2.3 Predictive performance of different approach on slope stability evaluation

Approach	Hyper-parameter value	Number of support vectors	Training performance	Test performance
GRNN	-	-	96.88	57.14
PNN	-	-	96.88	42.86
BP-ANN	-	-	95.7	-
Lib-SVM	C=2;g=1	32	100	64.29
P-SVM	10	11	100	85.71
RBF-SVM	100	14	100	78.57
S-SVM	100	10	100	78.57
G-RVM	20.51	7	100	71.43
C-RVM	61.51	5	100	71.43
L-RVM	66.51	7	100	71.43

Notes: Lib-SVM was provided by C.C. Chang and C.J. Lin (2011).

2.5 Further discussion

As mentioned before (Sakellariou and Ferentinou 2005), 15 cases in Table 2.1 present cohesion parameter $c = 0$, which implies the failure mode is planar but circular. Thus, these samples should be removed from the circular failure analysis in order to obtain more reasonable results. The predictive performance of the remained 31 cases is show in Fig. 2.6. As a whole, the best predictive accuracy in Fig. 2.6 is more satisfactory than that in Fig. 2.4-(a). This result tells that the removed slope cases do affect the performance of the models.

It is well know that it is always better to obtain as large data set as possible in the case-based evaluation of slope stability. Hence, influence of the removed cases on all the cases is more interesting. The predictive accuracy versus width hyper-parameter value is shown in Fig.6 for all the

remained 93 cases (Model 5). Compared to the performance of Model 3 in Fig. 2.4-(a), the performance of the 93 cases has greatly improved as shown in Fig. 2.7. This improvement can be manifested by the best predictive accuracy as well as the number of support vectors as shown in Fig. 2.8. Thus, special attention should be paid to the quality of slope cases to avoid affection of the cases of different failure mechanisms.

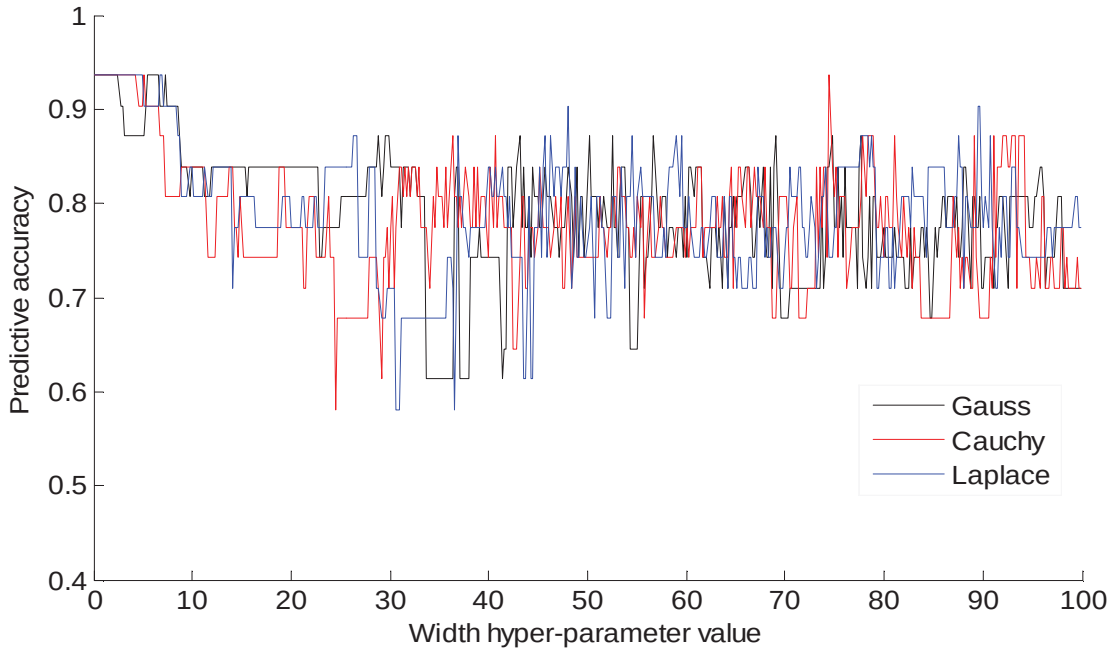

Fig. 2.6 Predictive performance of the 31 cases (filtered)

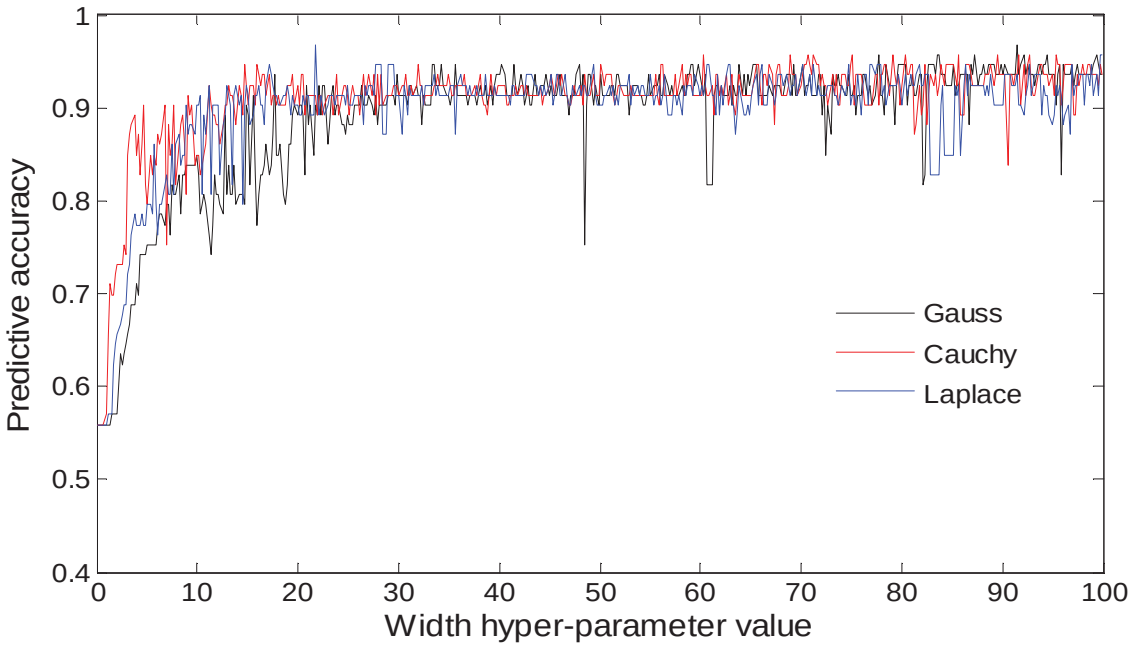

Fig. 2.7 Predictive performance of the 93 filtered cases

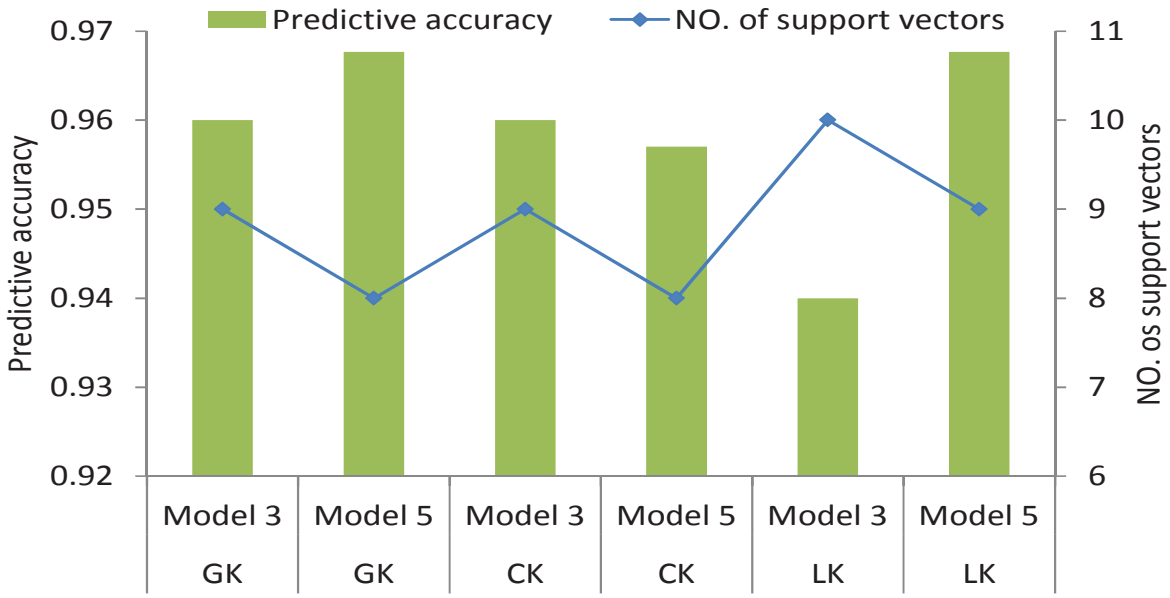

Fig. 2.8 Comparison of Model 3 and Model 5 on evaluation of slope stability

2.6 Conclusions

This chapter investigates the applicability and effectiveness of ARVM for slope stability evaluation and illustrates its performance with variant hyper-parameters of different kernels. The effect of kernel type is demonstrated with the Gaussian kernel, Cauchy kernel and Laplace kernel. The effect of the width hyper - parameter is described for each kernel type. The effect of sample size is also investigated with four models of different sample size. Based on these results, the following conclusions can be achieved.

(a) The strategy using ARVM is feasible and effective in the evaluation of slope stability based on former slope case data. The excellent performance on training cases has well illustrated this. The over 70% accuracy of test samples has well demonstrated its generalization ability.

(b) The kernel type of RVMs has no apparent effect on the predictive performance on condition that the optimal hyper-parameter is given. The width hyper-parameter values however has an evident effect on the performance of the RVMs, thus it is necessary to obtain an optimal width hyper-parameter value. The sample size shows certain influences on predictive results but the influences are mainly on the different optimal hyper-parameter values.

(c) Comparisons of different approaches show that the ARVMs have a powerful ability on training like the Neural Networks and SVMs. Also, the ARVMs have the better generalization ability than the widely used LIBSVM in the evaluation of slope stability. It is feasible and effective for application in slope stability evaluation. Also, it is a potential and promising tool for application in slope stability evaluation and can be used in other problems in earth science.

Nevertheless, the adaptive process of searching the optimal hyper-parameter is time consuming;

some optimization algorithms like the genetic algorithm and the particle swarm optimization may be applied to accelerate the optimizing process in future. And the stabibility evaluation should also be further undertaken for analysis of slopes of different failure mechanisms.

Chapter 3 Comprehensive evaluation of slope stability using the cloud models

3.1 Introduction

Stability evaluation acts as an important and continuous issue during the design and construction stage for slopes in hydropower stations, especially for the dam abutment slopes in mountainous areas. The abutment slope is a geological structure with stability problems over the dam and thus its failure would do great harm to the safety of the dam. For arc dams, the abutment slope is even an essential part of the resisting system to undertake the loads transferred from the arc dam. In this way, the stability assessment of abutment slopes in dam area has been paid much attention by geological engineers and associated researchers. Currently, several types of methods are being used for the evaluation of slope stability: the empirical method(Hoek and Bray 1981; Bieniawski 1979; Goodman 1989; Aydan et al. 1989; Romana et al. 2003; Rodrigo and Hürlimann 2008; Pantelidis 2009; Taheri and Tani 2010; Jhanwar 2012), the analytical analysis(Hoek and Bray 1991; Lam and Fredlund 1993; Nawari et al. 1997; Bye and Bell 2001; Rodrigo and Hürlimann 2008; Liu et al. 2008; Latha and Garaga 2010; Saada et al. 2012) the numerical modeling(Goodman and Shi 1985; Hoek and Bray 1991; Jeongi-gi and Kulatilake 2001; Wang et al. 2003; Hatzor et al. 2004; Stead et al. 2006; Kveldsvik et al. 2009; Alejano et al. 2011). These approaches have been recognized as the conventional methods for study of slope stability with great emphasis on empirical opinions of expert experience.

In the past decade, some newly developed methods, like the fuzzy method, the matter-element model and the extension method, have been proposed for application for comprehensive assessment of slope stability, such as (Li 1997b; Qin et al. 2001; Wang and Pan 2004; Shu et al. 2005; Xu et al. 2007; Liu and Chen 2007; Tan et al. 2009; Kang et al. 2009; Liang et al. 2010; Guo et al. 2010; Abbas et al. 2011; Samui and Kotharib 2011). These methods have been developed based on certain mathematical model and provide comprehensive evaluation of slope stability by taking accounts all the factors that have no negligible effects on slope performances. They are advancing since that the mathematical models can manage both quantitative and qualitative data and partially account for the uncertainties in slope engineering(Liu et al. 2012). For example the fuzzy method can take into account the fuzziness during the assessing procedure of slope stability(Park and West 2001; Park et al. 2005; Jimenez-Rodriguez et al. 2006; Aksoy and Ercanoglu 2007; Duzgun and Bhasin 2009; Abbas et al. 2011; Park et al. 2012). Three steps are to be processed for implementation of the methods: i) collect data of the slope; ii) classify the rating factors; iii) execute the comprehensive evaluation of slope

stability.

With the thorough researches on the topic of uncertainties, more and more scientists are coming to believe that the uncertainty is the nature of the world and nothing is assured except for the uncertainty itself(Li and Du 2007). The most elementary features among the uncertainties are the randomness and the fuzziness which is discussed in probability theory and fuzzy mathematics, respectively. As known, either of the two theories is capable of accounting for randomness or fuzziness but not sufficient enough to handle the both. Slope engineering is associated with nature data full of randomness and fuzziness. The fuzzy theory can account for the fuzziness but it is not capable of expressing the randomness in the slope data. In 1995, the concept of “cloud” is proposed on the basis of probability theory and fuzzy mathematics (Li et al. 1995) to overcome this problem. In the literatures (Li et al. 2004; Li et al. 1998b), the randomness and fuzziness were deeply studied as well as the relationship between them. Cloud model was proposed to portray the randomness and fuzziness as well as their relationship in linguistic terms(Li 1997a). The cloud model synthesizes the characteristics of both fuzzy mathematics and probability theory and it can generate results with fuzzy and random signification.

The application of cloud models for slope stability assessment is introduced in this work closely related to the left abutment slope of Jinping 1 Hydropower Station, southwest of China. A brief introduction is given first in both conventional and unconventional methods for slope stability evaluation problems as well as cloud models. Then, the characterization of the discussed slope and the evaluation system are discussed with concern to the problems on site characterization, potential slope failure, slope reinforcement and treatment, categories of evaluating factors, classification of the factors and rock slope stability classification. These evaluating factors of slope stability are adopted according to slope conditions and with reference to the previous rock mass rating systems. The classifications of these factors are obtained from Chinese slope design standard and the previous work related to this slope. Afterwards, the cloud mode method is introduced with special regard to slope stability problems. Also, the weighted AHP is presented for comprehensive evaluation of slope stability with the outputs of cloud models. In section 4, basing on the data collected, the implementation of the presented approach is executed to evaluate the stability of left abutment slope of Jinping 1 Hydropower Station. Then the conclusions are finally followed in section 5.

3.2 Slope characterization and evaluation system

Slope conditions are introduced in the following as well as the slope stability evaluation system. Cite characterization is first presented with special regard to geological features. These characteristics are followed by potential slope failures in different parts of the left bank slope and the corresponding

slope reinforcement and treatments. Then, the evaluating factors are adopted and sorted into four categories with respect to slope condition and previous rock mass rating systems. The monitoring factors with a few records in existing systems are managed in the form of four basic factors according to the monitoring analysis results of the left abutment slope. Classifications of these factors are obtained according to the results of the literatures and the Chinese standard for engineering classification of rock masses(PRC 1994).

3.2.1 Cite characterization

Jinping 1 Hydropower Station is the critical hydroelectric project in the midstream and downstream of Yalong River which is located to the east of Qinghai-Tibet plateau in Yanyuan and Muli district Liangshan state, Sichuan Province of China as shown in Fig. 3.1. This region is of complex topographical and geological conditions formed by the comprehensive effects of continuous uplifting of Qinghai-Tibet plateau and rapidly sapping of the steep valleys. The 305m water retaining structure of the project is currently the top highest arch dam with double curvatures worldwide. The height of dam crest is 1 885m and its ratio of thickness to height is 0.207. The capacity of the reservoir is 7.76×109 m3 and the power capacity is 3 600MW. An overview of the slope is given in Fig. 3.2.

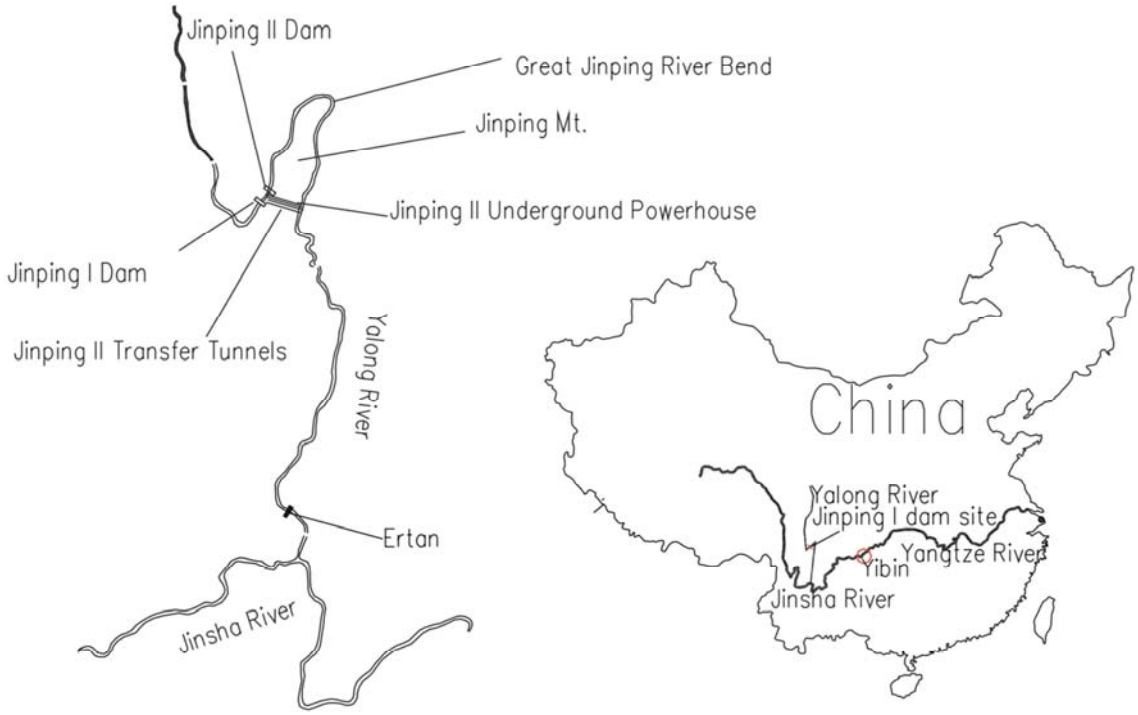

Fig. 3.1 Location of Jinping 1 Hydropower Station

The deep stream valley is steep with the typical shape like “V” round the dam area. The analysis of

valley development history show that the average sapping velocity of the valleys is about 3mm/a and the maximum velocity is about 3.9 mm/a ~4.4mm/a in the mid-downstream of Yalong River. The rock mass round the dam area is composed of inverted syncline. The attitude of rock formation mainly situates N15º~60ºE, SE∠35º~45º and the strike direction of rocks generally accords with that of the river. The bedding rock mainly consists of Triassic metamorphic rocks. The first segment of the bed rock is consisted of the green schist, the second is marble and the third is sandy slate.

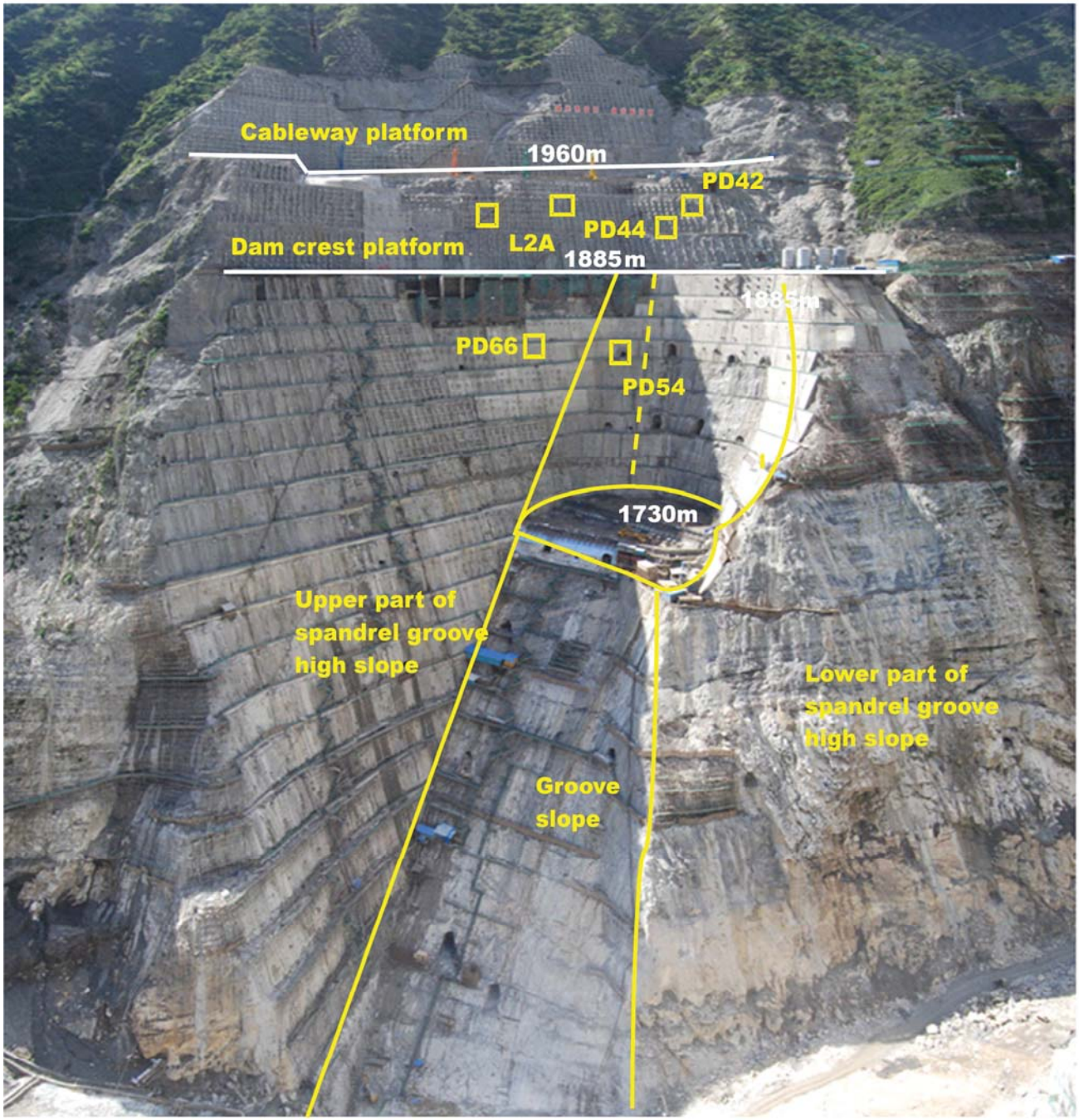

Fig. 3.2 Overview of the evaluated slope

The left bank slope in the dam area is a reverse slope and presents the interphase micro-geomorphology of the ridge and the super fissure. The lower part under height 1 820m~1 900m of the slope is formed by marble with the slope ratio between 55ºand 70º; the upper part is of sandy slate with the slope ratio between 40º~50º. There exist faults, joints and disturbed belts extruded between rock layers growing intensively in the rock mass of left bank slope. Typical features of the weak rocks are shown in Fig. 3.3 with applied supports.

Fig. 3.3 Typical weak rocks in the left abutment slope and the supports

Among the faults, most are in the direction NE~NNE and of large scale. The attitude situates mostly in N30º~50ºE, SE∠60º~80º for the faults with crush width between 1m and 3m, for example the faults f_5, f_8, f_2 and the spot dike(X). Faults in the direction NEE~EW develop secondly, represented by f_{42-9} with attitude EW, S∠40º~60º. Joints are principally developing into three categories: (1) N15º~35ºE, NW∠30º~45º, mainly fractures in the bedding plane; (2) SN~N30ºE, SE∠60º~80º;(3) N50º~70ºE, SE∠50º~80º, mostly rigid structure plane. The assembly of those joints would lead to formation of potential unstable blocks.

The height of the arch dam and other water retaining structures is far less than that of the slope and thus the high-steep slope forms the severe regional environment of the dam abutment buildings. The global stability and local stabilization would have significant influence on potential damage of the dam abutment buildings. Also, the stability of the slope is very important to the security of the arch dam.

Thus it is critical important for the stability analysis and the reinforcement design of the slope. The monitoring system is therefore designed to monitor and safeguard the safety of the slope.

3.2.2 Potential slope instability

The geological weaknesses that would affect the stability of this slope are principally: faults, joint fissures, unloading tension cracks in the rock mass, toppling deformation and deep-seated cracks. The global stability of the left bank slope is dominated originally by the safety of the wedge-shaped block with tensional deformation over the jetty head in the dam area. There would be the potential slipping damage mode for the wedge-shaped block which is formed by the crossing of loose rip zone SL_{44-1}(the upstream boundary), the fault f_{42-9} (the downstream boundary) and the Lamprophyre dike (the trailing edge cutting surface). Typical cracked rocks of the left abutment slope in the arch dam foundation are shown in Fig. 3.4 after slope excavation.

Fig. 3.4 Cracked rocks of left abutment slope in the arch dam foundation after excavation

Fortunately, this failure mode has been blocked thanks to slope reinforcement and treatment. As for local stabilities, the left abutment slope can be divided into three zones with different potential failures according to the slope structure, slope height and the developing degree of weak planes and discontinuities in the rock mass. The potential failures are summarized in Table 3.1 for the left abutment slope(Song et al. 2009).

3.2.3 Slope reinforcement and consolidation

Various kinds of reinforcement and treatment measures are utilized for stabilization of this slope. Water interception and drainage ditches are used in and round the slope excavating zone. The pre-stress anchor cable is used massively for reinforcement on the rip deformation block and potential toppling rock mass. Frame beams or the carlings are installed to join the anchor cables together at the slope positions of fractured rock mass according to the fracture degree of rocks.

Table 3.1 Geological features and potential failures of different zones of the slope

Slope height	Basic geological feature	Descriptive status of the cutting slope	Stability zone	Potential damage
Over 2000m	Sandy slates; reverse slope; moderate crush rock mass; minor faults and extruded inter laminar belts growing	Entire moderate stable; local weak stable in the shallow	C	Toppling-slippage; slippage-rip damage; local wedged unstable
1800m~2000m	The wedged block; sandy slates; reverse slope; weak discontinuities f_5, f_8, X; extruded inter laminar belts and minor faults medially dipped	Entire weak stable; rock mass ripping with severe relaxation	D	Wedged block damage; local toppling-slippage
	Outside the wedge block; sandy slate; reverse slope; weak to strong unloading; moderate crush rocks; minor faults and extruded inter laminar belts growing	Entire moderate stable; local weak stable in the shallow	C	Down slope fracture slipping and crump; local minor wedge block damage
Under 1800m	Marble; reverse slope; moderate intact rock mass; down slope fracture growing	Good stable conditions	A	Down slope fracture slipping and crump; local minor wedge block damage

Hints: in the column of stability zone: A-very stable; B-stable; C-moderate stable; D-weak stable; E-unstable.

The wedge block is originally the critical unstable part of left abutment slope. Grouting replacement is used to treat the fault f_{42-9} in the wedge block with anti-shear tunnels. The fault f_{42-9} is also the weak layer dominating the deformation of the rip deformation block. Thus substituting treatment of the fault f_{42-9} with anti-shear tunnel can largely promote the behavior of shearing resistance of the slope mass. The anti-shear tunnels are installed at the height 1883m, 1860m and 1834m with section size 9m×10m according to the strike of the fault $f_{42-9}$and the dyke of Lamprophyre$X$. The strengthen grooves are settled perpendicularly in the anti-shear tunnels. The upper and lower plates of the anti-shear tunnels are all penetrated into the rock mass with a depth of double tunnel diameter. Anchored bundled bars are installed on the wall and embedded into the upper and lower plates of the tunnels. The anti-shear tunnel is backfilled with reinforced concrete. Replacement and backfill are also used to improve the condition of the fault f_5. The resistant rock mass below the fault f_5 has good stable conditions and can resist the sliding of the rip deformation wedge block. Partial replacement of the faulty f_5 can greatly promote the resistant behavior of the rock mass below the fault f_5. The replacement treatments are conducted at a certain range along the fault f_5 at each pack-way. These treatments have greatly changed the condition of the wedge block and make it not the most vulnerable part for the slope.

Meanwhile, some rock mass are crushed, loose and incised by the faults and fissures, which makes

the integrity and stability of the slope position between the height 1885m and 1960m need to be strengthened by grouting. Typical fissures in the deep of the left abutment slope are shown in Fig. 3.5. Because of gathering decoration of buildings, grouting tunnels cannot be assigned at these positions. The grouting of the fractured rock mass is implemented by the anchor cable holes which can go through deeply in the slope.

Fig. 3.5 Typical fissures in the deep of the left abutment slope

Although the stability of this slope is originally dominated by the compositions of structural planes, the situation has greatly changed due to slope reinforcement and special treatment like excavating and grouting part of the fault f_5 and f_8. These treatments have improved intensively the conditions of the faults and possible failures of the slope would not be controlled by these weak planes anymore.

3.2.4 Category of evaluating factors

There are various kinds of factors that affect rock slope stabilities. These affections are often showing characteristics with randomicity and fuzziness since they would change with time or circumstances and cannot be quantified easily. The impactions of factors have been considered in many classification systems for rating rock mass quality. A rearrangement of the characteristics of the existing rock mass classification systems(Bieniawski 1976; Chen 1995) leads to the following findings: (i) the factors related to the general condition of rock slopes and the condition and geometric characteristics of discontinuities constitute the base of the existing classifications; (ii) the factors

commonly adopted are related to the geometric, excavation and supports of the rock slope; (iii) the factors relevant to the environmental changes such as the precipitation and the seismic characteristics are also listed in most systems. These factors above are all taken into account in this chapter for the stability evaluation of left abutment slope of Jinping 1 Hydropower Station, and named as geological factors, engineering factors and environmental factors, respectively. With the results of different classification systems, it should be convinced that slope stability is related to various factors but all the factors are not needed to be counted for evaluation of slope stability. Only the factors with evident effects need to be taken into account. The three types of factors adopted are shown in Fig. 3.6.

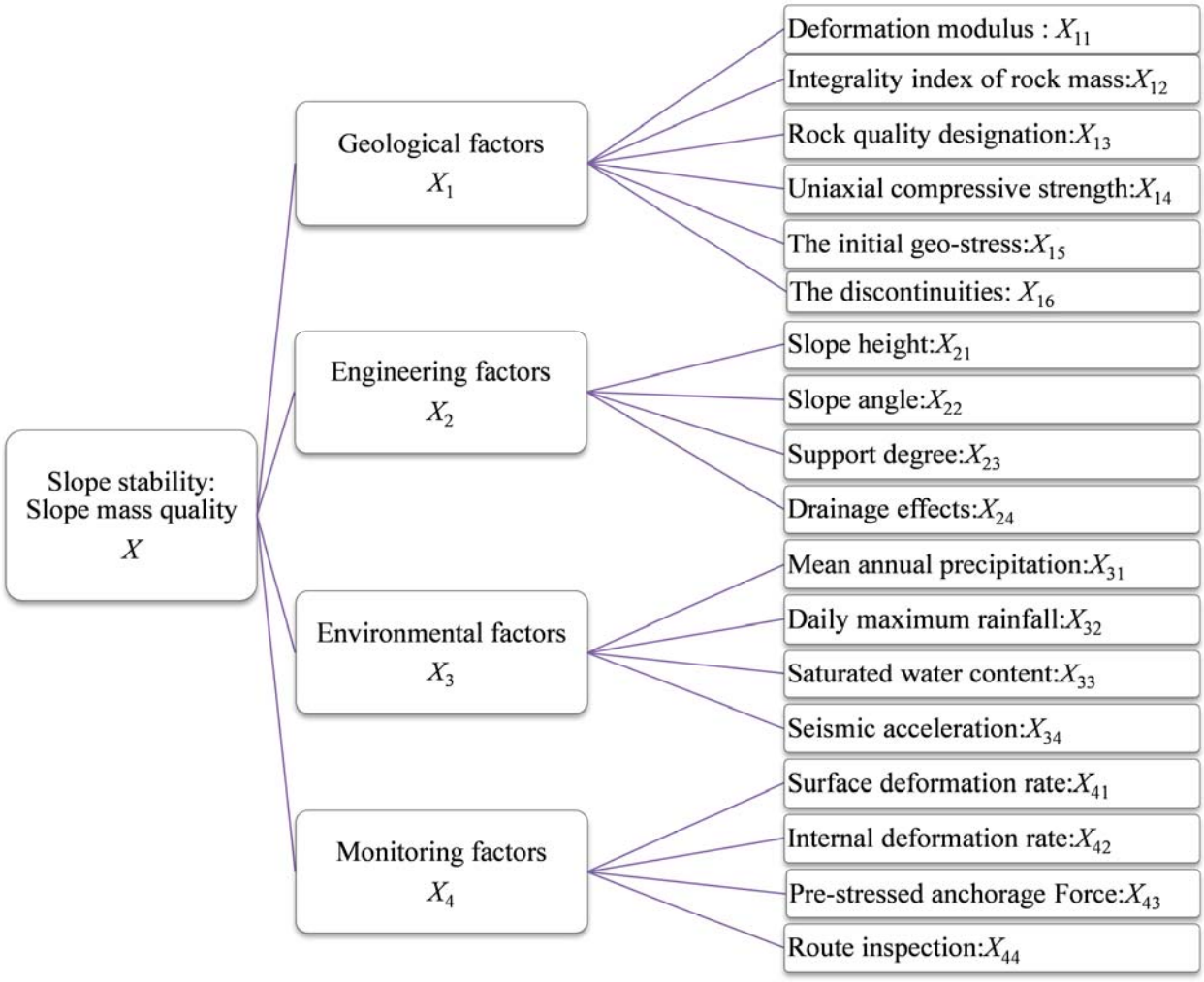

Fig. 3.6 Rating factors for stability assessment of the left abutment slope of Jinping 1

Besides the above three types of factors, the other type of factor come up to be important as a result of usage of field monitoring technologies. The blooming undergoing development of hydro-electricity project in West of China results in more and more huge rock slopes which cannot be pre-controlled so far without filed monitoring data. These slopes, such as the left bank slope of Jinping

1 hydropower station (more than 1000m with 350-500m cuttings), the left/right bank slope of Xiaowan hydropower station (400-700 meters), are quite different from that of Three Georges. No experienced design code can be account for these kinds of slope in China. Thus field monitoring are thought as another efficient way to know well of the slope performance. In this chapter the factors associated with safety monitoring results are also adopted to make the comprehensive evaluation of the left abutment slope. This rock slope is very complicated and the results of field monitoring are thought to be able to provide data for better understanding of the slope. In fact, pre-designs are mostly reinforced and many supplementary designs have been made owing to the results of filed monitoring for the left abutment slope during the construction period. Thus it is necessary to promote the results of safety monitoring for comprehension evaluation of slope stability.

A complete filed monitoring system is installed on the left bank slope of Jinping 1 Hydropower Station to reveal the slope performance during the construction period. The geological, hydrological and environmental factors have been strengthened in field monitoring for the purpose of disaster prevention during constructions. On view that data may not be sufficient enough for pre-designs of the complicated slope in early stage, monitoring results are treated as the supplements for better understanding during the construction period. In this way, monitoring results are to be analyzed for assessment of slope stabilities. In general, there are several kinds of variables that can be monitored in rock slope engineering: (i) displacement, (ii) force, (iii) strain; (iv) the environmental variables. Other variables can be deprived from these basic ones. For example, displacement rate can be derived from the original displacement with changes of the time period. Displacement is the most widely used in safety monitoring for the reason of data availability and reliability. The factors associated with safety monitoring are taken into account and named as four sub-factors shown in Fig. 3.6.

It must be convinced that the stability of the left abutment slope of Jinping 1 Hydropower Station is coupling affected by various factors. The factors shown in Fig.5 are thought to be important as a result of cite characteristics and slope conditions and the effects of them cannot be neglected for stability evaluation.

The parameter “Integrality index” in Fig. 3.6 (also known as velocity index of rock mass) is the quantitative evaluation of the degree of intactness of rock mass. It is calculated as

$$X_{12} = K_v = (V_{pm}/V_{pt})^2 \quad \text{.....(3.1)}$$

where V_{pm} is the velocity of elastic P-wave in the rock mass; V_{pt} is the velocity of elastic P-wave in rock sampling of the corresponding rock mass. If discontinuities exist in the rock mass, then V_{pm} is smaller than V_{pt}. The more and the wider is the discontinuities, the much smaller is V_{pm} than V_{pt}. Thus this parameter, to some extent, can be recognized as an evaluation associated with discontinuities in

the rock mass.

The parameter "Number of joints per m^3" is used to evaluate rock mass integrity on the case of unavailability of the parameter "integrality index". It is calculated as

$$J_v = S_1 + S_2 + \cdots + S_n + S_k \quad \text{.....(3.2)}$$

where J_v is the number of joint per cubic meter; S_n is the number of the n^{th} group of joints counted in the length of one meter; S_k is the number of ungrouped joints per cubic meter. This parameter is also one quantitative way to evaluate the discontinuities in the rock mass.

3.2.5 Classification of the evaluating factors

Each of the factors is classified into five grades in most rock mass classification systems according to the descriptions or the distribution of values. In this chapter, the values of the rating factors are classified into five intervals each of which represents a level of rock mass quality. The classification of geological factors is listed in Table 2 for assessing rock mass quality, including the (i) deformation modulus X_{11}, (ii) the integrity index of rock mass X_{12}, (iii) rock quality designation (RQD)X_{13}, (iv) the uniaxial compressive strength (UCS) X_{14} , (v) initial geo-stress X_{15} , (vi) the condition of discontinuities X_{16}. These factors can be classified into two categories: the physical and mechanical parameters of the rock mass and the conditions of discontinuities. The classification of geological factors is shown in Table 3.2 except for the condition of discontinuities.

The condition of discontinuities is often thought to be important for the stability of slopes in case of presence of discontinuities. Several structural planes, like the f_5, f_8, X mentioned in Table 3.1, go through the left abutment slope of the Jinping 1 Hydropower station which has made it a great challenge for the stability control of the slope without treatments. Thus special treatments have been proposed for reinforcement and stabilization of this slope, such as the re-excavation and grouting of part of the discontinuities f_5, f_8 and the reinforcement with plenty of pre-stressed anchor cables. Those treatments have intensively changed the condition of the discontinuities and thus greatly improved the stability of the slope. Therefore the discontinuities would not be the controlling factor to govern the stability of the left abutment slope with implementation of the special treatments, even though in many cases they are thought to be the main reason for slope instabilities. The classification of discontinuities is shown inTable 3.3.

Table 3.2 Classification of geological factors (X_1)

Rating factor	Rock mass quality level				
	V	IV	III	II	I
Deformation modulus(GPa)	0~1.3	1.3~6.0	6.0~20.0	20.0~33.0	33.0~50.0
Integrality index X_{12}	0~0.15	0.15~0.35	0.35~0.55	0.55~0.75	0.75~1

RQD X_{13}	0~30	30~50	50~75	75~90	90~100
UCS X_{14}(MPa)	0-25	25-50	50-100	100-250	>250
Initial geostress X_{15}(MPa)	20-25	14-20	8-14	2-8	0-2

Table 3.3 Classification of the discontinuities (X_{17})

Rating factor	Rock mass quality level				
	V	IV	III	II	I
Cohesion (Mpa)	0~0.05	0.05~0.08	0.08~0.12	0.12~0.22	0.22~0.32
Friction angle (°)	0~13	13~21	21~29	29~37	37~45
Number of joint per m3: J_V	>35	20~35	10~20	3~10	0~3
Integrity description of rock mass	very bad	bad	moderate	good	Very good

The classification of engineering factors: (i) slope height X_{21}; (ii) slope angle X_{22};(iii) support condition X_{23} ; (iv) drainage condition X_{24} , and environmental factors: (i) mean annual precipitation X_{31}, (ii) daily maximum rainfall X_{32}, (iii) saturated water content of slope X_{33}, (iv) seismic acceleration X_{34}, are discussed by (Li 1997b; Shu et al. 2005; Tan et al. 2009) for the purpose of global slope stability assessment in hydropower projects. The results of classification of engineering factors and environmental factors are shown in Table 3.4 and Table 3.5 respectively. The "initial geo-stress" in Table 3.2 could be recognized as one of the environmental parameters. The geo-stress is mainly formed by crustal movement and the self-gravity of the slope both of which are closely related to the geology of the site characteristics. Thus in this chapter the initial geo-stress is categorized in geological factors.

As mentioned above, a complete monitoring system is installed in the left abutment slope of the project. The monitoring system can provide data on surface deformation and internal deformation of the slope as well as the force of the pre-stressed anchorage. Of course, many other data can also be obtained, such as the data related to anchored bolts, but in this chapter only four kinds of data listed in Table 3.6 are adopted for analysis. This is because these kinds of data have a good duration and can be obtained from the left abutment slope. Generally, the monitoring instruments, like the displacement gauge and the graphite rod convergence gauge, can obtain displacement data; the anchor load meter and the bolt stress meter can obtain force changes in the anchorages or the bolts. For the left abutment slope the surface deformation data are mainly obtained by the monitoring points settled on the slope surface throughout the dam area. The internal deformation rate is calculated from the data acquired by the displacement gauges in the shallow and the graphite rod convergence gauges in the deep-seated position of the slope.

It is not easy to manage the monitoring factors for different rock slopes as a result that the monitoring data varies tremendously for different rock slopes. As recorded by landslide researchers(Li 2004), displacement rate of Huangnashi landslide is 50 mm/month for surface deformation and 10mm/month for inner deformation, while for Xintan landslide it is 85.9~399mm/day. Deformations

of rock slopes are much smaller than that of soil like slopes. And they vary massively as a result of diversity of the rock formations and conditions of the slope. The classification of monitoring factors of the left abutment slope is also discussed by (Tan et al. 2009). The classification results given in Table 3.6 are obtained from monitoring analysis on the longtime monitoring data from the year 2005 to 2010.

Table 3.4 Classification of engineering factors (X_2)

Rating factor	Rock mass quality level				
	V	IV	III	II	I
Slope height X_{21}(m)	80~100	60~80	45~60	30~45	0~30
Slope angle X_{22}(°)	60~75	45~60	35~45	20~35	0~20
Support degree X_{23}	very bad	bad	faire	good	very good
Drainage effects X_{24}	very bad	bad	faire	good	very good

Table 3.5 Classification of environmental factors (X_3)

Rating factor	Rock mass quality level				
	V	IV	III	II	I
Mean annual rainfall X_{31}(mm)	1500~2000	1100~1500	800~1100	600~800	0~600
Daily maximum rainfall X_{32}(mm)	100~150	70~100	50~70	25~50	0~25
Saturate water content X_{33}(%)	75~100	55~75	40~55	20~40	0~20
Seismic acceleration X_{34}(m/s2)	0.20~0.40	0.15~0.20	0.1~0.15	0.05~0.1	0~0.05

Table 3.6 Classification of monitoring factors (X_4)

factors	Slope rock mass quality level				
	V	IV	III	II	I
Surface deformation rate X_{41}(mm/month)	8~10	5~8	3~5	2~3	0~2
Internal deformation rate X_{42}(mm/month)	2~3	1.5~2	0.8~1.5	0.3~0.8	0~0.3
Pre-stressed anchorage force X_{43}(%)	25~30	20~25	15~20	8~15	0~8
Route inspection of slope condition X_{44}	very bad	bad	moderate	good	very good

3.2.6 Rock slope stability classification

In this chapter we think that slope stability is depending on slope mass quality which includes rock mass quality, slope condition and monitoring results. The result of slope stability assessment is mainly used to guarantee the safety of the slope and for possible slope reinforcement or re-excavation. The stability of rock slope is also classified into five levels according to the comprehensive evaluating results of slope mass quality. The final comprehension level of rock mass quality indicates the corresponding class of slope stability. The classification of rock slope is shown in Table 3.7 with empirical descriptions of slope conditions and possible treatments for reinforcement.

Table 3.7 Rock slope stability classification and the empirical descriptions

Class No.	V	IV	III	II	I
Description	Very bad	Bad	Fair	Good	Very good
Stability	Completely unstable	Unstable	Partially stable	Stable	Completely stable
Safety	Dangerous	Unsafe	Moderate safe	Safe	Completely safe
Failures	Big planar of soil-like	Planar or big wedges	Some joints or many wedges	Some Blocks	None
Treatment	Re-excavation	Important/corrective	Systematic	Occasional	None

3.3 Methodology—Cloud model and weighted AHP

3.3.1 Cloud model

Cloud model is defined as the uncertain transformation model between the qualitative concept expressed by linguistic terms and the corresponding quantitative representation expressed by three numerical descriptors(Liu et al. 2004). The normal cloud model is fundamental in cloud theory. The normal cloud model is quite different from a normal distribution and the universality of normal cloud has been proved theoretically(Li et al. 1998c). The normal cloud model conveys the numerical features of the qualitative concept with a group of independent parameters to represent the uncertainties. The parameters are named as the numerical descriptors of cloud model including the expectation E_x, the entropy E_n and the hyper entropy H_e. It represents the overall quantitative features of the qualitative concept and is used to describe the mathematical properties of linguistic terms. There are bell-shaped cloud as well as the half bell-sharp cloud and trapezium sharp cloud which is called the half cloud and trapezoidal clouds, respectively(Li et al. 1998c). The cloud model proved to be an effective tool for application in data mining(Li et al. 2000b) and uncertainty reasoning(Li et al. 1998a) as well as time series prediction(Zhang and Hu 2003). The results of these applications have greatly proven the applicability of cloud models.

An example of cloud membership is shown comparatively with the membership function of fuzzy set in Fig. 3.7 for the linguistic term “numbers close to zero”. The result of membership function is a definite curve but that of the membership cloud is formed by lots of cloud drops. The micro-features of membership cloud may differ randomly with time, while it can truly describe the overall features of the concept with the outline of the clouds. Cloud model does not emphasize on the precision of function denoting and it realizes the uncertainty reasoning by the outline of clouds of the concept. In general, the membership cloud can randomly generate the cloud drops and the outline of the all cloud drops can be recognized similarly as the membership function in fuzzy sets. A cloud drop naturally belongs to a cloud model representing certain linguistic concepts with cloud membership values from the interval [0, 1].

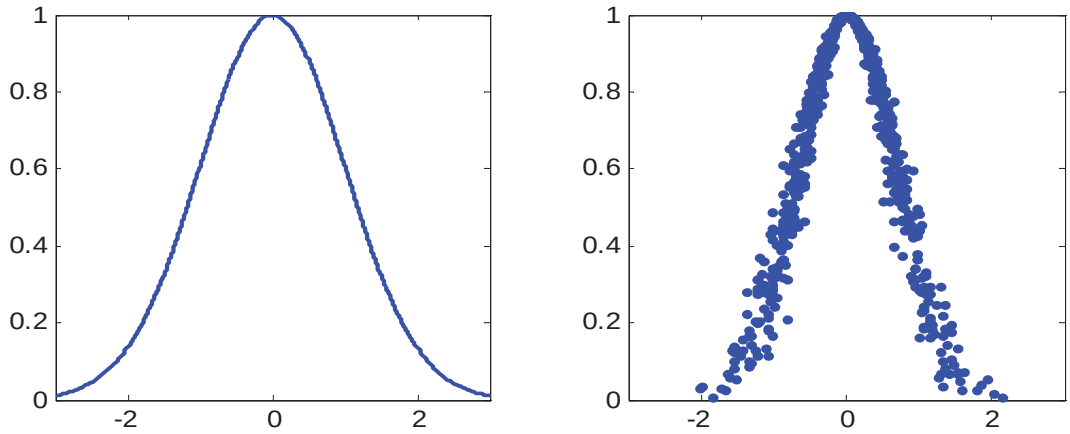

Fig. 3.7 Membership function and the membership cloud for "numbers close to zero"

3.3.2 Cloud generators

Cloud models are executed by cloud generators. There are generally two kinds of cloud generators: the forward and the backward cloud generators. The forward cloud generator is used to generate the cloud drops $P(x_i, \mu_i)(i = 1,2, \cdots n)$ given the cloud descriptors $N(E_x, E_n, H_e)$, which is the transformation from the qualitative knowledge to the quantitative representation and denoted with CG. And the backward generator is the transferring process to derive the qualitative concept represented by three descriptors from cloud drops $P(x_i, \mu_i)(i = 1,2, \cdots n)$, which is denoted with CG^{-1}. The forward and backward cloud generators are shown in Fig. 3.8. The combinations of the two kinds of generators can be used interchangeably to derive various kinds of clouds to bridge the gap between the qualitative concept and the quantitative knowledge. It is obvious that approximations should be taken if only a few cloud drops are given for backward cloud generators. The more cloud drops the more accurate to generate the three numerical descriptors $N(E_x, E_n, H_e)$.

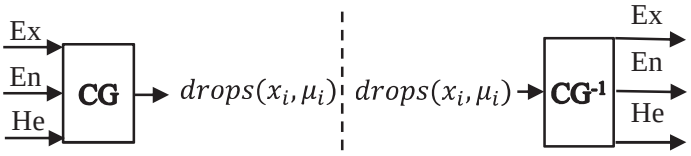

Fig. 3.8 Process of forward generator and backward generator

Given the three numerical descriptors of cloud and the specified $x = x_0$, the combination to generate the cloud drops $drop(x_0, \mu_i)$ is called the front-condition cloud generator or the X-condition cloud; given the three numerical descriptors of cloud and the specified $y = \mu_i$, the combination to generate the cloud drops $drop(x_i, \mu_i)$ is named as back-condition cloud generator or the Y-condition cloud. The X-condition and Y-condition cloud generator are both shown in Fig. 3.9.

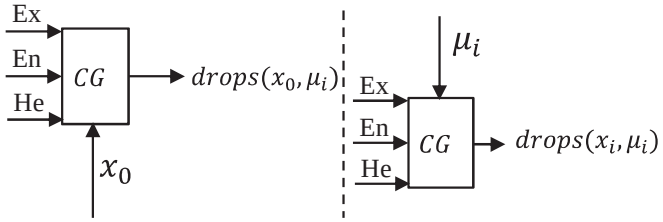

Fig. 3.9 Graphic expression of X-condition and Y-condition cloud

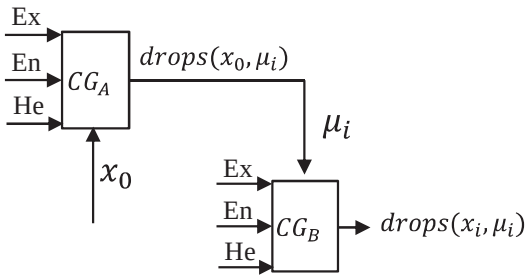

Fig. 3.10 Reasoning generator of one condition and one rule

Cloud generators are fundamental for uncertainty reasoning with cloud models. The combination of X-condition cloud and Y-condition cloud can be structured to obtain the reasoning generator for the rules like "IF A THEN B", which can be named as one condition and one rule generator. As shown in Fig. 3.10, if the input x_0 activates the forward generator CG_A, a certainty μ_i, which denotes the intensity of input x_0 to activate the qualitative rule, will be randomly generated by CG_A; meanwhile μ_i is an input of cloud generator CG_B and thus a cloud drop (x_i, μ_i) will be produced randomly. The qualitative rule structured by cloud models makes the hereditability and transitivity of reasoning system favorable. The generators with multiple conditions and multiple rules can be obtained in the similar way of structuring one condition and one rule generator.

Cloud models can accept input data and generate output knowledge with the cloud generators above. For example, x_0 can be the parameter value of a rating factor in Fig. 3.6; μ_i can be the cloud membership of x_0 to different cloud models representing different rock mass quality levels. The outputs of cloud models are cloud memberships which represent the quality level of each factor and can be used for further analysis on comprehension evaluation.

3.3.3 Cloud transformation

Cloud transformation is the process utilizing cloud models to represent continuous data intervals. It can also be named as cloudification in the similar way of fuzzification in fuzzy theory. It can transform data from the original data space to cloud model space. As stated above cloud models can be

represented by the numerical descriptors (E_x, E_n, H_e) thus the process of cloud transformation is to make up and identify the values of (E_x, E_n, H_e) from the original data. There are many different methods to execute cloud transformation. The numerical descriptors of the cloud models can be obtained as follows, given that the features of the data in Table 3.2~Table 3.6 in can be treated as data intervals.

Assume that data in the universe of discourse U after normalization can be divided into n grades denoted as $\{C_1, C_2, \ldots, C_{\mathrm{n}}\}$, and the corresponding data set is $[0, a_1], [a_1, a_2], \ldots, [a_{\mathrm{n}-1}, 1]$, then the numerical descriptors of each cloud model representing a concept can be obtained by the following expressions (3.3). Given the three numerical descriptors of each level, n cloud models could be generated with the forward cloud generator shown in Fig. 3.8.

$$\begin{cases} C_1 & Ex_1 = 0 & En_1 = a_1/3 & He_1 = k \\ C_2 & Ex_2 = (a_1 + a_2)/2 & En_2 = (Ex_2 - \frac{3}{2}En_1)/3 & He_2 = k \\ C_3 & Ex_3 = (a_2 + a_3)/2 & En_3 = (Ex_3 - \frac{3}{2}En_2)/3 & He_3 = k \\ \cdots & \cdots & \cdots & \cdots \\ C_n & Ex_n = 1 & En_n = (Ex_n - Ex_{n-1})/3 & He_n = k \end{cases} \quad \ldots\ldots\ldots\ldots (3.3)$$

Note that normalization of data should be implemented before cloud transformation. Data normalization is executed mainly to get rid of the influence of dimensions of different kinds of data. It makes the data dimensionless and thus they can be treated under the same rule. It can be executed with either of the two methods below depending on the effects of the factors to slope rock mass quality. If the larger is the value of the factors, the more positively it contributes to rock mass quality, then normalization of data can be executed as

$$x'_{ij} = \frac{x_{ij} - x_{i\max}}{x_{i\max} - x_{i\min}} \quad (3.4)$$

Otherwise

$$x'_{ij} = \frac{x_{i\max} - x_{ij}}{x_{i\max} - x_{i\min}} \quad (3.5)$$

In the above expression, x'_{ij} is the normalized value of factors; x_{ij} is the original value of factors; $x_{i\max}$ and $x_{i\min}$ are the maximum value and the minimum value of the factors, respectively. After execution of the above normalization, the values of the factors are transferred in the interval [0, 1] for the quantitative data.

Also, for the qualitative data of descriptive factors it can be assumed that each grade of description contributes the same weight. Thus, the value of each level can be obtained in the form of subinterval of [0, 1] for the five level assessment of rock slope stability.

Production process of cloud memberships are shown in Fig. 3.11.

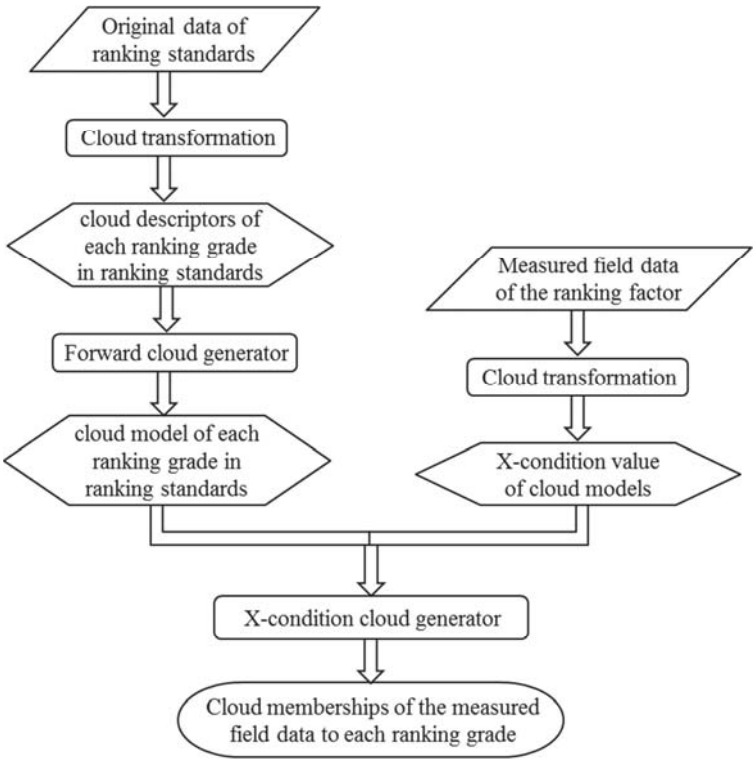

Fig. 3.11 Production of cloud memberships

3.3.4 Comprehensive evaluation based on weighted AHP

The cloud memberships of each factor can only represent the evaluating level of slope mass quality according to data of the unique factor. Rock slope stability is coupling affected by all the related factors. Each of the factors only contributes its portion and has a different weight for the final result of slope stability. The stability status of rock slope is the comprehensive result caused by these factors with different weights. Thus comprehensive assessment as well as variant weight analysis is needed for all the factors that have evident effects on rock slope stability. The weight values of all the factors can form a weight matrix. The weight matrix is generally specified according to experts' opinions and evaluations on the factors.

Each rating factor will have a rating class of rock mass quality according to the classifications in Table 3.2~Table 3.6 given the data of the slope at a time. The comprehensive classification of all factors results in an overall evaluation of the slope rock mass quality which determines the stabilities of the rock slope. The classification of each rating factor is represented with cloud models which can blur the boundaries between the adjacent classes. Each classification result is given in the form of a cloud membership vector. As it is shown in Fig. 3.6, the structure of the rating factors is multi-level with the structure of three hierarchies. The comprehensive assessment of slope stability could be recognized as a typical decision-making problem. This problem can be analyzed with the Analytic Hierarchy Process(AHP) (Saaty 1980)with different weights of the elements. The final assessment of

slope stability class is given by a cloud membership vector but a single value in this chapter, which is similar to the result of fuzzy set theory. The implementing procedure of the approach introduced in this chapter is shown in Fig. 3.13.

Given the value of the factors $x_{ij} = x_0(i = 1,2,3,4; j = 1,2,\cdots,n, n = 4\ or\ 6)$ in Fig. 3.6, the cloud membership $\mu_{ij} = U_S(x_{ij})(S = \mathrm{I, II, III, IV, V})$ of each factor to a certain rock mass quality level can be calculated with X-condition cloud generator. This cloud membership $U_S(x_{ij})$ represents the evaluating result of rock mass quality according to the factor X_{ij} when $x_{ij} = x_0$, which can only determine the grading level of a single factor but cannot evaluate the effects of all factors working together. Therefore, a comprehensive evaluation is in need to make out a final result of slope rock mass quality with all the factors. These factors are managed into three hierarchies shown in Fig. 3.6, where slope mass quality, four kinds of factor categories and the 18 basic factors are listed in the bottom, in the middle and in the bottom, respectively. On the basis of the cloud membership values of the basic factors

$$R_{Xi} = U_S(i) = [U_S(i1), U_S(i2), \cdots, U_S(in)]^{\mathrm{T}} \quad \text{..... (3.6)}$$

If the weight matrix W_{Xi} is obtained for the factors in the bottom hierarchy, the cloud membership of the factors in the middle hierarchy can be calculated

$$R_X = B_{Xi} = W_{Xi} \oplus R_{Xi} \quad \text{.....(3.7)}$$

Then similarly, if the weight matrix W_X of the factors in the middle level is given, the comprehension of cloud membership of slope rock mass quality in the top hierarchy can be computed as

$$B_X = W_X \oplus B_{Xi} \quad \text{.....(3.8)}$$

In the above expression, i is the category number; j is the factor number in the i^{th} category; S is the quality level of factors. The symbol $\oplus$ is fuzzy operator. The final result is calculated as a vector of cloud memberships.

The implementation of the strategy is shown in Fig. 3.12.

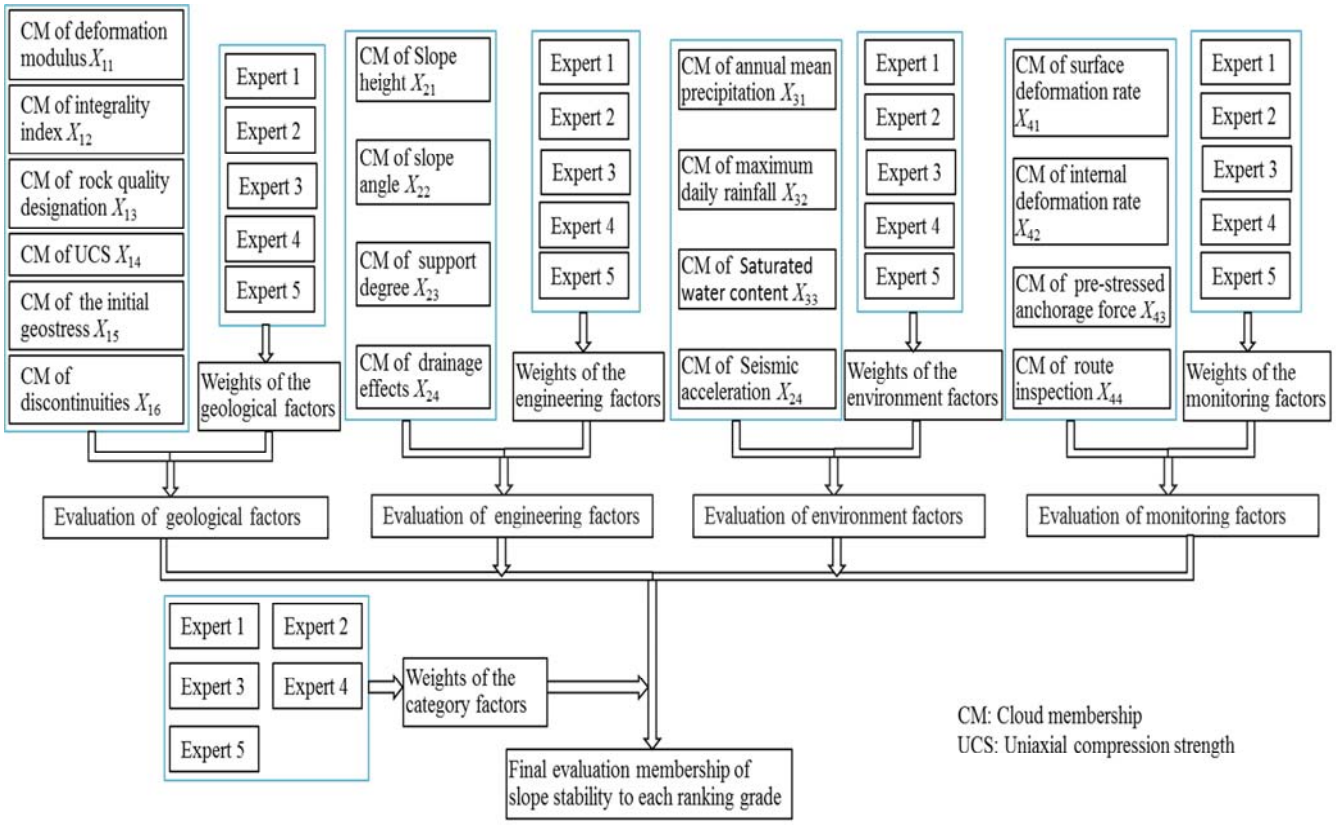

Fig. 3.12 Graphic view of the comprehensive evaluation

3.4 Stability assessment of the left abutment slope of Jinping 1

3.4.1 Slope data collection

The left abutment slope is about 110m high over the platform of the dam crest of height 1885m. The rock formations are consisted of Triassic metamorphic rocks and the strike of the rock formation is mainly in the direction of N70°E. As stated in Section 3.2, the overall attitude of the rock formation is N15~35°E, NW∠30~45° in the dam abutment area. The rock faults f_{42-9}, f_5 and the lamprophyre rock dike X go through the dam area in the left abutment slope. The data of the geological factors are obtained by field measurements or laboratory test of the rock samples. These results are given in Table 3.8.

As for the qualitative factors, like the support degree and drainage effect, evaluations are usually given empirically by experts or engineers in the form of linguistic language. In this chapter, the five quality levels of qualitative factors (V, IV, III, II, I) are represented quantitatively by each of the five data intervals [0.0, 0.2), [0.2, 0.4), [0.4, 0.6), [0.6, 0.8), [0.8, 1.0], respectively. In this way, the data can be treated easily in a cloud model without the effect of sorting dimension. Each expert invited to give his empirical value describing the quality of the qualitative factors of this slope. The final result of each factor is then calculated from the average of all experts' evaluation values. These results are also given

in Table 3.8. Data in the column “Original” are originally obtained by various measurements and tests; Data in the column “Cloudification” are the corresponding results of original data after cloudification.

Table 3.8 Original data and the cloudification values of the factors of left abutment slope

Evaluation Factor	Original	Cloudification	Evaluation factor	Original	Cloudification
Deformation modulus	1.9GPa	0.038	Support degree	0.70	0.700
Integrality index of rock mass	0.72	0.720	Drainage effect	0.75	0.750
Rock quality designation	85%	0.850	Mean annual precipitation	607mm	0.697
Wet uniaxial compressive strength	105Mpa	0.131	Daily maximum rainfall	49.2mm	0.672
The initial geo-stress	21.49Mpa	0.140	Water content	13%	0.130
Cohesion of discontinuity	0.02Mpa	0.063	Seismic acceleration	0.1g	0.750
Internal friction angle of discontinuity	16.7°	0.371	Surface deformation rate	1.89mm/m	0.811
Joint number	17/m3	0.283	Internal deformation rate	0.27mm/m	0.910
Integrity description of rock mass	0.60	0.600	Prestressed anchorage force	8.73%	0.709
Slope height	110m	0.000	Route inspection	0.75	0.750
Slope angle	50°	0.375			

3.4.2 Data cloudification

Classifications data in Table 3.2~Table 3.6can be processed with cloud transformation in order to obtain the numerical descriptors of each cloud model. Eq(4.4) or (4.5) is firstly applied to normalize the data so that they could be processed under the same space. Then Eq(4.3) is applied to derive the three numerical descriptors of each cloud model representing one level of the classifications of the factors. And the results are given in Table 3.9. The cloud models of each factor can be generated with the numerical descriptors in Table 3.9 by means of cloud generators shown in Fig. 3.9. Also, Eq(3.4) or (3.5) is applied for cloudification of the original data in Table 3.8 to be well accorded with the form of classification data for cloud models.

3.4.3 Calculation of cloud membership

As stated in Fig. 3.6, cloud membership can indicate the features of both fuzziness and randomness of a cloud drop to a certain cloud model. Calculation of cloud membership is one of the key parts for application of cloud models. Hereby as an example, the cloud membership of the mean annual precipitation X_{31} is calculated in detail. The cloud memberships of other factors can be computed in the same way.

Table 3.9 Cloudification results of the classification data of the factors

factors \ level	V	IV	III	II	I
X11	(0,0.052,0.003)	(0.203,0.042,0.003)	(0.313,0.036,0.003)	(0.531,0.073,0.003)	(1,0.156,0.003)
X12	(0,0.096,0.003)	(0.378,0.078,0.003)	(0.556,0.059,0.003)	(0.733,0.059,0.003)	(1,0.089,0.003)
X13	(0,0.050,0.003)	(0.250,0.058,0.003)	(0.450,0.067,0.003)	(0.650,0.067,0.003)	(1,0.117,0.003)
X14	(0,0.100,0.003)	(0.400,0.083,0.003)	(0.625,0.075,0.003)	(0.825,0.067,0.003)	(1,0.058,0.003)
X15	(0,0.100,0.003)	(0.400,0.083,0.003)	(0.625,0.075,0.003)	(0.825,0.067,0.003)	(1,0.058,0.003)
X16	(0,0.080,0.003)	(0.320,0.073,0.003)	(0.560,0.080,0.003)	(0.800,0.080,0.003)	(1,0.067,0.003)
X21	(0,0.080,0.003)	(0.300,0.067,0.003)	(0.475,0.058,0.003)	(0.625,0.050,0.003)	(1,0.125,0.003)
X22	(0,0.080,0.003)	(0.300,0.067,0.003)	(0.467,0.056,0.003)	(0.633,0.056,0.003)	(1,0.122,0.003)
X23	(0,0.067,0.003)	(0.300,0.067,0.003)	(0.500,0.067,0.003)	(0.700,0.067,0.003)	(1,0.100,0.003)
X24	(0,0.067,0.003)	(0.300,0.067,0.003)	(0.500,0.067,0.003)	(0.700,0.067,0.003)	(1,0.100,0.003)
X31	(0,0.083,0.003)	(0.350,0.075,0.003)	(0.525,0.058,0.003)	(0.650,0.042,0.003)	(1,0.117,0.003)
X32	(0,0.111,0.003)	(0.433,0.089,0.003)	(0.600,0.056,0.003)	(0.750,0.050,0.003)	(1,0.083,0.003)
X33	(0,0.083,0.003)	(0.350,0.075,0.003)	(0.525,0.058,0.003)	(0.700,0.058,0.003)	(1,0.100,0.003)
X34	(0,0.167,0.003)	(0.563,0.104,0.003)	(0.688,0.042,0.003)	(0.813,0.042,0.003)	(1,0.063,0.003)
X41	(0,0.067,0.003)	(0.350,0.083,0.003)	(0.600,0.083,0.003)	(0.750,0.050,0.003)	(1,0.083,0.003)
X42	(0,0.111,0.003)	(0.417,0.083,0.003)	(0.617,0.067,0.003)	(0.817,0.067,0.003)	(1,0.061,0.003)
X43	(0,0.056,0.003)	(0.250,0.056,0.003)	(0.417,0.056,0.003)	(0.617,0.067,0.003)	(1,0.128,0.003)
X44	(0,0.067,0.003)	(0.300,0.067,0.003)	(0.500,0.067,0.003)	(0.700,0.067,0.003)	(1,0.100,0.003)

Hints：The value of hyper entropy for each cloud model is 0.003; the level V and I is described by the left and right part of cloud, respectively.

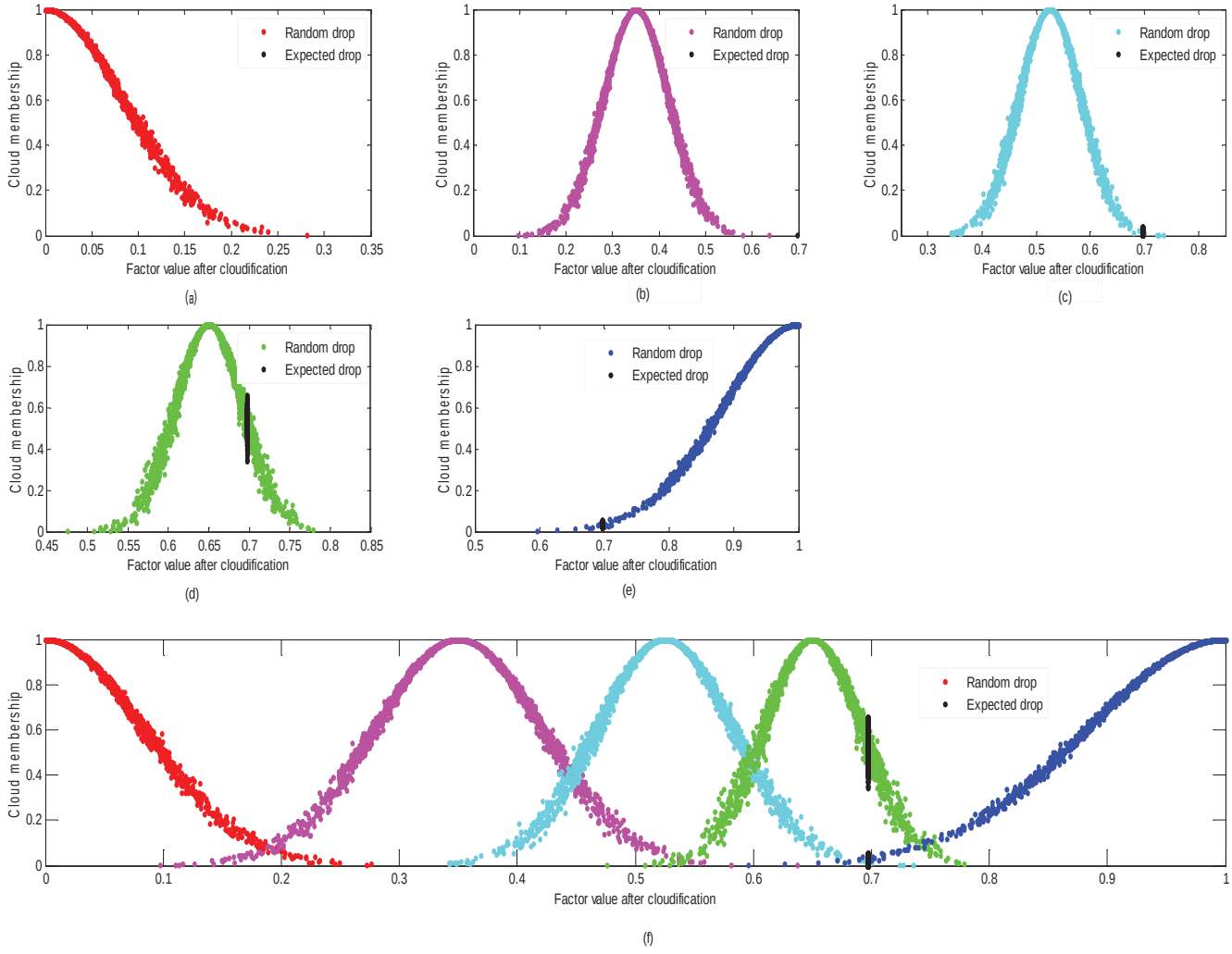

Fig. 3.13 Cloud model of each level of the factor X_{31} and the generation of membership

According to the numerical descriptors of X_{31} given in Table 3.9, the graphs of the cloud model of each quality level of the factor X_{31}can be generated as shown in Fig. 3.13. The subfigure (a), (b), (c), (d) and (e) in different color represent the concept that slope mass quality is level V, level VI, level III, level II and level I, respectively. If the value of the factor is given, its cloud membership to a certain quality level can be calculated by X-condition cloud generator. And thus the rating quality level is obtained for this factor.

The mean annual precipitation X_{31} is 607mm which is 0.697 after cloudification. Then the input $x_0 = 0.697$ is preceded as an input of each cloud model to generate cloud drops with X-condition cloud generator. For the cloud models of level V and IV, no cloud drops can be shown for $x_0 = 0.697$ since $x_0 = 0.697$ is too far from its counting range which depends on the numerical descriptors. It should be noted that there may be several cloud drops generated due to randomicity of cloud models. For the cloud models of level III, level II and level I, each can generate some cloud drops shown in figure 5 with $x_0 = 0.697$ as input. Different cloud memberships μ_i of x_0 to each level can be calculated randomly as outputs of X-condition cloud generator. Two ways can be chosen to determine the final cloud membership μ_i : $\mu = Average(\mu_i)$ or $\mu = Maximun(\mu_i)$. The former way is adopted in this chapter. As displayed in Fig. 3.13, the cloud memberships of X_{31} are calculated originally as $U = (0.0000, 0.0000, 0.0138, 0.5277, 0.1670)$. To normalize the cloud memberships, the corresponding values of memberships are obtained as $U_V(X_{31}) = 0, U_{IV}(X_{31}) = 0, U_{III}(X_{31}) = 0.019$, $U_{II}(X_{31}) = 0.745, U_I(X_{31}) = 0.236$. The value of cloud memberships of the other factors can be calculated in the similar way and the results are given in Table 3.10.

The figures are obtained with X-condition cloud generator of the factorX_{31}. Figure(a) represents the quality level V of X_{31} with CG (0, 0.08333,0.003); figure(b) represents the quality level IV of X_{31} with CG (0.35, 0.07083, 0.003; figure (c) represents the quality level III of X_{31} with CG (0.525, 0.058333, 0.003); figure(d) represents the quality level II of X_{31} with CG (0.65, 0.041667, 0.003); figure(e) represents the level I of $X_{31}$with CG(1, 0.155, 0.003). Figure (f) is the comprehension of all the levels of X_{31}. All these figures are generated under the same condition $X_{31} = x_0 = 0.697$.

Table 3.10 Cloud membership values of all factors

Level / Factors	V	IV	III	II	I
X11	0.027	0.973	0.000	0.000	0.000
X12	0.018	0.954	0.028	0.000	0.000
X13	0.000	0.000	0.000	0.107	0.893
X14	0.000	0.000	0.003	0.475	0.522
X15	0.000	0.000	0.000	0.027	0.973
X16	0.782	0.218	0.000	0.000	0.000
X21	1.000	0.000	0.000	0.000	0.000

X22	0.915	0.085	0.000	0.000	0.000
X23	0.000	0.000	0.035	0.930	0.035
X24	0.000	0.000	0.003	0.932	0.065
X31	0.000	0.000	0.019	0.745	0.236
X32	0.000	0.026	0.396	0.550	0.028
X33	0.000	0.000	0.001	0.025	0.974
X34	0.000	0.077	0.431	0.458	0.034
X41	0.000	0.000	0.035	0.391	0.574
X42	0.000	0.000	0.029	0.426	0.545
X43	0.000	0.000	0.002	0.823	0.175
X44	0.000	0.000	0.016	0.616	0.368

3.4.4 Weighted AHP analysis

The weight matrix in this chapter is obtained from the evaluating results of 7 experts from different design institutes and universities who have taken part in work associated with this slope project. The evaluating results are given in Table 3.11.

Table 3.11 Assembly weight of evaluation factors

Impact factors	Assembly weight
X	AX=(0.321,0.232,0.221,0.226)
X1	AX1=(0.155,0.158,0.171,0.173,0.180,0.163)
X2	AX2=(0.207,0.229,0.288,0.276)
X3	AX3=(0.266,0.240,0.263,0.231)
X4	AX4=(0.236,0.264,0.239,0.262)

Due to the multi-layer structure of the rating factors shown in Fig. 3.6, calculation of the comprehensive evaluation matrix of cloud model should be executed first for the four categories in the middle hierarchy. It follows as

$$R_{X1}=\begin{bmatrix} U_{\mathrm{S}}(X_{11}) \\ U_{\mathrm{S}}(X_{12}) \\ \vdots \\ U_{\mathrm{S}}(X_{16}) \end{bmatrix}=\begin{bmatrix} U_{\mathrm{I}}(X_{11}) & U_{\mathrm{II}}(X_{11}) & \cdots & U_{\mathrm{V}}(X_{11}) \\ U_{\mathrm{II}}(X_{12}) & U_{\mathrm{II}}(X_{12}) & \cdots & U_{\mathrm{V}}(X_{12}) \\ \vdots & \vdots & \cdots & \vdots \\ U_{\mathrm{V}}(X_{16}) & U_{\mathrm{II}}(X_{16}) & \cdots & U_{\mathrm{V}}(X_{16}) \end{bmatrix}$$

$$=\begin{bmatrix} 0.027 & 0.973 & 0 & 0 & 0 \\ 0.018 & 0.954 & 0.028 & 0 & 0 \\ 0 & 0 & 0 & 0.107 & 0.893 \\ 0 & 0 & 0.003 & 0.475 & 0.522 \\ 0 & 0 & 0 & 0.027 & 0.973 \\ 0.782 & 0.218 & 0 & 0 & 0 \end{bmatrix}$$

In the similar way, the value of R_{X2}, R_{X3}, R_{X4} can be obtained according to the data in Table 3.10. Taking account the weight matrix, the following results can be achieved

$$B_{X1} = A_{X1} \oplus R_{X1} = [0.281 \quad 0.191 \quad 0.005 \quad 0.105 \quad 0.418]$$

$$B_{X2} = A_{X2} \oplus R_{X2} = [0.407 \quad 0.029 \quad 0.011 \quad 0.525 \quad 0.028]$$

$$B_{X3} = A_{X3} \oplus R_{X3} = [0.000 \quad 0.024 \quad 0.200 \quad 0.443 \quad 0.333]$$

$$B_{X4} = A_{X4} \oplus R_{X4} = [0.000 \quad 0.000 \quad 0.021 \quad 0.561 \quad 0.418]$$

In the above expression, the average weighting operator denoted by $M(+,\cdot)$ is chosen for the fuzzy operator calculation. The average weighting operator can cover the effect of a unique factor as well as the overall effects of all factors.

Therefore, the matrix R_X representing effects of the factors in the middle hierarchy can be expressed as

$$R_X = \begin{bmatrix} B_{X1} \\ B_{X2} \\ B_{X3} \\ B_{X4} \end{bmatrix} = \begin{bmatrix} 0.281 & 0.191 & 0.005 & 0.105 & 0.418 \\ 0.407 & 0.029 & 0.011 & 0.525 & 0.028 \\ 0.000 & 0.024 & 0.200 & 0.443 & 0.333 \\ 0.000 & 0.000 & 0.021 & 0.561 & 0.418 \end{bmatrix} \quad \text{.....(3.9)}$$

Similarly, if the weight matrix is given, the final evaluation result can be calculated as

$$B_X = A_X \oplus R_X = [0.185 \quad 0.073 \quad 0.053 \quad 0.380 \quad 0.309] \quad \text{.....(3.10)}$$

The elements in the vector B_X represent the quality level of rock slope mass. The larger of the element value, the more likely is the slope mass to the corresponding quality level. The elements in B_X indicate that the discussed slope mass quality is most likely situating in quality level II and I.

3.4.5 Discussion

As shown above, the final evaluating result is obtained by means of cloud model and weighted AHP analysis. Factors in the bottom hierarchy are firstly analyzed by cloud models with cloud generators which make out the cloud memberships for each associated factor. Then these cloud memberships are synthesized by means of AHP analysis with variant weights. Then the final membership vector is made out to represent the slope quality level which can be accounted for slope stability.

The final cloud membership vector B_X indicates the comprehensive effect of all factors to influence slope stability. It can be drawn from the evaluation result B_X that the maximum membership is 0.380 of level II with a small difference 0.072 of the level I. The membership value of other levels is much smaller than that of level II and I. Thus the stability status of the left bank slope upper the height

1885m of Jinping 1 hydropower station is firstly close to level II (stable) and secondly close to level I (completely stable). If the maximum membership method is applied to give the final evaluation of level II (stable), too much information will be omitted. Thus other methods should be applied to give more proper explanations. According to the final cloud membership vector, the value of cloud membership is 0.380 and 0.309 for the stability level II and level I respectively; the cloud membership of the level V, IV and III add up to 0.311, it can be concluded that the stability status at present is between level II and level I, and squint towards level II. This result is more practical than that of the maximum membership method for the special purpose of slope reinforcement and treatments.

The study carried out by (Hydro-China 2008) on numerical modeling of this slope showed that the stability of the slope would improve greatly as a result of slope reinforcement and treatment measures. And due to grout replacement, the weak planes would not be the controlling factors to trigger potential slope failures. This is essential to apply the proposed approach to stability evaluation of the rock slope. They concluded that the stability of this slope would be lying in class I in normal situations and class II in seismic condition with earthquake intensity less than M8.0. Moreover, field monitoring and manual inspection have all proved that at present this slope is under good situation of stability. These results have good consistency with that of the approach presented in this chapter.

Some extra results can be found from the cloud membership values of the four rows in R_X. The first row denotes the effects of geological factors, and the other three rows denote the effects of engineering factors, environmental factors and monitoring factors, respectively. The values of memberships in the first row indicate that the quality of geological factors is most likely of level I with moderate possibility of level V and IV. This result is caused by the divergence of evaluating the results of the single factors. The second row indicates that the quality engineering factors have large divergent evaluating results. This result is caused by the super slope height and proper slope treatment. The membership values show that the slope reinforcement and treatment have greatly improved the situation of the slope. The membership values in the second row show this slope is under good environment favorable to slope stability. And the memberships of the monitoring factors show that this slope is under very good situation of stability.

It would be interesting to discuss the effects of monitoring factors. The cloud memberships have nothing in crossing for the factors in the bottom hierarchy and thus the effects of the four categories (geological factors, engineering factors, environmental factors and monitoring factors) are obtained independently. If the monitoring factors are not taken into account, the matrix R_X would be

$$R_X^{'} = \begin{bmatrix} B_{X1} \\ B_{X2} \\ B_{X3} \end{bmatrix} = \begin{bmatrix} 0.281 & 0.191 & 0.005 & 0.105 & 0.418 \\ 0.407 & 0.029 & 0.011 & 0.525 & 0.028 \\ 0.000 & 0.024 & 0.200 & 0.443 & 0.333 \end{bmatrix} \quad \text{.....(3.11)}$$

The relative weight contributions of the other factors keep the same, it would be obtained $A'_X = (0.415, 0.300, 0.285)$. Then final evaluation result will be

$$B'_X = A'_X \oplus R'_X = [0.241, 0.094, 0.062, 0.327, 0.276] \quad \text{.....(3.12)}$$

Each membership in B'_X indicates the probability of the slope mass belongs to the corresponding quality level. It can be observed that the memberships in B_X and B'_X are variant especially for that of level V. The membership of level V in B'_X contributes much more than that in B_X. This result gives out a much larger probability of the left abutment slope to situate in quality level V than that of considering the monitoring factors, which is not accord with the real situation of the slope at present. In fact, the situation of the slope will not change at all whether the monitoring factors are considered. Taking account the monitoring factors have reduced the weight of other factors. Thus, taking account the monitoring factors are more reasonable to give out a proper evaluation result of the stability and safety of this rock slope. Of course, these evaluating results are greatly related with the classifications of the factors. Thus it's very important to progress the classifications of the factors constantly.

3.4.6 Comparison and validation

The research work has been conducted by (Kang et al. 2009)on the stability features of this slope from the view of monitoring behaviors. The deformation trend, spatial distribution and the relationship between the deformation and the excavation were investigated in the study. They concluded that the excavating activities influenced the deformation of the slope with a very high depth (more than 80 meters deep in the slope). They also concluded that the stress releasing process of the slope would continue and not come to be completely stable in a short time. In all, their study showed that this slope would be in a good global stability status with some local stability problems. These local stability problems would be probably caused by the influence of stress releasing of the rock mass as a result of the excavation activities. After the excavations, this slope will be in good stability status. To this end, this is consistent with the result of this chapter.

Also, the extenics method has been applied by (Tan et al. 2009) to evaluate the comprehensive safety of this rock slope. Their results show that the safety status of the left abutment slope of Jinping 1 Hydropower Station is ranked in class II prone to class I, which gives that the slope is stable as shown in Table 3.7. Thus the result of this chapter also accords with that of their results. And at present, this high rock slope is in good stability status owing to special treatments and consolidation measures.

3.5 Conclusions

The factors adopted in this chapter are thought to have evident effects on the stability of left abutment slope of Jinping 1 Hydropower Station based on its cite characteristics and rearrangement

results of existing rock mass rating system. These factors are managed into four categories according to different attributions. The classifications of these factors for slope mass quality are obtained mainly from Chinese Standard for engineering classification of rock masses and the work of previous researchers. Cloud model which concerns randomness and fuzziness is firstly applied to evaluate effects of the factors in the bottom hierarchy. The output of cloud model is cloud membership representing the quality level of slope mass basing on the data of each rating factor. Then AHP analysis is executed to integrate the outputs of all cloud models of the factors with different weights. Taking account the effects of all factors, the final result is obtained to be the comprehensive membership vector which represents the stability level of the studied slope. Based on the work above, the following conclusions can be made.

(a) The factors adopted in this chapter can account for the stability of the discussed slope since the result is proved to be accorded with that of numerical modeling and manual inspection of this slope. Thus it's true that all the factors related to slope stability are not essential to be taken into account in stability evaluation of a specific rock slope.

(b) The federal approach can be recognized as a unconventional way for modeling the factors in the bottom hierarchy with cloud transformation and cloud generators. With slope data it can produce cloud memberships which can be analyzed with weighted AHP to obtain the comprehensive evaluation result of slope stability by synthesis calculation of cloud memberships. The results prove that this approach is feasible and reliable for stability evaluation of the studied slope. While, this approach may not be able to account for slope failures dominated by structural planes since no other factors than the discontinuities that can account for this kind of slope failure.

(c) Monitoring information is covered for slope stability evaluation in the study since the studied slope is complicated without experienced design standards for reference and data obtained by the monitoring system is essential for modification and supplementation of slope design. Theoretically the evaluating result can be more reliable with the monitoring information.

Nevertheless, it must be convinced that the factors adopted for rock slope stability evaluation would be probably different due to data availability and slope conditions. And the classifications would consequently change slightly for different slopes in a different area with different conditions. The classification data in this chapter are mainly counted for rock slopes in hydroelectric projects with the similar conditions. What's more, the classifications of the monitoring factors presented in this chapter need to be further proved with many more cases. And the weight matrix of the factors would be more proper if more experts and more experiences could have been obtained.

Chapter 4 Rock burst classification with cloud models synthesized by attribution weights

4.1 Introduction

Rock burst is one of the most common failures caused by overstressing of the continuous rock in hard rock mining and civil construction. It is often accompanied by rock fragments, platelets or slabs which may result in dreadful disasters. Rock burst often occurs suddenly if there is not sufficient time to reinforce the rock surroundings. Rock burst hazards are often great challenges to the stability of underground openings, the safety of field workers and even cause other serious accidents. Thus, prediction and control of rock burst s are very important for the purpose of disaster prevention and reduction in the related projects. A great deal of valuable results on the topic have been extracted by a number of authors from a variety of aspects such as the triggering mechanism, the probabilistic prediction reducing measures (Ortlepp 1993; Hoek et al. 1995; Palmström 1995; Tang 2000); and application of Acoustic technique(Hahnekamp and Gluckauf 1983; Will and Gluckauf 1985; Young et al. 1987; Yuan and Li 2009; He et al. 2010; Ishida et al. 2010) for study on rock burst hazards. The present study focuses on the prediction of rock burst events with proposed models.

In the topic of prediction of rock burst event, those factors related to the stress and the energy indexes are recognized as the main indicators for the prediction and classification of rock burst intensity. Several criteria have been proposed worldwide. Russenes criterion (Russenes 1974)sets up the classification graph of rock burst intensity by taking the ratio of the maximum tangential stress around the tunneling(σ_θ) and the point loading strength of rock(I_s) which can be expressed by the uniaxial compressive strength(σ_c). Turchaninov criterion (Turchaninov et al. 1972) gives that the behaviors of rock burst depend on the ratio of σ_c and the sum of σ_θ and the axial stress around the opening (σ_L). Hoek criterion (Hoek and Brown 1980) took the ratio of the uniaxial compressive strength(σ_c) and the maximum tangential stress around the tunneling(σ_θ) as the rule to determine the occurring time and intensity of rock burst.

Besides the stress-related criteria, the energy-related indexes were also applied as rock burst criteria. The strain energy storage index the brittle deformation coefficient and the elastic strain energy index were presented by Neyman for classification of rock burst (Neyman et al. 1972). The elastic energy index(W_{et}) was presented by Kidybinskia to evaluate the intensity of rock burst s(Kidybinskia 1981). Also, combinations of single factors were proposed for the comprehensive evaluation of rock burst intensity like the stress coefficient (σ_θ/σ_c), rock brittleness coefficient (σ_c/σ_t) and elastic

energy index(W_{et})(Wang et al. 1998). Also, another work (Tang and Wang 2002) suggested the rock brittleness index, the stress index and the intact coefficient of rock mass(K_v) to evaluate and classify the intensity of the rock burst hazard. In the work of (Zhang and Fu 2008), five factors were applied as the comprehensive criteria for prediction of rock burst classifications. Most of the work ranked rock burst intensity into four classes according to the factor values. The factors associated with these criteria can thus be recognized as the potential indicators of rock burst event.

Besides the work mentioned above, the predictive method or model is another imperative issue on the predictions of rock burst classification. Various types of methods were applied throughout the world including the empirical methods, the neural networks, and the support vector machines etc. for prediction of rock burst intensity.

An empirical approach was presented for the prediction of rock burst intensity and applied it for the gold mine of Kolar Gold Fields, wherein rock burst were predicted in an ensemble in a specific seismic zone with a lead time of 6 months (Jha and Chouhan 1994). Case studies were presented using a kinematics of failure approach for rock burst prediction (Beer and Mendecki 1998). An approach was presented for the prediction of rock burst by analysis of induced seismicity data (Mansurov 2001). Another seismological method was introduced for prediction of area rock burst in deep mines based on the analysis of the seismic source mechanism and unstable failure theory (Tang and Xia 2010). A finite element perturbation method (Sharan 2004) was executed for the prediction of rock burst which was the numerical modeling method for rock burst prediction.

Besides the above methods, the computational intelligent methods are widely used for prediction of rock burst classification. The neural network was proposed for the prediction of rock burst intensity based on knowledge learning ability of neural networks from the rock burst cases in underground openings (Feng and Wang 1994). Singh T. N. and Singh V. (Singh and Singh 2005) presented an intelligent approach to predict and control ground vibration in mines with artificial neural network(ANN) incorporating a large number of parameters associated with the ground vibration. A new model using the concept of the matter - element and dependent function was introduced for prediction of rock burst and applied it to analyze the rock burst classification of underground projects (Yang and Zhu 2000). A distance discriminant analysis method introduced for application on prediction of possibility and classification of rock burst based on the case data (Gong and Li 2007). A study was presented on the attribute synthetic evaluation system for application in the production of possibility and classification of rock burst (Wen 2008). Xu F. and Xu W.Y. (Xu and Xu 2010b) presented a study on rock burst prediction using the projection pursuit model with the particle swarm optimization. A study was presented on intensity prediction of rock burst based on the efficacy coefficient method (Wang et al. 2010). At the same time, the support vector machine is another

commonly used method for this task. A study was presented on the probability integral method for predicting mining subsidence and the SVM model was applied to estimate the parameters of the integral method (Zhang et al. 2009). The support vector machine was introduced for evaluation and prediction of blast-induced ground vibration by taking into consideration the maximum charge per delay and the distance between the blast force and monitoring point (Khandelwal 2010). A study was presented on a long-term prediction model for classification of rock burst intensity in underground openings using the heuristic algorithms and support vector machines (Zhou et al. 2012).

Also, some comprehensive evaluation techniques have been applied for rock burst prediction. The fuzzy set theory was proposed for application on comprehensive evaluations of rock burst prediction based on several recorded cases (Wang et al. 1998). A study was introduced on the comprehensive prediction of rock burst events based on the analysis of the strain energy of the rock (Wang and Park 2001). A comprehensive forecasting method was proposed for estimating rock burst intensity based on the analytic hierarchy process (AHP) and fuzzy set theory (Yang and Wu 2005). Some other works can also be found in the application of computational intelligence approaches (Vardhan et al. 2009; Verma and Singh 2012a, b; Khademi Hamidi et al. 2010; Sobhani et al. 2010; Cevik et al. 2011; Ceryan et al. 2012; Rabbani et al. 2012; Rajabzadeh et al. 2012; Rezaei et al. 2012; Rajesh Kumar et al. 2013; Yesiloglu-Gultekin et al. 2013).

Truly, these works have been approaching the problems of rock burst, but it never comes to the end of solving it completely. Meanwhile, the methods mentioned above may not sufficient enough to work well in all cases. A certain method may be favorable for some cases but may not be good enough for other cases. For example, the seismic sources are not widely obtained at present, the seismological method cannot work in many cases and thus other methods need be exploited. And for the comprehensive evaluation methods, the weights of evaluating factors given by the experts could probably be different if different experts are inquired, which may result in different effects on the final evaluating results. Thus using the objective weights may be an alternative way to overcome this problem (Liu et al. 2013).

In this paper, the prediction and classification of rock burst are focused on using the technique synthesizing cloud models with the objective attribution weight. The cloud model, which is brought forward to cope with randomness and fuzziness (Li et al. 1998d), is presented for the prediction of rock burst classification with the potential six rock burst indicators ($\sigma_\theta, \sigma_c, \sigma_t, \sigma_\theta/\sigma_c, \sigma_c/\sigma_t, W_{et}$) based on the recorded rock burst cases in the literatures. The adopted parameters in this chapter are selected based on former works on rock burst criteria. In consideration of the varied contributions of the indicators, the effect of each parameter is investigated by computing the corresponding attribution which is objectively obtained on the basis of the dataset. In all, the present work presents a study on the

feasibility and applicability of the proposed technique for prediction of rock burst classification. Study of rock burst criteria is actually important and interesting but it is not concentrated in this work. The aim is to investigate the effect of each indicator and arrive at an attribution based approach for prediction of rock burst classification.

4.2 Empirical classification and indicator analysis

4.2.1 Empirical classification

In the underground openings of hard rock, rock burst is caused by both the internal factors (associated with rock mass properties) and the external factors (referring opening activities). The occurrence of rock burst is associated with multiple factors such as the geological structures of the rock mass, the geo-stress conditions, rock mass strength, the excavation method and shape of the opening, the ground water, rock blasting and earthquake. As a result of opening, the occurrence environment of the underground rock mass changes intensively, causing stress redistribution and concentration around the openings. By the energy theory, rock burst happens when the elastic deformation energy stored in the process of deformation and failure can not only provide sufficient energy for the deforming and rupturing of the rock mass but also remain enough energy for transferring into the kinetic form resulting in the ejection of rock fragments or blocks.

The occurrence of rock burst events are often accompanied by other kinds of phenomena such as rock crackling, rock fragment thrown and sound roaring. The characteristic behavior of the four classes of rock burst intensity is given in Table 4.1[after (Palmström 1995)]. These descriptive characteristic behaviors have been recognized as the empirical classification for rock burst events and used as the standard to evaluate and record the intensity of rock burst events.

Table 4.1 Characteristic behavior of the tunnels subjected to different rock burst intensities

Rock burst intensity	Rock burst class	Descriptive characteristic behavior of the tunnels
None	I	No sound of rock burst and absence of rock burst activities
Light	II	May cause loosening of a few fragments. The surrounding rock will be deformed, cracked or rib spalled. There would be a weak sound but no ejection phenomenon.
Moderate	III	Spalling and falls of thin rock fragments. The surrounding rock will be deformed and fractured, there may be a considerable number of rock chip ejections, loose and sudden destructions, accompanied by crisp crackling, and often presented in the local cavern of surrounding rock.
Strong	IV	Loosening and falls, often as a violent detachment of fragments and platy blocks. The surrounding rock will be bursting severely and suddenly thrown out or ejected into the tunnel, accompanied by strong bursts and roaring sound, and will expand rapidly to the deeper surrounding rock.

4.2.2 Indicator analysis

Rock bursts are mainly caused by overstressing of the ground around the hard rocks although various factors may have effects on them. The occurrence of rock burst is depended by the ratio between the stresses set up in the ground surrounding the opening and the strength of the ground rocks. Thus the factors associated with stresses are treated the most often as the criteria for prediction of rock burst intensity. The tangential stress σ_θ around the opening is co-affected by the ground water, the rock stress, the shape and diameter of the opening (Palmström 1995). Thus tangential stress σ_θ can be thought as the comprehensive effect of those four factors which are thus not included as indicators in context to rock burst event. To take into account the rock material strength, the tangential stress is also expressed as $Ts = \sigma_\theta/\sigma_c$ (Hoek and Brown 1997). In fact, this factor has been adopted in many rock burst prediction criteria. Therefore, both the tangential stress and the rock material strength are adopted in this chapter as possible indicators.

The influence of joints and the block size of the rock mass can be described by the rock brittleness index. It is defined as the ratio of uniaxial compressive strength to tensile strength of rock, i.e. $B = \sigma_c/\sigma_t$. The rocks with higher strength will accumulate large amounts of elastic strain energy prior to failure. They can contribute more to the problem of rock bursting than that of lower strength (Singh 1988). Therefore the tensile strength σ_t is also selected as a potential indicator as well as the uniaxial compressive strength σ_c in this chapter.

In the view of energy theory, the energy related index is the energy measure for evaluation of rock burst intensity. The energy in rocks is widely studied by the acoustic emission (AE) technique. AE occurs in crack form in rocks under high stress condition. AE is also described by failure of large areas of material or relative motion between structural units (Shiotani et al. 2001) in earthquakes. Stored elastic energy is released suddenly when new cracks are generated or the existing cracks make an extension. The elastic energy is often released in the form of elastic stress wave which travels from the releasing point within the rocks to a certain boundary where it is observed as an AE signal. In laboratory experiments, AE is caused by the creation, propagation and sliding of micro-cracks. Thus AE is the result of energy release of rocks, which can be expressed by the energy related index. The elastic strain energy storage index W_{et} is defined as the proportion of strain energy retained to that dissipated during a single loading-unloading cycle of uniaxial compression (Kidybinskia 1981). Also, there are other energy indexes such as the Burst Proneness Index, the Burst Energy Release Index. The Burst Proneness Index is an indicator of the rock's ability to store recoverable and irrecoverable strain energy. The Burst Energy Release Index is a measure of the energy released and dissipated at the time of specimen fracture. The study (Singh 1988) showed that these energy indexes correlated with each other and can thus be similarly related to rock burst. The higher the maximum strain energy stored in

the rock, the larger the value of energy index and the more likely the rock will be subject to bursting. Thus only one energy index W_{et} is selected as the energy indicator for prediction of rock burst classification in this chapter.

Therefore potential indicators adopted in this chapter are the tangential stress σ_θ around the openings, the uniaxial compressive strength σ_c of rock, the tensile strength σ_t, the stress ratio $Ts = \sigma_\theta/\sigma_c$, the rock brittleness index $B = \sigma_c/\sigma_t$ and the elastic strain energy storage index W_{et}. Besides, these indicators are adopted because of availability and reliability of the rock burst case data. There may be other indicators theoretically, but the data collection is a big challenge for their applicability. Therefore those indicators are recognized as the major parameters to quantitatively discover the activities in context to rock burst. The compositions of the indicators are investigated in this paper in order to discover the effects of different indicators.

4.3 Cloud model and attributive weight

4.3.1 The cloud models

The cloud model is defined as the uncertain transformation model between the qualitative concept expressed by linguistic terms and the corresponding quantitative representation expressed by three numerical descriptors (Liu et al. 2004) which are named as the expectationEx, the entropy En and the hyper entropy He. It represents the overall quantitative features of the qualitative concept and is used to describe the mathematical properties of linguistic terms. There are bell-shaped cloud as well as the half bell-sharp cloud and trapezium sharp cloud which is called the half cloud and trapezoidal clouds, respectively (Li et al. 1998e). The cloud models prove to be an effective tool for application in data mining (Li et al. 2000a) and uncertainty reasoning (Li et al. 1998d). The results of these applications have greatly improved the applicability of cloud models.

In short, given the test sample x, the output of the cloud model $\mathrm{CG}(Ex, En, He)$ can be expressed in the membership form as

$$\mu = \exp\left[-\frac{1}{2}\frac{(x-Ex)^2}{(En')^2}\right] \quad \text{.....(4.1)}$$

where x is the data sample to be classified; $\mu \in [0, 1]$ is the cloud membership of x belonging to the cloud model $\mathrm{CG}(Ex, En, He)$; En' is the normal random vector generated by $N(En, He)$.

Suppose that the cloud model be applied to analyze the classification problem of the data set X with m data samples and $D(D \geq 1)$ attributions. And the data set can be classified into $p(p \geq 2)$ classes, i.e. $X = [X_1, X_2, \cdots, X_p]$. The samples $X_k(k = 1,2 \cdots, p)$ of the class k can be denoted by one D-dimension cloud model which can be expressed as $\mathrm{CG}_k(Ex_k, En_k, He_k)$ and calculated by

$$Ex_k = mean(X_k);\ \ En_k = \frac{\max(X_k)-\min(X_k)}{6};\ He_k = constant \quad \text{.....(4.2)}$$

Cloud models are executed by cloud generators. There are generally two kinds of cloud generators: the forward and the backward cloud generators. The forward cloud generator is used to generate the cloud drops $\mathrm{P}(\mathrm{x_i}, \mu_\mathrm{i})(\mathrm{i} = 1,2, \cdots \mathrm{n})$ given the cloud descriptors $\mathrm{N}(\mathrm{E_x}, \mathrm{E_n}, \mathrm{H_e})$, which is the transformation from the qualitative knowledge to the quantitative representation and denoted with CG. And the backward generator is the transferring process to derive the qualitative concept represented by three descriptors from cloud drops $\mathrm{P}(\mathrm{x_i}, \mu_\mathrm{i})(\mathrm{i} = 1,2, \cdots \mathrm{n})$, which is denoted by CG^{-1}. The forward and backward cloud generators are shown in Fig. 3.8. The combinations of the two kinds of generators can be used interchangeably to derive various kinds of clouds to bridge the gap between the qualitative concept and the quantitative knowledge. It is obvious that approximations should be taken if only a few cloud drops are given for backward cloud generators. The more cloud drops the more accurate to generate the three numerical descriptors $\mathrm{N}(\mathrm{E_x}, \mathrm{E_n}, \mathrm{H_e})$.

Given the three numerical descriptors of cloud and the specified $\mathrm{x} = \mathrm{x_0}$, the combination to generate the cloud drops $(\mathrm{x_0}, \mu_\mathrm{i})$ is called the front-condition cloud generator or the X-condition cloud; given the three numerical descriptors of cloud and the specified $\mathrm{y} = \mu_\mathrm{i}$, the combination to generate the cloud drops $(\mathrm{x_i}, \mu_\mathrm{i})$ is named as back-condition cloud generator or the Y-condition cloud (Liu et al. 2004).The X-condition and Y-condition cloud generator are shown in Fig. 3.9.

With the three numerical descriptors, the cloud drops (X, μ) can be produced using the forward cloud generator. Given the test sample $x_i(i = 1,2, \cdots, m)$, we can generate the cloud membership μ_{ik} for the cloud model $\mathrm{CG}_k(E_{xk}, E_{nk}, H_{ek})$ using the X-conditional cloud generator. If $\mu_{ik} = \max(\mu_{i1}, \mu_{i2}, \cdots, \mu_{ip})(k = 1,2 \cdots, p)$, we conclude that the test sample x_i belongs to the class k.

4.3.2 Attribution weight

In the above classification, the effects of the attributions of the data samples are not considered. In fact, different attributions often have different effects for the classification problems. Some attributions may probably contribute much more than the other attributions. In this way, the weight of the attributions should be taken into account. Generally, there are two ways to determine the attributive weight: the subjective method and objective method. The subjective method is to inquire the experts' opinions on the weighting values of the attributions. In this paper, we use the objective method which obtains the weighting values from the similarity of each attribution of the data samples. The larger value of similarity of an attribution, the much less it can contribute to the classification.

If the distance of the j^{th} attribution of the class X_s and class X_t is define as

$$d(X_{sj}, X_{tj}) = \begin{cases} 0 & X_{sj} \subseteq X_{tj} \text{ or } X_{sj} \supseteq X_{tj} \\ \frac{|Ex_{sj} - Ex_{tj}|}{3(En_{sj} + En_{tj})} & X_{sj} \subset X_{tj} \text{ or } X_{sj} \supset X_{tj} \end{cases} .. \quad (4.3)$$

$$En_{sj} = \frac{Ex_{sj} - \min(X_{ij})}{3} \ or \ En_{sj} = \frac{\max(X_{ij}) - Ex_{sj}}{3} \quad ..... \quad (4.4)$$

The similarity of the j^{th} attributions can be calculated by

$$S(j) = S(X_{sj}, X_{tj}) = \begin{cases} 1 & d(X_{sj}, X_{tj}) = 0 \\ 1 - \min(d(X_{sj}, X_{tj})) & 0 < d(X_{sj}, X_{tj}) < 1 \\ 0 & d(X_{sj}, X_{tj}) \geq 1 \end{cases} ..... \quad (4.5)$$

Then the weight of j^{th} attribution can be obtained as

$$\omega(j) = \frac{1 - S(j)}{\sum_{j=1}^{D} [1 - S(j)]} \quad .....(4.6)$$

This weight can be added to calculate the cloud membership of the *D* dimensional cloud model as to indicate the divergent contributions of different attributions. In this way, given the test sample x, the cloud membership that x belongs to class k will be obtained as

$$\mu_k = \sum_{j=1}^{D} \omega(j) \exp\left[-\frac{1}{2} \frac{(x - Ex_{kj})^2}{2En_{kj}^2} \right] \quad .....(4.7)$$

4.3.3 Implementation procedure of the approach

There are two problems to be figured out to this end. The first is to establish the cloud models of each class of rock burst intensity. The second is to calculate the corresponding outputs for the test samples. The cloud models can be set up on the basis of the statistical features of the rock burst instances. The procedure of the strategy of this paper can be processed as follows.

a) Establishment of cloud models. Compute the numerical descriptors of the cloud model $\mathrm{CG}(Ex, En, He)$ for each class of rock burst intensity by *Eq.*(4.2).

b) Calculation of the weight of each rock burst indicator. Compute the similarity of each rock burst indicator among the four different rock burst intensities by *Eq.*(4.3)-(4.5), then calculate the weight of each indicator by *Eq.*(4.6). The large of the weight of an indicator, the much more the corresponding indicator contributes to the classification of the rock burst instances.

c) Preparation of the test samples. First take each class of instances as the test samples to verify the performance of the strategy introduced in this paper; then select randomly some instances from the rock burst dataset as the test samples.

d) Calculation of the cloud memberships of the test samples. Calculate the cloud memberships of

each test sample to the four classes of rock burst intensities according to *Eq*.(4.1) or *Eq*.(4.7). Then the output of the strategy in this paper is generated.

The values of the cloud memberships give out the degree of the test samples belonging to the corresponding rock burst intensity class. They can indicate the performance of the cloud model for classification.

4.4 Results and discussion

Preliminary analysis is undertaken first on statistical features of the parameters as well as single parameter analysis in context of rock burst class. Then the weight of each indicator is calculated and thus the relative sensitivity is obtained. The clustering figures are generated by cloud models for every rock burst class. Afterwards, predictive performance of the proposed strategy is given comparatively with other techniques like the empirical methods, the regression analysis, the neural networks and support vector machines.

4.4.1 Case data of rock burst intensities

The occurrence of rock burst events has been reported throughout the world in underground openings, for example, the mines and the underground caverns of civil infrastructures. The work (Feng and Wang 1994) showed that they collected 201 rock burst case histories from 25 underground coal mines and hydroelectric tunnels in China and used them as learning patterns for neural networks. The 30 rock burst data samples were generated by Xu F. and Xu W.Y. (Xu and Xu 2010b) based on forecasting criteria to be used for the learning and training of the projection pursuit model for rock burst intensity prediction. Another 132 rock burst data samples were collected from the literatures and applied the heuristic algorithms and support vector machines for prediction of rock burst classification(Zhou et al. 2012). In total, the 162 rock burst shown in Table 4.2 are collected in this chapter for prediction of rock burst classification, among which 152 instances randomly chosen are used for establishing the cloud models(i.e. training) and the left 10 instances are used to validate the generalization ability(i.e. testing) of the approach.

These rock burst instances have a wide range of engineering type(like the hydropower stations tunnels, road tunnels, railway tunnels, nuclear cooling tunnels, coal mines and metal mines) and location(China, Norway, Sweden, Japan, Italy, etc.). The box graph of these cases is shown in Fig. 4.1. The factors σ_θ, σ_c and σ_c/σ_t are divided by 10 in Fig. 4.1 in order to well display all the indicators in one figure.

Table 4.2 Rock burst cases with parameter value and empirical classification

NO.	Engineering	Rock type	H/m	σθ (MPa)	σc (MPa)	σt (MPa)	σθ /σc	σc /σθ	Wet	Rock burst class
1	Diversion Tunnels of Yuzixi Hydropower Station	Granodiorite	200	90	170	11.3	0.53	15.04	9	III
2	2# Sub Tunnel of Ertan Hydropower Station	Syenite	194	90	220	7.4	0.41	29.73	7.3	II
3	Underground Cavern of Taipingyi Hydropower Station	Granodiorite	400	62.6	165	9.4	0.38	17.53	9	II
4	Underground powerhouse of Laxiwa Hydropower Station	Granite	300	55.4	176	7.3	0.32	24.11	9.3	III
5	Diversion Tunnels of Tian shengqiao -II Hydropower Station	Dolomitic limestone	400	30	88.7	3.7	0.34	23.97	6.6	III
6	Underground cavern of Norwegian Sima Hydropower Station	Granite	700	48.75	180	8.3	0.27	21.69	5	III
7	Diversion Tunnels of Swedish Vietas Hydropower Station	Quartzite	250	80	180	6.7	0.44	26.87	5.5	II
8	Japanese Guanyuk Tunnel	Quartz diorite	890	89	236	8.3	0.38	28.43	5	III
9	Diversion Tunnels of Jingping Hydropower Station	Marble	150	98.6	120	6.5	0.82	18.46	3.8	III
10	Italian Raibl Lead Zinc de Working	Lead and zinc ore		108.4	140	8	0.77	17.5	5	IV
11	Soviet Rasvumchorr Workings	Ni nepheline-P nepheline		57	180	8.3	0.32	21.69	5	III
12	Cooling Diversion Tunnels of Swedish Forsmark Nuclear Station	Gneissic granite		50	130	6	0.38	21.67	5	III
13	Norwegian Heggura Road Tunnel	Granitic gneiss		62.5	175	7.25	0.36	24.14	5	III
14	Norwegian Sewage Road Tunnel	Granite		75	180	8.3	0.42	21.69	5	III
15	Underground Cavern of Lijiaxia Hydropower Station	Biotite angle, flash plagioclase schist		11	115	5	0.1	23	5.7	I
16	Underground Cavern of Pubugou Hydropower Station	Diorite granite		43.4	123	6	0.35	20.5	5	III
17	Underground Cavern of Longyangxia Hydropower Station	Granite		18.8	178	5.7	0.11	31.23	7.4	I
18	Underground Cavern of Lubuge Hydropower Station	Limestone		34	150	5.4	0.23	27.78	7.8	I
19	Qinling Tunnel of Xikang Railway Dyk77 + 176	Granite		56.1	132	9.44	0.43	13.98	7.44	III
20	Qinling tunnel of Xikang railway T1	Granite		54.2	134	9.1	0.4	0.147	7.1	III
21	Qinling tunnel of Xikang railway T2	Granite		70.3	128.3	8.7	0.55	0.148	6.4	III
22	Qinling Tunnel of Xikang Railway Dyk72 + 440	Granite		60.7	111.5	7.86	0.54	14.19	6.16	IV
23	Qin-ling Tunnel	Migmatite	<1600	54.2	134	9.09	0.404	15	7.08	III
24	Qin-ling Tunnel	Migmatite	<1600	70.3	129	8.73	0.547	11.4	6.43	III
25	Kuocang Mountain Tunnel	Crystal tuff	204	35	133.4	9.3	0.26	14.34	2.9	II
26	Riverside Hydropower Station diversion tunnel	Sandstone	203	157.3	91.23	6.92	0.58	13.18	6.27	IV
27	Riverside Hydropower Station diversion tunnel	Dolomite	827	148.4	66.77	3.81	0.45	17.53	5.08	II
28	Riverside Hydropower Station diversion tunnel	Ore	896	132.1	51.5	2.47	0.39	20.86	4.63	III
29	Riverside Hydropower Station diversion tunnel	Red Shale	1117	127.9	35.82	1.24	0.28	28.9	3.67	II

NO.	Engineering	Rock type	H/m	σθ (MPa)	σc (MPa)	σt (MPa)	σθ /σc	σc /σθ	Wet	Rock burst class
30	Riverside Hydropower Station diversion tunnel	Sandstone	1124	107.5	21.5	0.6	0.2	36.04	2.29	I
31	Riverside Hydropower Station diversion tunnel	Dolomite	1140	96.41	18.32	0.38	0.19	47.93	1.87	I
32	Riverside Hydropower Station diversion tunnel	Ore	983	167.2	110.3	8.36	0.66	13.2	6.83	IV
33	Riverside Hydropower Station diversion tunnel	Red shale	853	118.5	26.06	0.77	0.22	33.75	2.89	II
34	Huize Lead–Zinc Mine	Sandstone	920	34.15	54.2	12.1	0.63	4.48	3.17	II
35	Jinchuan 2nd Mine	Granite	1000	60	135	15.04	0.444	8.976	4.86	II
36	Jinchuan 2nd Mine	Marble	1000	60	66.49	9.72	0.902	6.841	2.15	II
37	Jinchuan 2nd Mine	Migmatite	1000	60	106.4	11.2	0.564	9.498	6.11	II
38	Jinchuan 2nd Mine	Peridotite	1000	60	86.03	7.14	0.697	12.05	2.85	II
39	Jinchuan 2nd Mine	Lherzolite	1000	60	149.2	9.3	0.402	16.04	3.5	II
40	Jinchuan 2nd Mine	Amphibolite	1000	60	136.8	10.42	0.439	13.13	2.12	II
41	Ma Luping mine	Sandstone	750	63.8	110	4.5	0.58	24.4	6.31	III
42	Ma Luping mine	Dolomite	750	2.6	20	3	0.13	6.67	1.39	I
43	Ma Luping mine	Phosphate rock	750	44.4	120	5	0.37	24	5.1	II
44	Ma Luping mine	Red Shale	750	13.5	30	2.67	0.45	11.2	2.03	II
45	Ma Luping mine	Sandstone	700	70.4	110	4.5	0.64	24.4	6.31	III
46	Ma Luping mine	Dolomite	700	3.8	20	3	0.19	6.67	1.39	I
47	Ma Luping mine	Phosphate rock	700	57.6	120	5	0.48	24	5.1	III
48	Ma Luping mine	Red shale	700	19.5	30	2.67	0.65	11.2	2.03	III
49	Ma Luping mine	Sandstone	600	81.4	110	4.5	0.74	24.4	6.31	IV
50	Ma Luping mine	Dolomite	600	4.6	20	3	0.23	6.67	1.39	I
51	Ma Luping mine	Phosphate rock	600	73.2	120	5	0.61	24	5.1	III
52	Ma Luping mine	Red shale	600	30	30	2.67	1	11.2	2.03	IV
53	Beiminghe iron mine	Limestone	510	15.2	53.8	5.56	0.283	9.68	1.92	I
54	Beiminghe iron mine	Diorite	510	88.9	142	13.2	0.627	10.7	3.62	IV
55	Beiminghe iron mine	Iron ore	510	59.82	85.8	7.31	0.697	11.7	2.78	III
56	Beiminghe iron mine	Skarn	510	32.3	67.4	6.7	0.479	10.1	1.1	I
57		Dolomitic limestone	225	30.1	88.7	3.7	0.34	23.97	6.6	IV
58		Granite	375	18.8	171.5	6.3	0.11	27.22	7	I
59		Limestone	435	34	149	5.9	0.23	25.25	7.6	II
60		Clay sandstone	250	38.2	53	3.9	0.72	13.59	1.6	I
61		Marble	100	11.3	90	4.8	0.13	18.75	3.6	I
62		Limestone	300	92	263	10.7	0.35	24.58	8	II
63		Diorite	330	62.4	235	9.5	0.27	24.74	9	IV
64		Granite	223	43.4	136.5	7.2	0.32	18.96	5.6	IV
65		Diastatite anorthose	425	11	105	4.9	0.1	21.43	4.7	I
66	Section 1–1 of diversion tunnel JinpingIIhydropower station	Breccia marble	<2520				0.62	20	3.1	III
67	Section 1–1 of diversion tunnel JinpingIIhydropower station	Grey-white marble	<2520				0.67	26.8	0.85	II
68	Section 2–2 of diversion tunnel JinpingIIhydropower station		<2520				0.9	25.7	0.9	IV
69	Section 3–3 of diversion tunnel JinpingIIhydropower station		<2520				0.83	28.9	3.2	IV

NO.	Engineering	Rock type	H/m	σθ (MPa)	σc (MPa)	σt (MPa)	σθ /σc	σc /σθ	Wet	Rock burst class
70	Section 4–4 of diversion tunnel JinpingIIhydropower station		<2520				0.93	28.9	3.2	IV
71	Section 5–5 of diversion tunnel JinpingIIhydropower station		<2520				0.74	28.9	3.2	III
72	Section 6–6 of diversion tunnel JinpingIIhydropower station		<2520				1.41	19.2	3.1	IV
73	Section 7–7 of diversion tunnel JinpingIIhydropower station		<2520				0.79	22	2	III
74	Long exploratory tunnel1 + 693 of Jinping II hydropower station	Mica marble					0.559	20.4	2	II
75	Long exploratory tunnel1 + 731 of Jinping II hydropower station	Mica marble		46.4	100	4.9	0.464	20.4	2	II
76	Long exploratory tunnel0 + 568 of Jinping II hydropower station	Gray-white marble					0.237	26.8	0.85	II
77	Long exploratory tunnel0 + 600 of Jinping II hydropower station	Gray-white marble		23	80	3	0.29	26.8	0.85	II
78	Long exploratory tunnel2 + 215 of Jinping II hydropower station	Gray-white marble					0.634	19.7	0.85	III
79	Long exploratory tunnel1 + 560 of Jinping II hydropower station	Granophyric marble					0.488	19.7	2.3	II
80	Long exploratory tunnel1 + 640 of Jinping II hydropower station	Granophyric marble		46.2	105	5.3	0.436	19.7	2.3	II
81	Long exploratory tunnel3 + 390 of Jinping II hydropower station	Granophyric marble					0.842	19.7	2.3	III
82	Long exploratory tunnel3 + 580 of Jinping II hydropower station	Granophyric marble					0.417	19.7	2.3	II
83	Long exploratory tunnel3 + 650 of Jinping II hydropower station	Granophyric marble					0.463	19.7	2.3	II
84	Long exploratory tunnel3 + 000 of Jinping II hydropower station	Black marble					0.846	27.3	3.1	III
85	Long exploratory tunnel3 + 800 of Jinping II hydropower station	Black marble					0.506	27.3	3.1	III
86	Cangling tunnel K97 + 102-K98 + 152	Weathered and fresh Tuff, breccia and K-feldspar granite porphyry					0.21	24.3	4.6	II
87	Cangling tunnel K98 + 152–K98 + 637						0.28	23.6	4.9	II
88	Cangling tunnel K98 + 637–K99 + 638						0.32	21.3	5.3	III
89	Cangling tunnel K99 + 638–K100 + 892						0.28	23.8	4.8	II
90	Erlang Mountain Tunnel level guide K261 + 939						0.52	21.2	5.5	III
91	Qinling Zhongnanshan highway tunnel						0.65	28.6	6.8	IV
92	Fujian Jiuhuashan Tunnel						0.52	24.6	7.3	III
93	Kuocangshan tunnel k155 + 200–k156 + 178		<504	13.9	124	4.22	0.112	29.4	2.04	I
94	Kuocangshan tunnel k156 + 203–k157 + 573		<504	17.4	161	3.98	0.139	31.4	2.19	II

NO.	Engineering	Rock type	H/m	σθ (MPa)	σc (MPa)	σt (MPa)	σθ /σc	σc /σθ	Wet	Rock burst class
95	Kuocangshan tunnel k157 + 573–k58 + 078		<504	19	153	4.48	0.151	28.1	2.11	II
96	Kuocangshan tunnel k157 + 078–kl59 + 250		<504	19.7	142	4.55	0.155	27.9	2.26	II
97	Chengchao iron mine	Marble	469	18.7	82	10.9	0.23	7.52	1.5	I
98	Chengchao iron mine	Granite porphyry	520	28.6	122	12	0.23	10.22	2.5	III
99	Chengchao iron mine	Diorite	552	29.8	132	11.5	0.23	11.52	4.6	III
100	Chengchao iron mine	Dioritic porphyrite	583	33.6	156	10.8	0.22	14.45	5.2	III
101	Chengchao iron mine	Magnetite	567	26.9	92.8	9.47	0.29	9.8	3.7	III
102	Chengchao iron mine	Granite	670	55.9	128	6.29	0.44	20.3	8.1	IV
103	Chengchao iron mine	Skarn	670	59.9	96.6	11.7	0.62	8.26	1.8	II
104	Chengchao iron mine	Quartz-feldspar porphyry	600	68	107	6.1	0.64	17.51	7.2	IV
105							0.514	15.908	4.198	III
106							0.652	18.195	4.204	III
107							0.694	23.558	4.795	III
108							0.697	15.193	4.745	III
109							0.108	69.359	0.153	I
110							0.052	67.536	0.012	I
111							0.125	74.056	0.505	I
112							0.254	78.634	0.143	I
113							0.107	71.872	0.034	I
114							0.823	10.614	5.976	IV
115							0.756	6.293	5.904	IV
116							0.975	10.142	6.201	IV
117							0.538	19.552	4.433	III
118							0.648	14.853	4.189	III
119							0.627	18.992	4.645	III
120							0.339	36.371	2.016	II
121							0.346	37.535	2.274	II
122							0.427	39.388	2.432	II
123							0.354	35.547	2.134	II
124							0.104	79.993	0.346	I
125							0.142	73.638	0.201	I
126							0.24	72.524	0.015	I
127							0.759	2.25	6.413	IV
128							0.982	8.865	7.882	IV
129							0.685	15.014	3.618	III
130							0.653	23.121	4.51	III
131							0.31	39.522	2.017	II
132							0.314	35.624	2.149	II
133							0.401	37.959	2.073	II
134							0.302	28.367	2.041	II
135	Dongguashan copper mine	Siltstone	850	105.5	187	19.2	0.56	9.74	7.27	III
136	Dongguashan copper mine	Garnet Skarn	850	105.5	170	12.1	0.62	14.05	5.76	III
137	Dongguashan copper mine	Skarn	790	105.5	190	17.1	0.55	11.11	3.97	III
138	Tongyu Tunnel K21 + 680	Limestone	900	47.56	58.5	3.5	0.81	16.71	5	II
139	Tongyu Tunnel K21 + 740	Limestone	1030	43.62	78.1	3.2	0.56	24.41	6	II

NO. Engineering	Rock type	H/m	σθ (MPa)	σc (MPa)	σt (MPa)	σθ /σc	σc /σθ	Wet	Rock burst class
140 Daxiangling tunnel YK55 + 119	Rhyolite	362	25.7	59.7	1.3	0.43	45.9	1.7	I
141 Daxiangling tunnel ZK55 + 154	Rhyolite	374	26.9	62.8	2.1	0.42	29.9	2.4	II
142 Daxiangling tunnel YK55 + 819	Rhyolite	775	40.4	72.1	2.1	0.56	34.3	1.9	II
143 Daxiangling tunnel ZK55 + 854	Rhyolite	799	39.4	65.2	2.3	0.6	28.3	3.4	III
144 Daxiangling tunnel YK56 + 080	Rhyolite	811	38.2	71.4	3.4	0.53	21	3.6	III
145 Daxiangling tunnel YK56 + 109	Rhyolite	816	45.7	69.1	3.2	0.66	21.5	4.1	III
146 Daxiangling tunnel YK56 + 177	Rhyolite	841	35.8	67.8	3.8	0.52	17.8	4.3	III
147 Daxiangling tunnel YK56 + 343	Rhyolite	959	39.4	69.2	2.7	0.57	25.6	3.8	III
148 Daxiangling tunnel ZK56 + 374	Rhyolite	984	40.6	66.6	2.6	0.61	25.6	3.7	III
149 Daxiangling tunnel YK56 + 421	Rhyolite	1112	39	70.1	2.4	0.56	29.2	4.8	III
150 Daxiangling tunnel YK61 + 305	Rhyolite	981	57.2	80.6	2.5	0.71	32.2	5.5	IV
151 Daxiangling tunnel YK61 + 382	Rhyolite	808	55.6	114	2.3	0.49	49.5	4.7	III
152 Daxiangling tunnel YK61 + 400	Rhyolite	799	56.9	123	2.7	0.46	45.5	5.2	III
153 Daxiangling tunnel ZK61 + 440	Rhyolite	768	62.1	132	2.4	0.47	55	5	III
154 Daxiangling tunnel YK61 + 445	Rhyolite	764	29.7	116	2.7	0.26	42.9	3.7	II
155 Daxiangling tunnel YK61 + 450	Rhyolite	760	29.1	94	2.6	0.31	36.1	3.2	II
156 Daxiangling tunnel YK61 + 493	Rhyolite	729	27.8	90	2.1	0.31	42.8	1.8	I
157 Daxiangling tunnel YK61 + 827	Rhyolite	724	30.3	88	3.1	0.34	28.3	3	II
158 Daxiangling tunnel YK61 + 382	Rhyolite	808	55.6	114	2.3	0.49	49.5	4.7	III
159 Daxiangling tunnel ZK56 + 451	Rhyolite	1048	41.6	67.6	2.7	0.61	25	3.7	III
160 Daxiangling tunnel ZK56 + 479	Rhyolite	1074	40.1	72.1	2.3	0.55	31.3	4.6	III
161 Daxiangling tunnel ZK61 + 201	Rhyolite	980	58.2	83.6	2.6	0.69	32.1	5.9	IV
162 Daxiangling tunnel ZK61 + 352	Rhyolite	839	56.8	112	2.2	0.5	50.9	5.2	III

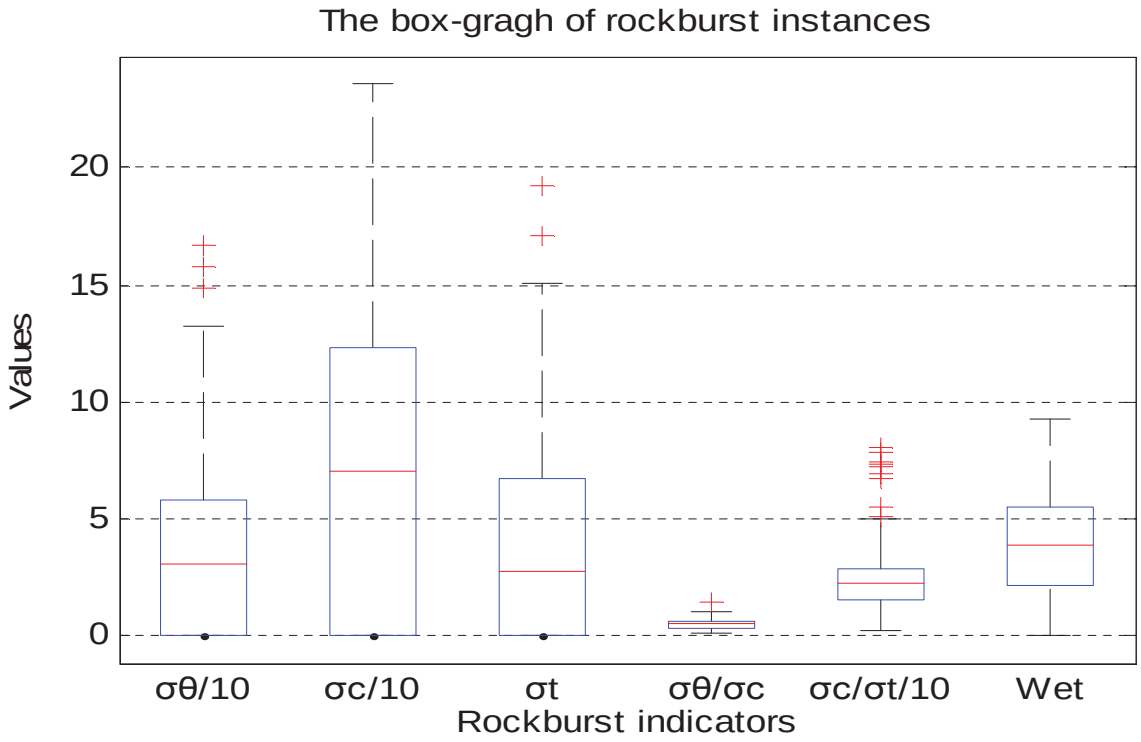

Fig. 4.1 Box graph of rock burst instances

4.4.2 Preliminary data analysis

The statistical features of these case data are summarized in Table 4.3. The maximum and minimum values of each attribution do not have apparent differences, respectively, among the four rock burst intensities. And each has large values of mean square deviation. The parameter value ranges intersect with each other and have very vague boundaries. This would make it difficult or even impossible to directly classify those rock burst instances with a satisfactory accuracy. On the contrary, the indicators' mean values of each rock burst class differ with each other with a big portion of percent judging from Table 4.3, especially for the indicator $Ts = \sigma_\theta/\sigma_c$. This feature would help to find the way of classifying those instances.

It can be noticed in Table 4.2 that some of the samples have missing values for certain attributions. Also, there may be noise data in recording the samples. Thus the dataset should be preprocessed with some mathematical technics in order to be better mannered and processed in the model programming. The mean imputation method is applied to deal with the missing values in this dataset. Also, the $n\sigma(\mathrm{n} = 2 \text{ or } 3)$ rule has been used to prune the data samples. During the investigation, the pre-treatments of the data samples are found important to obtain better mannered results. The graph of rock burst classes with respect to each single indicator after pre-treatments are shown in Fig. 4.2. Ideally, in order to be easily classified, every indicator value should not have more than one class label value in the figure. It is easy to know from Fig. 4.2 that some indicator values have more than one corresponding value of the rock burst class label in some cases. This is caused by the reason that the indicator values do not have clear boundaries at all among the four classes of rock burst. Thus, it's not possible to classify the rock burst cases correctly only using one of the indicators. Fortunately, the composition of the indicators may work. In the following section, combinations of the indicators are used in order to obtain as good classification results as possible.

Table 4.3 Statistical features of the recorded rock burst case data

Rock burst intensity	Indicators	σ_θ(MPa)	σ_c(MPa)	σ_t(MPa)	σ_θ/σ_c	σ_c/σ_t	Wet
None rock burst	Number of instances	26(2 as test sample)					
	Number of missing values	8	8	8	0	0	0
	Minimum value	2.6	18.32	0.38	0.052	6.670	0.012
	Maximum value	107.5	178.00	10.90	0.720	79.993	7.800
	Mean value	27.31	79.957	4.264	0.208	38.461	2.215
	Mean square deviation	29.11	52.513	2.512	0.147	26.550	2.362
Light rock burst	Number of instances	49(3 as test sample)					
	Number of missing values	17	17	17	0	0	0
	Minimum value	13.5	26.06	0.77	0.139	4.480	0.850
	Maximum value	148.4	263.00	15.04	0.902	42.900	9.000

	Mean value	53.74	110.321	6.094	0.405	24.388	3.359
	Mean square deviation	32.54	53.786	3.734	0.163	9.577	1.923
Moderate rock burst	Number of instances	63(3 as test sample)					
	Number of missing values	19	19	19	0	0	0
	Minimum value	19.5	30.00	2.20	0.220	9.740	0.850
	Maximum value	132.1	236.00	19.20	0.846	55.000	9.000
	Mean value	58.26	120.618	6.528	0.559	22.790	4.491
	Mean square deviation	24.51	44.940	4.086	0.141	10.920	1.545
Strong rock burst	Number of instances	24(2 as test sample)					
	Number of missing values	10	10	10	0	0	0
	Minimum value	30.0	30.00	2.50	0.270	2.250	0.900
	Maximum value	167.2	235.00	13.20	1.410	32.200	9.000
	Mean value	76.36	113.888	6.386	0.723	18.484	5.571
	Mean square deviation	42.08	52.231	3.036	0.251	8.545	1.967

4.4.3 Indicator weight and sensitivity

The similarity and the weight of each rock burst indicator are obtained in Table 4.4 by *Eq*.(4.3)-(4.5) according to the data instances shown in Table 4.2. It can be draw from Table 4.4 that these indicators all have large values of similarity among the four classes of rock burst intensities. None of the indicators is sufficient enough to solely classify the rock burst intensity because that the indicator values of one class are closely similar to that of another. Fortunately, these indicators can work synthetically with different contribution weight so as to generate much better results.

The weight values shown in Table 4.4 turn out that the indicator σ_θ/σ_c has the largest weight for classification prediction. It shows that the ratio plays a much more important role than the other factors to account for the occurrence of rock burst event. It should be noted that it is neither the tangential stress around the openings σ_θ nor the compressive strength of rock σ_c itself that plays the role. The elastic strain energy storage index W_{et} takes the second place of the attribution weights with value 0.266, which is followed by the brittleness index with weight value 0.142. In total, these three indicators contribute 87.0% of the weight. This would indicate that only using the three indicators for analysis of rock burst classification could obtain moderate satisfactory evaluation results.

The indicator sensitivity is thought to be related to the importance of the indicators for rock burst classification. The relative sensitivity of these indicators is obtained based on the weights of each indicator before implementation of the strategy. The relative sensitivity of the indicator is thus shown in Fig. 4.3. It is apparent as shown in Fig. 4.3 that σ_θ/σ_c is the most sensitive for rock burst classification, and the energy index W_{et} is the second sensitive and then the brittleness index $B = \sigma_c/\sigma_t, \sigma_\theta, \sigma_c$ and σ_t, successively.

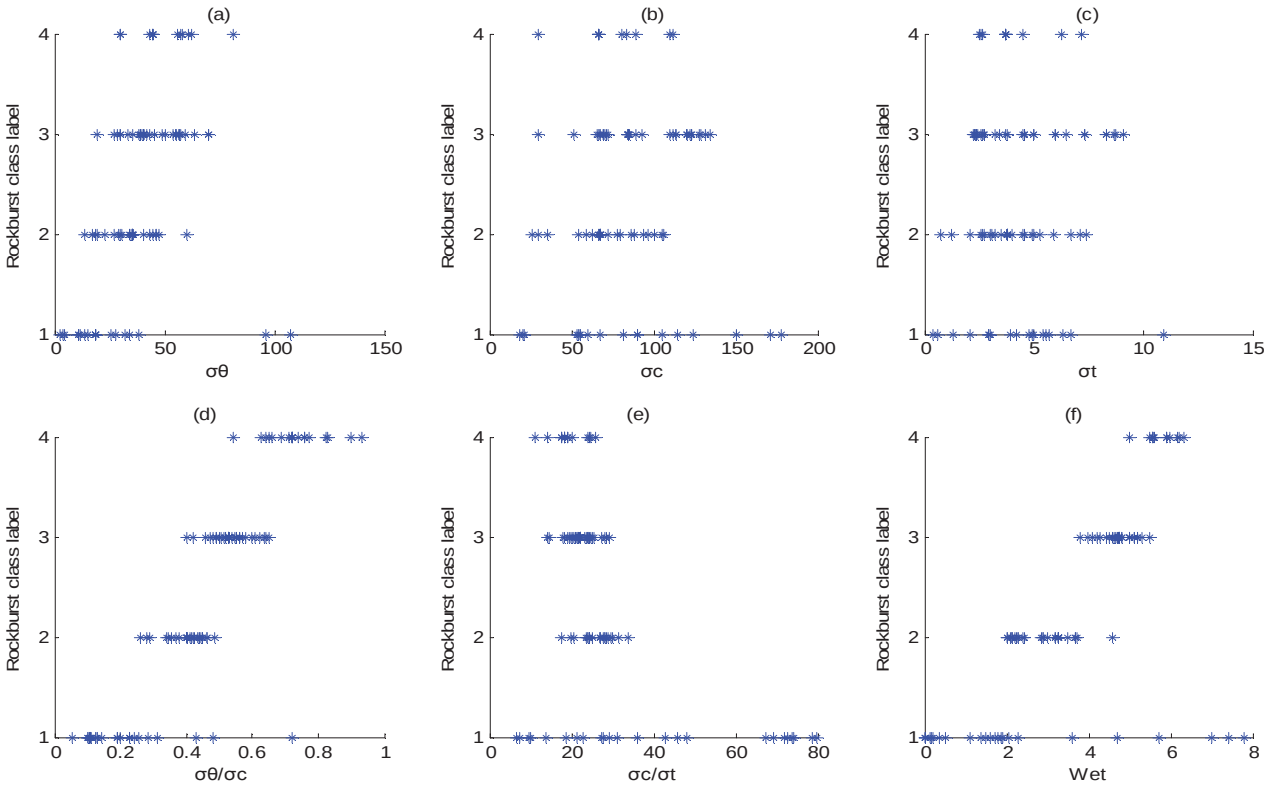

Fig. 4.2 Rock burst class with respect to each indicator (preprocessed data samples)

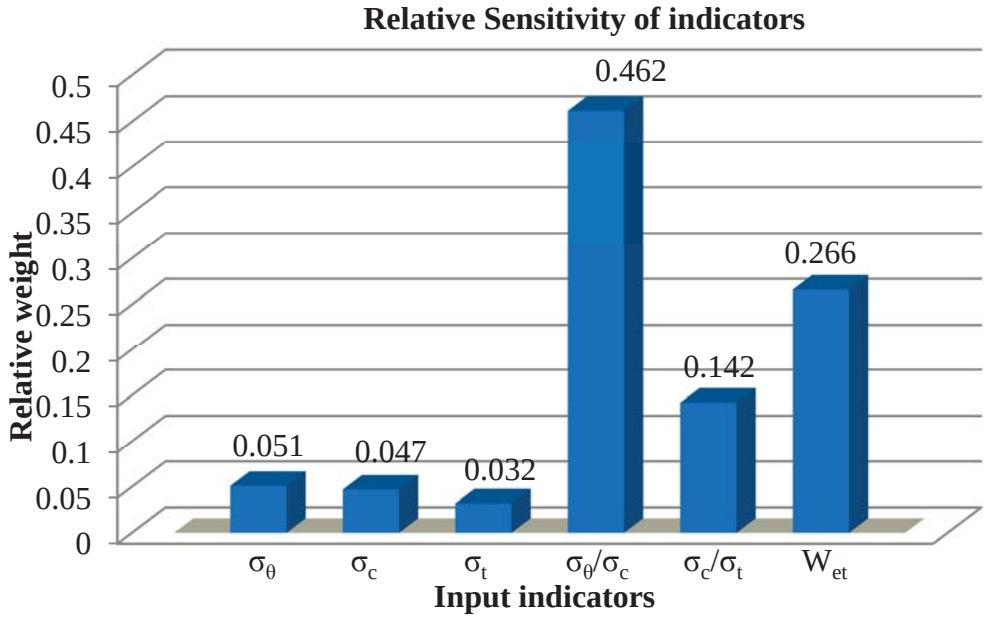

Fig. 4.3 Relative importance of the indicators for rock burst classification

4.4.4 Clustering figures by cloud models

The clustering figures of the rock burst instance are generated by the cloud models as shown in Fig. 4.4. The x-axis and y-axis of the figures is every two of the six indicator values, respectively, and the

z-axis is the corresponding cloud membership values. These values indicate the degrees of membership of the generated cloud drops. The cloud drops are produced with the forward cloud generators using the case data in Table 4.2. In the figures, each cloud drop denotes an instance; the cloud drops in the color blue, magenta, black and red denote the rock burst intensity class "None", "Light", "Moderate" and "Strong", respectively. The front of each arrow shows the center of each corresponding rock burst class.

It can be drawn from Fig. 4.4 that the four classes of rock burst intensities do not have a clear class boundary at all, especially for the light rock burst instances and the moderate rock burst instances. To some extent, the sub-fig.(a) to (c) give out much more satisfactory results than sub-fig.(d) to (f) for classifying the four classes of rock burst instances. These phenomena indicate that the indicators σ_θ/σ_c, W_{et} and σ_c/σ_t can perform much better than σ_θ, σ_c and σ_t for classifying these rock burst instances. The result is well accord with that of the attributive weight values given in Table 4.4.

Table 4.4 Values of the similarity and weight of rock burst indicators

Rock burst Indicator	σ_θ(MPa)	σ_c(MPa)	σ_t(MPa)	σ_θ/σ_c	σ_c/σ_t	W_{et}
The similarity	0.983	0.984	0.989	0.841	0.951	0.909
The weight	0.051	0.047	0.032	0.462	0.142	0.266

4.4.5 Predicted results and comparison

In this part, the predictions of the rock burst instances are firstly given for both the simple cloud models and the weighted cloud models. Following this, other techniques like the Neural Network and Support Vector Machines are applied to comparatively predict the rock burst classifications. Then variant models with different indictors are investigated in order to know the effects of different indictors for the rock burst classification.

4.4.5.1 Empirical method results

Some empirical criteria for rock burst classification are applied to give evaluations on these rock burst cases (162 cases). The applied empirical criteria are shown in Table 4.5 as well as the corresponding predictive performance. The predictive accuracy of these methods is between 50%-60% of the original data and less than 80% of the filtered data.

It is obvious judging from the predictive accuracy that the empirical methods cannot generate satisfactory predictions on these robust instances. These empirical methods are proposed based on some engineering experiences which could probably result in dependence of the methods on the engineering background. While, the rock burst cases collected in this chapter has a wide range of engineering type and location, thus the empirical methods cannot work well for all the cases.

Table 4.5 Classification results of some empirical methods

Empirical method	Equation	Classification criteria				Predictive accuracy (%) (original data)	Predictive accuracy (%) (filtered data)
		None	Light	Moderate	Strong		
Russenes criterion(1974)	σ_θ/σ_c	<0.25	0.25-0.33	0.33-0.55	>0.67	56.2	67.3
Hoek criterion(1980)	σ_c/σ_θ	>3.5	2.0-3. 5	1.7-2.0	<1.7	54.3	60.5
Rock brittleness criterion	$B=\sigma_c/\sigma_t$	>40	26.7-40	14.5-26.7	<14.3	51.2	49.4
Tangential stress criterion	$T_s=\sigma_\theta/\sigma_c$	<0.3	0.3-0.5	0.5-0.7	>0.7	58.0	70.1
Elastic energy index criterion	W_{et}	<2.0	2.0-3.5	3.5-5.0	>5.0	57.4	76.0

4.4.5.2 Regression analysis Results

Regression analysis is a commonly used technique to show the relationship between the targets and the related factors and can give regressive results for the given dataset. The multinomial logistic regression (MLR) method is implemented with the same cases (162 cases) in this chapter since the rock burst class labels are class-type data.

With rock burst class IV as the reference category, the parameter estimate results of MLR show the value of the significance level of each indicator is different for each of the three classes with a 95% confidence interval. For class I, it is 0.795, 0.222, 0.130, 0.000, 0.327, 0.000, successively for σ_θ, σ_c σt, σ_θ/σ_c, $\sigma c/\sigma t$, W_{et}. For class II, it is 0.894, 0.347, 0.304, 0.000, 0.643, and 0.000. For class III, it is 0.469, 0.679, 0.416, 0.001, 0.754, and 0.003. With the 95% confidence interval, it requires the significance levels of the factors should be less than 0.05 to well explain the model. These significance level values thus imply that only the indicator σ_θ/σ_c and W_{et} can be used to explain the model. What's more, for class I and class II, the indicator σ_θ/σ_c and W_{et} have the same significance level 0.000; for class III, they are 0.001 and 0.003, respectively. This phenomenon shows that $\sigma_\theta/\sigma_c$is relatively better than Wet to interpret class III of rock burst and thus more capable to classify these rock burst intensities.

The classification results using MLR are given in Table 4.6. The overall percentage correct shows that the MLR work better than the empirical methods while the predictive performance is still not very good.

Table 4.6 Results of Multinomial Logistic Regression on rock burst classification

Observed	Predicted				
	I	II	III	IV	Percent Correct
I	17	6	3	0	65.4%
II	4	33	11	1	67.3%
III	2	5	53	3	84.1%
IV	0	0	8	16	66.7%
Overall Percentage	14.2%	27.2%	46.3%	12.3%	73.5%

4.4.5.3 Results of cloud models

The predicting results of the 152 training instances are shown in Table 4.7 for both the simple cloud models (CM) and the attribution weighted cloud models (WCM). The numbers of the predicted instances are given for each class of rock burst intensity. The numbers in bold are the correctly predictive numbers and the others are the missed predictive numbers. These values give out the performance of the simple and weighted cloud models in the prediction of rock burst classification. It can be concluded according to the numbers in Table 4.7 that the cloud models with attributive weight can generate satisfactory results for the classification of these instances. The values of the accuracy rate of the weighted cloud models (94.1%) are a little bigger than that of simple cloud models (93.4%) in Table 4.7.Thus considering the attributive weight can improve the predictive performance of cloud models for the classification of these rock burst instances.

Beside the training instances, 10 rock burst instances randomly chosen are tested to validate the generalization ability of the strategy with cloud models and attributive weight for prediction of rock burst classification. The testing accuracy is 90% of the simple cloud models and 100% for the weighted cloud models. The results indicate that the strategy is capable of generating agreeable results for the predication of the rock burst classifications.

Table 4.7 Predictive results of both simple and weighted cloud models with six indicators

Class label	Data set	Simple cloud model				Weighted cloud model			
		I	II	III	IV	I	II	III	IV
I	Training set(24)	18	4	1	1	20	0	3	1
	Test set(2)	1	1	0	0	2	0	0	0
II	Training set(46)	0	46	0	0	0	46	0	0
	Test set(3)	0	2	1	0	1	2	0	0
III	Training set(60)	0	0	56	4	0	0	56	4
	Test set(3)	0	0	2	1	0	0	2	1
IV	Training set(22)	0	0	0	22	0	0	1	21
	Test set(2)	0	0	1	1	0	0	0	2
Accuracy (%)	Training set(152)	93.4				94.1			
	Test set(10)	90.0				100.0			

Notes: The digits in the brackets denote the total sample numbers. The other digits denote the number of samples predicted in the corresponding class.

4.4.5.4 Results of neural network and support vector machines

In order to compare the performance of the strategy, the methods of Neural Network and Support Vector Machines (SVM)(Chang and Lin 2011) are also applied comparatively to generate results on these rock burst instances. Before modeling, the data samples are normalized in order to reduce the

effect of units and range difference. In the neural network investigation, the General Regression Neural Network(GRNN)(Specht 1991) and Probabilistic Neural Network(PNN)(Specht 1990) is applied respectively. In the SVM investigation, the RBF kernel function is applied. The cost parameter of the SVM model is settled as $c = 2$ and the gamma parameter of the kernel function is $g = 1$.

The predictive performances of the above techniques are shown in for both the training samples and test samples with different indicators. Each accuracy rate of Model 1~Model 7 indicates that WCM can perform better than CM in classification of these rock burst samples. Meanwhile, the accuracy rate of the GRNN and PNN is bigger than all the other technics for the training samples, while that of the WCM and SVM is bigger than the Neural networks for the test samples. That's to say the Neural Networks have superior ability of training samples while the WCM and SVM the superior generalization ability over the samples.

Therefore the WCM performs much better than the empirical methods and regression approaches and that it has the better generalization ability than the GRNN and PNN on modeling these rock burst cases. Unlike the neural networks and SVMs, it is advantageous that there are no experience-depended hyper-parameters to adjust for the CM and WCM during the modeling. Also, the clustering figures in Fig. 4.4 can show visually the effect of each two indicators on rock burst classification. To this end, the WCM is superior to the SVMs in clusters visualization.

4.4.6 Validation of indicator sensitivity

The relative sensitivity shown in Fig. 4.3 is obtained based on the importance of the indicators for rock burst classification. The sensitivity analysis of the indicators is carried out at the same time with different models in order to validate the effects of varying indicators for classification of these rock burst instances. The effects of the indicators are already investigated in the former section by weight analysis, cloud clustering analysis and regression analysis; only some compositions of these indicators are executed as shown in Fig. 4.5 based on the former results. In all, seven models have been investigated for each strategy and the corresponding predicted performance is shown in Fig. 4.5.

The results of Model 1(with 6 parameters) and Model 2(without σ_c and σ_t) are mainly the same in Fig. 4.5, which indicates that the parameters σ_c and σ_t are not sensitive for the rock burst classification compared with other factors. The accuracy rates of Model 1 are bigger than that of the Model 3, which indicates that the parameter σ_θ/σ_c is relatively more sensitive than the others. Comparison of Model 1 and Model 4 gives out that W_{et} is also sensitive but less sensitive than σ_θ/σ_c. Comparison of Model 4 and Model 5 indicates that σ_θ is not very sensitive. The results of Model 5 and Model 6 give that σ_c/σ_t is a bit sensitive. The results of Model 7 show that only using σ_θ,σ_c, σ_t cannot generate as good predictive performance as using the other indicators for classification of the

samples(while similar to that of the empirical methods).

These results demonstrate that σ_θ/σ_c is the most sensitive factor among the indicators for the prediction of rock burst classification. The indicator W_{et} takes the second place of sensitivity. The brittleness index σ_c/σ_t is a bit sensitive. The factors σ_θ,σ_c, σ_t is not so sensitive as the former three factors. None of the indicators are capable to exclusively classify these rock burst instances well. The combination of the indicators works much better than single indicator.

These phenomena illustrate that the ratio of the stress parameters (like σ_θ/σ_c and σ_c/σ_t) is much more sensitive than the stress parameter itself. This feature shows that the stress ratio is more reasonable to account for rock burst events than the single stress parameter. In the stress-induced view, rock burst occurs when the stresses set up in the ground surrounding the rock openings surpass intensively the strength of the rocks and the stresses release and redistribute as a sudden with no time for deformation extension. Thus the occurrence of rock burst is closely related to the relation between the stress accumulated on the ground and the strength of the bursting rocks rather than the rock strength itself. The sensitivity analysis results demonstrate this well.

4.5 Further discussion

Besides the predictions, another purpose for studying rock burst event is to find possible measures which can prevent rock burst hazards. The different roles that those indicators play can give some indications in the selection of rock burst prevention measures. The indicator $\mathrm{Ts} = \sigma_\theta/\sigma_c$ takes the most important place in the classification of rock burst events among all the indicators. Large values of $\mathrm{Ts} = \sigma_\theta/\sigma_c$ results in large rock burst possibility. Thus reducing the value of $\mathrm{Ts} = \sigma_\theta/\sigma_c$ would provide a promising orientation for reducing and preventing rock burst hazards. As outlined (Hoek and Brown 1980), the tangential stress around the underground openings can be found from the vertical rock stress, the ground water pressure, and the shape and diameter of the openings. Therefore, controlling those factors is a good direction to find measures for rock burst hazard reduction and prevention. In practical projects, the shape and diameter of the openings are much easier to be controlled with proper design than the other factors. Thus it can be taken as the first measure for rock burst hazard reduction.

Nevertheless, work is still needed to record as large data sets as possible to better study on rock burst events. At present, rock burst hazards are far from being under control and work is continuously needed for supplementation. Also, further work on triggering mechanisms of different kinds of rock burst is very helpful for reducing rock burst hazards. The approach in this chapter is still helpful in predicting rock burst classification and to the future excavating activity, though it may not solve the whole problem of rock burst hazards. It is advisable to pay special attention to the rock burst prone

regions figured out by the prediction result.

4.6 Conclusions

Rock burst is a common type of hazard during the excavation of openings, which is a great challenge to the safety of staffs and properties. It is practical and significant to predict rock burst intensity before excavating activities. Cloud models and the attribution weight method are presented in this chapter to generate the predictions of rock burst classification. Based on the work above, conclusion can be made as follows.

(1) The weight values and the cloud clustering figures of the rock burst indicators show that the value of $\mathrm{Ts} = \sigma_\theta/\sigma_c$ plays a much more important role than the other parameters for classification of rock burst intensity. The sensitivity order of those factors is $Ts = \sigma_\theta/\sigma_c, W_{et}, B = \frac{\sigma_c}{\sigma_t}, \sigma_\theta, \sigma_c, \sigma_t,$ successively, according to the factor priority for rock burst classification.

(2) The predicted results of simple and weighted cloud models prove that the weighted cloud model performs much better for both training samples and generating predictions over the samples. Thus considering the weights of the indicators can contribute to obtaining more accurate predictive results. The weighted cloud model has the potential ability for rock burst classification.

(3) The cloud models and WCM perform much better than the mentioned empirical approaches and regression analysis in prediction of the rock burst classification. Also, the WCM has better generalization ability than the neural networks like GRNN and PNN on these rock burst cases and it has no hyper-parameters to adjust comparing to SVMs. Thus, the strategy introduced in this chapter is feasible and applicable for rock burst classification.

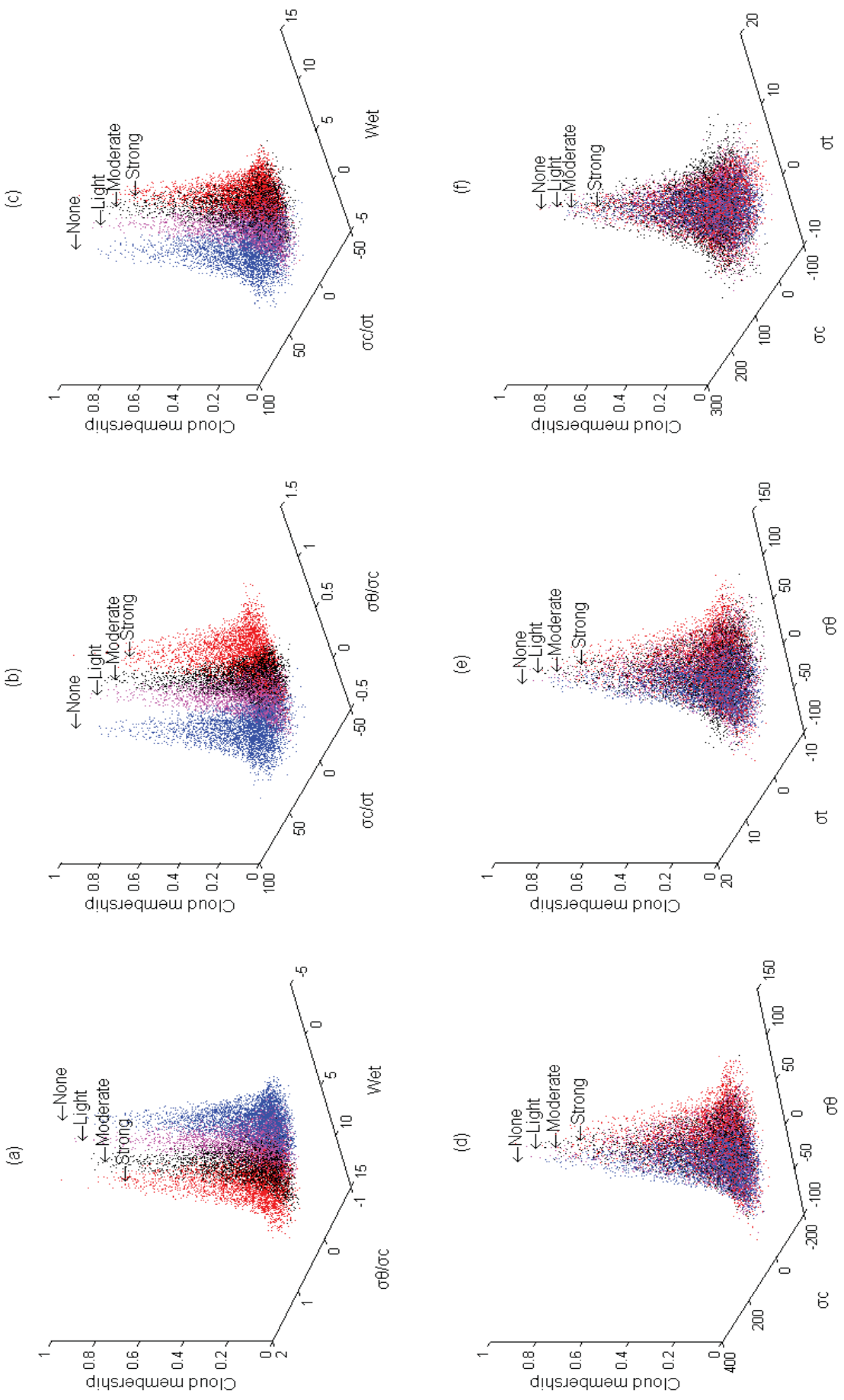

Fig. 4.4 Clustering figures of rock burst instances generated by the cloud models

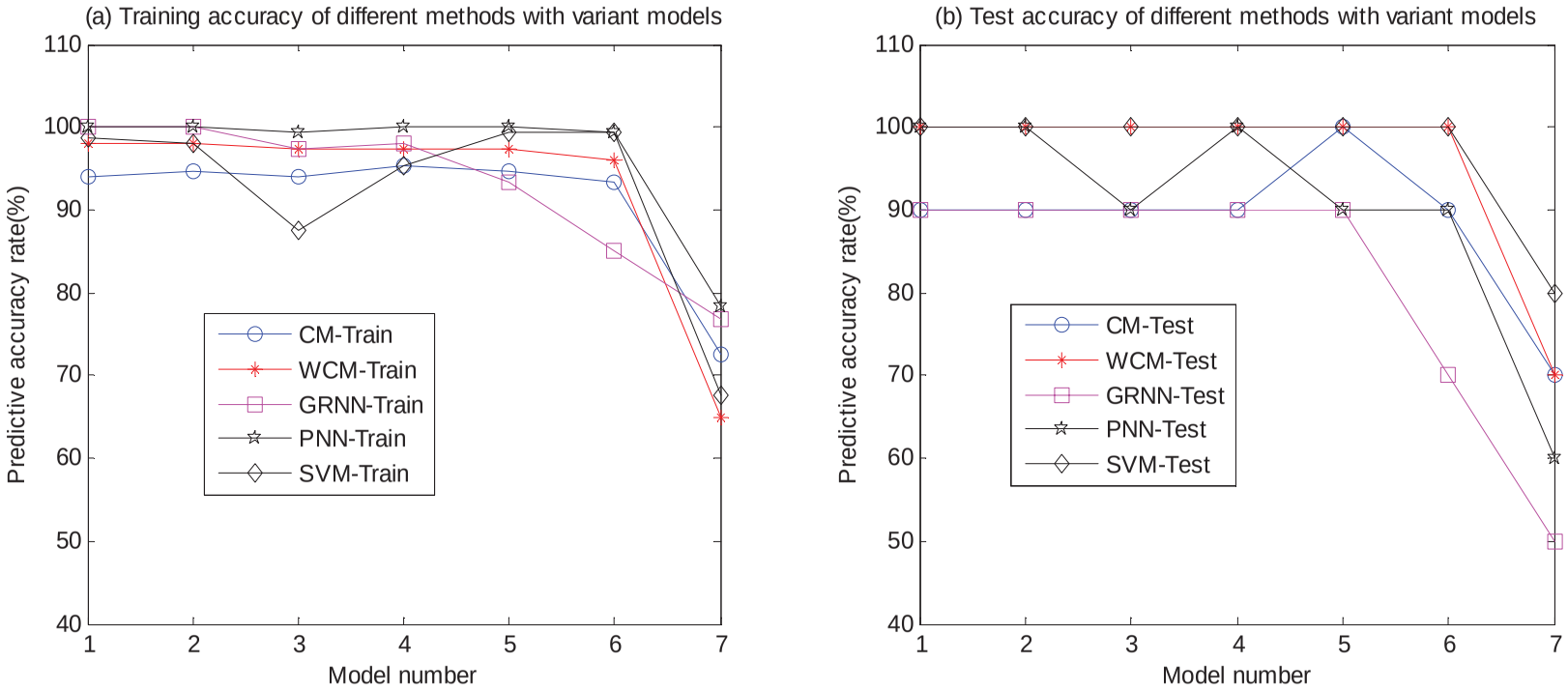

Notes: Each model adopts different indicators. Model 1 adopts σ_θ, σ_c, σ_t, σ_θ/σ_c,σ_c/σ_t,W_{et}. Model 2 adopts σ_θ,σ_θ/σ_c,σ_c/σ_t, W_{et}. Model 3 adopts σ_θ, σ_c, σ_t,σ_c/σ_t,W_{et}. Model 4 adopts σ_θ, σ_c, σ_t, σ_θ/σ_c,σ_c/σ_t.Model 5 adopts σ_θ/σ_c,σ_c/σ_t,W_{et}. Model 6 adopts σ_θ/σ_c,W_{et}. Model 7 adopts σ_θ, σ_c, σ_t.

The abbreviations are as follows. CM-Simple cloud model; WCM-Weighted cloud model; GRNN-General Regression Neural Network, PNN-Probabilistic Neural Network, SVM-support vector machines

Fig. 4.5 Predictive performances of different methods with variant mode

Chapter 5 Summary and recommendations

5.1 Summary

Many problems in rock mechanics and geotechnical engineering are extensively filled with uncertainties. This is because we often deal with the nature data (not man-made) in this field. The conventional methods are used in many cases but not capable enough to account for the variety of associated uncertainties in practical problems. This study has investigated the potential of computational intelligent methods for application in rock mechanics and geotechnical hazard modeling. Although it may not cover every problem, it has illustrated some aspects of these problems. In Chapter 1, landslide displacement analysis and prediction is implemented with the technique of Gaussian process and cross validation and at last a prediction criterion is put forward based on the results of Gaussian process. Different aspects of slope stability evaluation are discussed in Chapter 2 and Chapter 3. In Chapter 4, rock burst, one typical geotechnical hazard, is analyzed using different computational intelligent approaches with emphasis on cloud models. In each modeling, one technique is emphasized and compared with other techniques including the traditional regression analysis. Based on the findings in each chapter, final remarks can be made as follows.

The Gaussian process can take into account expert prior knowledge in the priority functions. This feature strengthens its possibility in application of landslide displacement analysis in which empirical experience is important. The Gaussian process is a satisfactory technique for modeling landslide displacement series. It has the superior ability of point predictions for landslide displacement with proper prior covariance functions. Also, it can provide good results for tracking tendency of the displacement series. The covariance functions and hyper-parameters are the main causes for model performances of the Gaussian process. It would be a sign for forecasting landslide if the intersection angle reaches 45° at the turnings of the predicted curve when modeling the observed displacement of the creep-typed slope.

The parameters of the state-of-art technique RVM is adapted by an iteration method for evaluation and prediction of slope stability based on the factors related to slope failure mechanism. The ARVM is feasible and effective for evaluation of slope stability with good quality of slope case data. The kernel type has no apparent effect on the predictive performance of RVMs on condition that the optimal hyper-parameter is given. The width hyper-parameter values however has an evident effect on the performance of the RVMs, thus it is necessary to obtain an optimal width hyper-parameter value. The sample size shows certain influences on predictive results but the influences are mainly on the different optimal hyper-parameter values. The ARVMs have a powerful training ability like the Neural

Networks and SVMs. Also, the ARVMs have the better generalization ability than the widely used LibSVM in the evaluation of slope stability. It is a potential and promising tool for application in slope stability evaluation.

Many factors are related to the stability of high steep rock slope. It's true that all the factors are not necessary to be considered in stability evaluation of a specific rock slope. The cloud model and analytical hierarchy process approach can be recognized as a unconventional way for modeling the variety of factors related with slope stability with cloud transformation and cloud generators. The approach is proved to be feasible and reliable for stability evaluation of the studied slope. While, this approach may not be able to account for slope failures dominated by structural planes since no other factors than the discontinuities that can account for this kind of slope failure. Monitoring information is considered for slope stability evaluation in the study for the complicated slope without experienced design standards for reference. Data obtained by monitoring instruments are helpful for modification and supplementation of slope design. And the evaluating result is more reliable taking into account the monitoring information.

Rock burst is a common type of hazard during the excavation of openings, which is a great challenge to the safety of staffs and properties. Among the adopted factors in Chapter 4, the value of $Ts = \sigma_\theta/\sigma_c$ plays a much more important role than the other parameters for classification of rock burst intensity. The sensitivity order of those factors is $Ts = \sigma_\theta/\sigma_c$, W_{et}, $B = \frac{\sigma_c}{\sigma_t}$, σ_θ, σ_c, σ_t, successively, according to the factor priority for rock burst classification. Considering weights of the indicators can contribute to obtaining more accurate predictive results. The cloud models and WCM perform much better than the empirical methods in prediction of rock burst classification. The WCM has no hyper-parameters to adjust comparing to SVMs and has better generalization ability than the neural networks like GRNN and PNN. The weighted cloud model has an outstanding ability for rock burst classification.

Nevertheless, the topic of rock mechanics and geotechnical hazard modeling is far more than the problems discussed in this study. And the computational intelligent approaches are being developed all the time. This study only illustrates the analysis of rock compressibility, landslide displacement and prediction, slope stability evaluation and rock burst classification by using the approaches like PLSR, ANNs, SVMs and the Cloud models as well as some parameter optimization techniques. It provides a guide on how to apply the computational intelligent techniques for analysis of rock mechanics and geotechnical hazard prediction.

5.2 Recommendations

This study discusses only the computational intelligent modeling; rock compressibility analysis can be implemented together with the theoretical analytical solutions despite that the analytical solutions have many assumptions.

Landslide is a complex system involving many disciplines. Displacement modeling is a phenomenal method for landslide study; further studies could be continued on landslide predictions by the composition of displacement study and the evolutionary mechanism analysis. Meanwhile, studies may also be carried out for the warning criteria of slopes with the mutant type and stepped type displacement features.

Slope stability analysis can also be continued for other type of failure for example the wedge failure. Also, the cloud model synthesized with analytical hierarchy

Nevertheless, it must be convinced that the factors adopted for rock slope stability evaluation would be probably different due to data availability and slope conditions. And the classifications would consequently change slightly for different slopes in a different area with different conditions. The classification data in this chapter are mainly counted for rock slopes in hydroelectric projects with the similar conditions. What's more, the classifications of the monitoring factors presented in this chapter need to be further proved with many more cases. And the weight matrix of the factors would be more proper if more experts and more experiences could have been obtained.

At last, the integrated systematic information system is to be developed for geotechnical hazard analysis and prediction using the computational intelligence techniques. In this way, these techniques can be applied for mapping regional geotechnical hazards.

References

Abbas D, Ataeib M, Sereshki F (2011) Assessment of rock slope stability using the Fuzzy Slope Mass Rating (FSMR) system. Applied Soft Computing 11 (8):4465-4473

Aksoy H, Ercanoglu M (2007) Fuzzified kinematic analysis of discontinuity-controlled rock slope instabilities. Eng Geol 89 (3-4):206-219

Alejano LR, Ferrero AM, Ramírez-Oyanguren P, Álvarez Fernández MI (2011) Comparison of limit-equilibrium, numerical and physical models of wall slope stability. Int J Rock Mech Min 48 (1):16-26

Aydan Ö, Shimizu Y, Ichikawa Y (1989) The effective failure modes and stability of slopes in rock mass with two discontinuity sets. Rock Mech Rock Eng 22 (3):163-188

Barber D, Saad D (1996) Does Extra Knowledge Necessarily Improve Generalisation. Neural Comput 8:202-214

Beer DW, Mendecki AJ (1998) Rockburst prediction-case studies using a kinematics of failure approach. Journal of South African Institute of Mining and Metallurgy 98:65-73

Belhouari SB, Bermak A (2004) Gaussian process for nonstationary time series prediction. Comput Stat Data An 47 (4):705-712

Belhouari SB, Vesin JM Bayesian learning using Gaussian process for time series prediction. In: 1th IEEE Statistical Signal Processing Workshop, 2001. pp 433-436

Berger JO (1985) Statistical Decision Theory and Bayesian Analysis. Second Edition. Springer-Verlag, New York

Bieniawski ZT Rock mass classification in rock engineering. In: the symposium on explorer for rock engineering, Johannesburg, 1976. pp 97-106

Bieniawski ZT The geomechanics classification in rock engineering applications. In: Proceedings of the 4th international congress on rock mechanics, 1979. pp 41-48

Bye A, Bell F (2001) Stability assessment and slope design at Sandsloot open pit, South Africa. Int J Rock Mech Min 38 (3):449-466

Ceryan N, Okkan U, Kesimal A (2012) Application of Generalized Regression Neural Networks in Predicting the Unconfined Compressive Strength of Carbonate Rocks. Rock Mech Rock Eng 45:1055-1072

Cevik A, Sezer EA, Cabalar AF, Gokceoglu C (2011) Modeling of the uniaxial compressive strength of some clay-bearing rocks using neural network. Applied Soft Computing 11 (2):2587-2594. doi:http://dx.doi.org/10.1016/j.asoc.2010.10.008

Chang CC, Lin CJ (2011) LIBSVM: a library for support vector machines. ACM Transactions on Intelligent Systems and Technology 2 (3):1-27

Chau KW (2006) Particle swarm optimization training algorithm for ANNs in stage prediction of Shing Mun River. J Hydrol 329 (3-4):363-367

Chen C, Xiao Z, Zhang G (2011) Stability Assessment Model for Epimetamorphic Rock Slopes based on Adaptive Neuro-Fuzzy Inference System. the Electronic Journal of Geotechnical Engineering 16 (A):93-107

Chen WF, Snitbhan N (1975) On slip surface and slope stability analysis. Soils and Foundations 15 (3):41-49

Chen Z (1995) Recent developments in slope stability analysis. Paper presented at the Proceedings of the 8th international congress ISRM, Tokyo,

Chenga M-Y, Roya AFV, Chena K-L (2012) Evolutionary risk preference inference model using fuzzy support vector machine for road slope collapse prediction. Expert Syst Appl 39 (2):1737-1746

Choobbasti AJ, Farrokhzad F, Barari A (2009) Prediction of slope stability using artificial neural network (case study: Noabad, Mazandaran, Iran). Arabian Journal of Geosciences 2 (4):311-319

Clark ARJ, Everson RM (2012) Multi-objective learning of Relevance Vector Machine classifiers with multi-resolution kernels. PatternRecognition 45:3535-3543

Dixon B (2009) A case study using support vector machines, neural networks and logistic regression in a GIS to identify wells contaminated with nitrate-N. Hydrogeology 17:1507-1520

Dong H, Fu H, Leng W (2007) Landslide Displacement Prediction Based on Takens Theory and SVM. China Journal of Highway and Transport 20 (5):13

Duzgun HS, Bhasin R (2009) Probabilistic stability evaluation of Oppstadhornet rock slope, Norway. Rock Mech Rock Eng 42 (5):729-749

Elguebaly T, Bouguila N (2011) Bayesian learning of finite generalized Gaussian mixture models on images. Signal Process 91 (4):801-820

Feng X, Zhao H, Li S (2004) Modeling non-linear displacement time series of geo-materials using evolutionary support vector machines. Int J Rock Mech Min 41 (7):1087-1107

Feng XT, Wang LN (1994) Rockburst prediction based on neural networks. T Nonferr Metal Soc 4 (1):7-14

Feng XT, Wang Y, Yao J (1996) A neural network model on real-time prediction of roof pressure in coal mines. Int J Rock Mech Min 33 (6):647-653

Ferentinou MD, Sakellariou MG (2007) Computational intelligence tools for the prediction of slope performance. Comput Geotech 34 (5):362-384

Fukuzono T A new method for predicting the failure time of a slope. In: the 4th International Conference and Field Workshop on Landslides, Tokyo, 1985. Tokyo University Press, pp 145-150

Gong FQ, Li XB (2007) A distance discriminant analysis method for prediction of possibility and classification of rockburst and its application. Chin J Rock Mech Eng 26 (5):1012-1018

Goodman RE (1989) Introduction to Rock Mechanics. Wiley, New York

Goodman RE, Shi G-H (1985) Block Theory and its application to rock ngineering. NJ, Prentice-Hall

Guo F, Xu WY, Xu F (2010) Optimized Based on Cloud Model Extension Assessment of Slope Stability. Advanced Materials Research (163-167):2709-2714

H.B.Wang, W.Y.Xu, R.C.Xu (2005) Slope stability evaluation using Back Propagation Neural Networks. Eng Geol 80 (7):302-315

Hahnekamp HG, Gluckauf F (1983) Simple seismo-acoustic monitoring system for use in rockburst-prone zones (in German) V43, N6, Dec 1982, P256–259. International Journal of Rock Mechanics and Mining Sciences & Geomechanics Abstracts 20 (6):A182. doi:10.1016/0148-9062(83)90726-X

Hatzor YH, Arzi AA, Zaslavsky Y, Shapira A (2004) Dynamic stability analysis of jointed rock slopes using the DDA method: King Herod's Palace, Masada, Israel. Int J Rock Mech Min 41 (5):813-832. doi:http://dx.doi.org/10.1016/j.ijrmms.2004.02.002

He MC, Miao JL, Feng JL (2010) Rock burst process of limestone and its acoustic emission characteristics under true-triaxial unloading conditions. International Journal of Rock Mechanics and Mining Sciences 47 (2):286-298. doi:10.1016/j.ijrmms.2009.09.003

Herbrich R (2002) Learning Kernel Classifiers. MIT Press, Cambridge MA

Hoek E, Bray JW (1981) Rock Slope Engineering. Institute of Mining and Metallurgy, London

Hoek E, Bray JW (1991) Rock Slope Engineering. Elsevier Science Publishing, New York

Hoek E, Brown ET (1980) Underground Excavation in Rock. Institute of Mining and Metallurgy, London

Hoek E, Brown ET (1997) Practical estimates of rock mass strength. Int J Rock Mech Min 34:1165-1186.

Hoek E, Kaiser PK, Bawden WF (1995) Support of Underground Excavations in Hard Rock. Rotterdam:Balkema

Hydro-China CEC (2008) Special research report on left bank slope stability analysis of Jinping 1 hydropower station in Yalong river. Hydro-China Chengdu Engineering Corporation, Chengdu

Ishida T, Kanagawa T, Kanaori Y (2010) Source distribution of acoustic emissions during an in-situ direct shear test: Implications for an analog model of seismogenic faulting in an inhomogeneous rock mass. Engineering Geology 110 (3–4):66-76. doi:10.1016/j.enggeo.2009.11.003

Janbu N (1973) Slope Stability Computations in Embankment Dam Engineering , Casagrande Vol., pp.47-86. Paper presented at the Embankment-Dam Engineering,

Jeongi-gi U, Kulatilake PHSW (2001) Kinematic and block theory analyses for shiplock slope of the three gorges dam site in china. Geotech Geol Eng 19:21-42

Jha PC, Chouhan RKS (1994) Long range rockburst prediction: a seismological approach. Int J Rock Mech Min Sci Geomech Abstr 31 (1):71-77

Jhanwar J (2012) A Classification System for the Slope Stability Assessment of Opencast Coal Mines in Central India. Rock Mech Rock Eng 45 (4):631-637

Jimenez-Rodriguez R, Sitar N, Chacón J (2006) System reliability approach to rock slope stability. Int J Rock Mech Min 43 (6):847-859

K.Liu, Liu B, Xu C, al e (2009) Intelligent analysis model of slope nonlinear displacement time series based on genetic-Gaussian process regression algorithm of combined kernel function. Chin J Rock Mech Eng 28 (10):2128-2134

Kang ZQ, R.S.Wang, Guo LW, al e Rock Slope Quality Evaluation Based on Matter Element Model. In: Proceedings of Selected Papers from the 2009 GeoHunan International Conference, 2009. ASCE, pp 190-196

Khademi Hamidi J, Shahriar K, Rezai B, Bejari H (2010) Application of Fuzzy Set Theory to Rock Engineering Classification Systems: An Illustration of the Rock Mass Excavability Index. Rock Mech Rock Eng 43 (3):335-350. doi:10.1007/s00603-009-0029-1

Khandelwal M (2010) Evaluation and prediction of blast-induced ground vibration using support vector machine. Int J Rock Mech Min 47 (3):509-516

Kidybinskia (1981) Bursting liability indices of coal. Int J Rock Mech Min Sci Geomechanics Abstract 18 (4):295-304

Kveldsvik V, Einstein HH, Nilsen B, Blikra LH (2009) Numerical analysis of the 650,000 m 2 Åknes rock slope based on measured displacements and geotechnical data. Rock Mech Rock Eng 42 (5):689-728

Lam L, Fredlund DG (1993) A general limit equilibrium model of three-dimensional slope stability analysis. Can Geotech J 30 (6):905-919

Latha GM, Garaga A (2010) Seismic Stability Analysis of a Himalayan Rock Slope. Rock Mech Rock Eng 43 (6):831-843

Li D (1997a) Knowledge representation in KDD based on linguistic atoms. Journal of Computer Science and Technology 12 (6):481-496

Li D, Cheng D, Shi X (1998a) Uncertainty reasoning based on cloud models in controllers. Computers and Mathematics with Applications 35 (3):99-123

Li D, Di K, Li D (1998b) Mining association rules with linguistic cloud models. Lect Notes Comput Sc 1394:392-393

Li D, Du Y (2007) Artificial intelligence with uncertainty. Chapman & Hall/CRC, Boca Raton USA

Li D, Han J, Shi X, al. e (1998c) Knowledge representation and discovery based on linguistic atoms. Knowl-based Syst 10 (7):431-440

Li D, Liu C-y, Du Y, Han X (2004) Artificial intelligence with uncertainty Journal of Software 15 (11):1-13

Li D, Meng HJ, Shi XM (1995) Membership clouds and membership cloud generators. Computers Research and Development 32 (6):16~21

Li DY, Cheng D, Shi XM (1998d) Uncertainty reasoning based on cloud models in controllers. Computers and Mathematics with Applications 35 (3):99-123

Li DY, Di KC, Li DR (2000a) Mining association rules with linguistic cloud models. Journal of Software 11 (2):143-158

Li DY, Di KC, Li DR, Song ZL (2000b) Mining association rules with linguistic cloud models. Journal of Software 11 (2):143-158

Li DY, Han JW, Shi XM (1998e) Knowledge representation and discovery based on linguistic atoms. Knowl-based Syst 10 (7):431-440

Li H, Sun J (2009) Gaussian case-based reasoning for business failure prediction with empirical data in China. Inform Sciences 179:89-108

Li S, Liu Y (2004) Intelligent Forecast Procedures for Slope Stability with Evolutionary Artificial Neural Network, Advances in Neural Networks - ISNN 2004. Lect Notes Comput Sc 3174:792-798

Li X (2004) Research on time prediction for landslide hazard. Chengdu university of technology, Chengdu

Li Z (1997b) Application of fuzzy analysis to slope stability evaluation. Chin J Rock Mech Eng 16 (5):490-495

Liang G, Xu W, Tan X (2010) Application of extension theory based on entropy weight to rock quality evaluation. Rock and Soil Mechanics 31 (2):535-540

Liu CH, Jaksa MB, Meyers AG (2008) Improved analytical solution for toppling stability analysis of rock slopes. Int J Rock Mech Min 45 (8):1361-1372

Liu CY, Li DY, Pan LL (2004) Uncertain knowledge representation based on cloud model. Computer Engineering and Applications (2):32-35

Liu YC, Chen CS (2007) A new approach for application of rock mass classification on rock slope stability assessment. Eng Geol 89:129-143

Liu Z, Shao J, Xu W, Meng Y (2013) Prediction of rock burst classification using the technique of cloud models with attribution weight. Nat Hazards. doi: 10.1007/s11069-013-0635-9

Liu Z, Xu W, Shao J (2012) Gaussian Process Based Approach for Application on Landslide Displacement Analysis and Prediction. CMES: Comp M Eng & Sci 84 (2):99-122. doi:doi:10.3970/cmes.2012.084.099

Liu ZB, Xu WY, Meng YD, Chen H Modification of GM (1, 1) and its Application in Analysis of Rock-slope Deformation. In: Proc. of 2009 IEEE Int. Con. on GSIS, Nanjing China, 2009. pp 415-419

Lu P, Rosenbaum MS (2003) Artificial Neural Networks and Grey Systems for the Prediction of Slope Stability. Nat Hazards 30 (3):383-398

MacKay DJC (1994) Models of Neural Networks III: Bayesian Methods forBack propagation Networks.

Mansurov VA (2001) Prediction of rockbursts by analysis of induced seismicity data. International Journal of Rock Mechanics & Mining Sciences 38 (7):893-901

Matías JM, Taboada J, Taboada J, al e (2010) Partially linear support vector machines applied to the prediction of mine slope movements. Math Comput Model 51 (3-4):206-215

Mehdi K, Mehdi B (2011) A novel hybridization of artificial neural networks and ARIMA models for time series forecasting. Applied Soft Computing 11 (2):2664-2675

Mehrabi Mazidi S, Haftani M, Bohloli B, Cheshomi A (2012) Measurement of uniaxial compressive strength of rocks using reconstructed cores from rock cuttings. J Petrol Sci Eng 86–87 (0):39-43. doi:http://dx.doi.org/10.1016/j.petrol.2012.03.015

Mishra DA, Basu A (2012) Use of the block punch test to predict the compressive and tensile strengths of rocks. Int J Rock Mech Min 51 (0):119-127. doi:http://dx.doi.org/10.1016/j.ijrmms.2012.01.016

Mohamed T, Kasa A, Mukhlisin M (2012) Prediction of slope stability using statistical method and fuzzy logic. the Online Journal of Science and Technology 2 (4):68-73

the Ministry of Land Resouces of China (2010) http://www.mlr.gov.cn/mlrenglish/.

Nawari O, Hartmann R, Lackner R (1997) Stability analysis of rock slopes with the direct sliding blocks method. Int J Rock Mech Min 34 (3-4):220.e221-220.e228

Neal RM (1996) Bayesian Learning for Neural Networks. Springer, New York

Neyman B, Szecowka Z, Zuberek W Effective methods for fighting rock burst in Polish collieries. In: In: Proceedings of the 5th International Strata Control Conference, 1972. pp 1-9

Ortlepp WD The design of support for the containment of rockburst damage in tunnels-an engineering approach. In: proceedings in international symposium on rock support, Rotterdam: Balkema, 1993. Sudbury, pp 593-609

Palmström A Characterizing rock burst and squeezing by the rock mass index. In: International Conference in Design and Construction of Underground Structures, 1995. p 10

Pantelidis L (2009) Rock slope stability assessment through rock mass classification systems. Int J Rock Mech Min 46 (2):315-325. doi:http://dx.doi.org/10.1016/j.ijrmms.2008.06.003

Park H-J, West TR, Woo I (2005) Probabilistic analysis of rock slope stability and random properties of discontinuity parameters, Interstate Highway 40, Western North Carolina, USA. Eng Geol 79:230-250

Park H, West TR (2001) Development of a probabilistic approach for rock wedge failure. Eng Geol 59 (3-4):233-251

Park HJ, Um J-G, Woo I, Kim JW (2012) Application of fuzzy set theory to evaluate the probability of failure in rock slopes. Eng Geol 125 (1):92-101

Pradhan B (2012) A comparative study on the predictive ability of the decision tree, support vector machine and neuro-fuzzy models in landslide susceptibility mapping using GIS. Computers & Geosciences.

PRC MoC (1994) Standard for engineering classification of rock masses(GB50218-94). China Planninc Press,

Psorakis I, Damoulas T, Girolami MA (2010) Multiclass Relevance Vector Machines: Sparsity and Accuracy. Ieee T Neural Networ 21 (10):1588-1597

Qin S, Jiao JJ, Wang S, Long H (2001) A nonlinear Catastrophe Model of Instability of Planar-slip Slope and Chaotic Dynamical Mechanisms of Its Evolutionary Process. Int J Solids Struct 38:8093-9109

Rabbani E, Sharif F, Koolivand Salooki M, Moradzadeh A (2012) Application of neural network technique for prediction of uniaxial compressive strength using reservoir formation properties. Int J Rock Mech Min 56 (0):100-111. doi:http://dx.doi.org/10.1016/j.ijrmms.2012.07.033

Rajabzadeh MA, Moosavinasab Z, Rakhshandehroo G (2012) Effects of Rock Classes and Porosity on the Relation between Uniaxial Compressive Strength and Some Rock Properties for Carbonate Rocks. Rock Mech Rock Eng 45 (1):113-122. doi:10.1007/s00603-011-0169-y

Rajesh Kumar B, Vardhan H, Govindaraj M, Vijay GS (2013) Regression analysis and ANN models to predict rock properties from sound levels produced during drilling. Int J Rock Mech Min 58 (0):61-72. doi:http://dx.doi.org/10.1016/j.ijrmms.2012.10.002

Rasmussen CE, Williams CKI (2006) Gaussian Processes for Machine Learning. MIT

Rezaei M, Majdi A, Monjezi M (2012) An intelligent approach to predict unconfined compressive strength of rock surrounding access tunnels in longwall coal mining. Neural Comput & Applic:1-9. doi:10.1007/s00521-012-1221-x

Rodrigo dP, Hürlimann M (2008) Geotechnical classification and characterisation of materials for stability analyses of large volcanic slopes. Eng Geol 98 (1-2):1-17

Romana M, Seron J, Montalar E SMR Geo-mechanics classification: application, experience and validation. In: the international symposium on role of rock mechanics, South African Institute of Mining and Metallurgy, 2003. pp 1-4

Russenes BF (1974) Analysis of Rock Spalling for Tunnels in Steep Valley Sides(in Norwegian). Master Thesis of Science, Norwegian Institute of Technology, Trondheim

Saada Z, Maghous S, Garnier D (2012) Stability analysis of rock slopes subjected to seepage forces using the modified Hoek-Brown criterion. Int J Rock Mech Min 55 (0):45-54

Saaty TL (1980) The Analytic Hierarchy Process. McGraw-Hill International Book Company, New York

Saito M Forecasting the time of occurrence of slope failure. In: Proceedings of the 6th International Conference on Soil Mechanics and Foundation Engineering, Montréal, Que, 1965. University of Toronto Press, pp 537-542

Sakellariou MG, Ferentinou MD (2005) A study of slope stability prediction using neural networks. Geotech Geol Eng 24 (3):419-445

Samui P (2008) Slope stability analysis: a support vector machine approach. Environ Geol 56:255-267

Samui P, Kotharib DP (2011) Utilization of a least square support vector machine (LSSVM) for slope stability analysis. Scientia Iranica 18 (1):53-58

Samui P, Lansivaarab T, Kim D (2011) Utilization relevance vector machine for slope reliability analysis. Applied Soft Computing 11 (5):4036-4040

Schölkopf **B**, Burges CJC, Smola AJ (1999) Advances in Kernel Methods: Support Vector Learning.

Sharan SK (2004) A finite element perturbation method for the prediction of rockburst. Computers and Structures 85:1304-1309

Shiotani T, Ohstu M, Ikeda K (2001) Detection and evaluation of AE waves due to rock deformation. Construct Build Maters 15:235-246

Shu J, Cai Q, Hao H (2005) Use of extenics theory in recognizing failure mode of slope. Journal of China University of Mining and Technology 34 (5):591-595

Singh SP (1988) Burst energy release index. Rock Mech Rock Eng 21:149-155

Singh TN, Singh V (2005) An intelligent approach to prediction and control ground vibration in mines. Geotech Geol Eng 23:249-262

Sobhani J, Najimi M, Pourkhorshidi AR, Parhizkar T (2010) Prediction of the compressive strength of no-slump concrete: A comparative study of regression, neural network and ANFIS models. Constr Build Mater 24 (5):709-718. doi:http://dx.doi.org/10.1016/j.conbuildmat.2009.10.037

Song S, Xiang B, Yang J, al e (2009) Stability analysis and reinforcement design of high and steep slopes with complex geology in abutment of Jinping 1 Hydropower Station. Chin J Geotech Eng 29 (3):442-458

Specht DF (1990) Probabilistic neural networks. Neural Networks 3 (1):109-118

Specht DF (1991) A general regression neural network. IEEE Trans Neural Networks 2 (6):568-576

Stead D, Eberhardt E, Coggan JS (2006) Developments in the characterization of complex rock slope deformation and failure using numerical modelling techniques. Eng Geol 83 (1-3):217-235

Steihaug T (1983) The Conjugate Gradient Method and Trust Regions in Large Scale Optimization. Siam J Numer Anal 20 (3):626-637

Taheri A, Tani K (2010) Assessment of the Stability of Rock Slopes by the Slope Stability Rating Classification System. Rock Mech Rock Eng 43 (3):321-333

Tan X, Xu W, Liang G (2009) Application of extension method to comprehensive safety evaluation of rock slope. Chinese Journal of Rock Mechanics and Engineering 28 (12):2503-2509

Tang BY (2000) Rockburst Control using Distress Blasting. McGill University, Montreal, Canada

Tang LZ, Wang WX (2002) New rock burst proneness index. Chin J Rock Mech Eng 21 (6):874-878

Tang LZ, Xia KW (2010) Seismological method for prediction of areal rockbursts in deep mine with seismic source mechanism and unstable failure theory. Journal of central south university of technology 17:947-953

Tayer DW (1937) Stability of Earth Slopes. Journal of the Boston Society of Civil Engineers 24 (3):337-386

Tipping ME The Relevance Vector Machine. In: Solla SA, Leen TK, Müller KR (eds) Advances in Neural Information Processing Systems, MIT, 2000. MIT, pp 652-658

Tipping ME (2001) Sparse Bayesian learning and the relevance vector machine. J Mach Learn Res 1:211-244

Tipping ME (2004) Bayesian inference: An introduction to principles and practice in machine learning. Paper presented at the Advanced Lectures on Machine Learning,

Turchaninov A, Markov GA, Gzovsky MV, al. e (1972) State of stress in the upper part of the Earth's crust based on direct measurements in mines and on tectonophysical and seismological studies. Phys Earth Planet In (6):229-234

Ulusay R, Erguler ZA (2012) Needle penetration test: Evaluation of its performance and possible uses in predicting strength of weak and soft rocks. Eng Geol 149–150 (0):47-56. doi:http://dx.doi.org/10.1016/j.enggeo.2012.08.007

Vapnik V (1998) Statistical Learning Theory. Wiley-Interscience, New York

Vardhan H, Adhikari GR, Govinda Raj M (2009) Estimating rock properties using sound levels produced during drilling. Int J Rock Mech Min 46 (3):604-612. doi:http://dx.doi.org/10.1016/j.ijrmms.2008.07.011

Verma AK, Singh TN (2012a) Comparative study of cognitive systems for ground vibration measurements. Neural Comput & Applic:1-10. doi:10.1007/s00521-012-0845-1

Verma AK, Singh TN (2012b) A neuro-fuzzy approach for prediction of longitudinal wave velocity. Neural Comput & Applic:1-9. doi:10.1007/s00521-012-0817-5

Wang C, Pan F (2004) Fuzzy matter-element model for evaluating geotechnical slope stability. Wat Res Hydro Eng 35 (9):591-595

Wang C, Tannant DD, Lilly PA (2003) Numerical analysis of the stability of heavily jointed rock slopes using PFC2D. Int J Rock Mech Min 40 (3):415-424

Wang HB, Xu WY, Xu RC (2005) Slope stability evaluation using Back Propagation Neural Networks. Eng Geol 80 (3-4):302-315

Wang JA, Park HD (2001) Comprehensive prediction of rockburst based on analysis of strain energy in rocks. Tunneling and Underground Space Technology 16 (1):49-57

Wang YC, Shang YQ, Sun HY, Yan XS (2010) Study on prediction of rockburst intensity based on efficacy coefficient method. Rock and Soil Mechanics 31 (2):529-534

Wang YH, Li WD, Li QG, Xu Y, Tan GH (1998) Method of fuzzy comprehensive evaluations for rock burst prediction. Chin J Rock Mech Eng 17 (5):493-501

Wasantha PLP, Ranjith PG, Viete DR, Luo L (2012) Influence of the geometry of partially-spanning joints on the uniaxial compressive strength of rock. Int J Rock Mech Min 50 (0):140-146. doi:http://dx.doi.org/10.1016/j.ijrmms.2012.01.006

Wen CP (2008) Application of attribute synthetic evaluation system in prediction of possibility and classification of rockburst. Engineering Mechanics 25 (6):153-158

Will M, Gluckauf F (1985) Seismo-acoustic measurements for monitoring rockburst-prone zone (In German) : V44, N4, Aug 1983, P171–174. International Journal of Rock Mechanics and

Mining Sciences & Geomechanics Abstracts 22 (3):A86. doi:10.1016/0148-9062(85)93418-7

Williams CKI, Rasmussen CE Gaussian process for regression. In: Touretzky DS, Mozer MC, Hasselmo ME (eds) In: Advances in Information Processing Systems, Cambridge, 1996. MA. MIT, pp 111-116

Xu F, Xu W (2010a) Prediction of displacement time series based on support vector machines-Markov chain. Rock and Soil Mechanics 31 (3):944-948

Xu F, Xu WY (2010b) Projection pursuit model based on particle swarm optimization for rock burst prediction. Chin J Geotech Eng 32 (5):718-723

Xu W, Tan X, Jiang Z (2007) Research on fuzzy analytic approach for stability analysis of jointed rock slope. Chin J Rock Mech Eng 26 (6):1232-1236

Yang J, Wu X (2005) Comprehensive forecasting method for estimating rock burst. Chin J Rock Mech Eng 24 (3):411-416

Yang YC, Zhu J (2000) A new model for classified prediction of rockburst and its application. Journal of China Coal Society 25 (2):169-172

Yao X, Thamb LG, Dai FC (2008) Landslide susceptibility mapping based on Support Vector Machine: A case study on natural slopes of Hong Kong. China Geomorphology 101 (4):572-582

Yesiloglu-Gultekin N, Sezer EA, Gokceoglu C, Bayhan H (2013) An application of adaptive neuro fuzzy inference system for estimating the uniaxial compressive strength of certain granitic rocks from their mineral contents. Expert Syst Appl 40 (3):921-928. doi:http://dx.doi.org/10.1016/j.eswa.2012.05.048

Yilmaz I, Kaynar O (2011) Multiple regression, ANN (RBF, MLP) and ANFIS models for prediction of swell potential of clayey soils. Expert Syst Appl 38 (5):5958-5966. doi:http://dx.doi.org/10.1016/j.eswa.2010.11.027

Young RP, Hutchins DA, J MW, Urbancic T, Falls S, Towers J (1987) Concurrent seismic tomographic imaging and acoustic emission techniques: a new approach to rockburst. In: Proc 6th International Conference on Rock Mechanics, Montreal, 30 Aug 1987 1987. Publ Rotterdam: A A Balkema Rotterdam, pp 1333-1338. doi:10.1016/0148-9062(89)92642-9

Yuan R-f, Li Y-h (2009) Fractal analysis on the spatial distribution of acoustic emission in the failure process of rock specimens. International Journal of Minerals, Metallurgy and Materials 16 (1):19-24. doi:10.1016/S1674-4799(09)60004-2

Yuan Y, Xu Q, Guo K (2005) Search for the jump spot of a landslide using the nsmutation algorithm. Journal of Engineering Geology 2005 (13):4

Zhang H, Wang YJ, Li YF (2009) SVM model for estimating the parameters of the probability integral method of predicting mining subsidence. Mining Science and Technology 19 (2):385-388

Zhang J, Hu G (2003) Application of uncertainty reasoning based on cloud model in time series prediction. Journal of Zhejiang University SCIENCE 4 (5):578-583

Zhang JJ, Fu BJ (2008) Rock burst and its criteria and control. Chin J Rock Mech Eng 27 (10):2034–2042

Zhao H (2008) Slope reliability analysis using a support vector machine. Comput Geotech 35 (3):459-467

Zhou J, Li X, Shi X (2012) Long-term prediction model of rockburst in underground openings using heuristic algorithms and support vector machines. Safety Sci 50 (4):629-644. doi:http://dx.doi.org/10.1016/j.ssci.2011.08.065

Zhou P, Yao L (2009) Landslide hazard early warning system in China and future trends. Paper presented at the Engineering Geology for Tomorrow's cities, London,